Inaugural dissertation

for

obtaining the doctoral degree

of the

Combined Faculty of Mathematics, Engineering and Natural Sciences

of the

Ruprecht - Karls - University

Heidelberg

Presented by

M.S. Soham Basu

born in: Kolkata, India

Oral examination: June 11, 2024

The roles of basement membrane during larva-polyp morphogenesis of the starlet sea anemone *Nematostella vectensis*

Referees: apl. Prof. Dr. Suat Özbek

Prof. Dr. Detlev Arendt

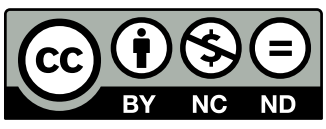

Declaration

This thesis was carried out at the European Molecular Biology Laboratory in Heidelberg from September 2019 to March 2024 under the supervision of Dr. Aissam Ikmi.

Acknowledgements

Around 5 years ago, I fell in love with biology. Doing my graduate studies in physics, biology seemed inaccessible to me. I was always passionate about the origins of complexity and from that point of view, biology seemed extremely rich. My interests moved me far from my home, and what follows up in this thesis is a very brief reflection on how the last 5 years of my life were. Thanks to EMBL and its PhD program with its support in my doctoral journey, and to allow me an excursion in biology.

This journey would not have been possible without the Ikmi lab, and definitely not possible without Aissam with whom I have enjoyed discussing science from the moment we have crossed paths. My sincere thanks to all the members in the past and the present of the Ikmi lab who have helped me beyond my expectations in scientific, even more in non-scientific matters. I would cherish all the coffee and the cakes and the laughter that we have shared together. Thank you for all the feedback throughout the years! It was a pleasure being surrounded by such lovely curious people. Thanks a ton, Peter, Marie, Anniek, Stephanie, Paolo, Giulia, Omar, Pauline, Julia, Richard, Kaushik, Florian, Alexandre, Lotta, Irié, Jaro, Levin, Silvia, Elody, Auriane, Mohannad and Sohsuke for the shared journey. The lab indeed grew big!

I would like to thank my TAC members, Suat, Detlev, Alba and Anna, who has followed through my research development over the years. Many thanks to the core facilities at EMBL for their input in my research over the years. My thanks also go to Krěso for taking good care of our animals, and to Alexandre for helping me with his expertise in genome editing.

Our Developmental Biology Unit also needs a lovely mention. I was blessed to have lovely colleagues all around. Thanks to all the joint lab meetings, the retreats, the beer sessions and the bustling seminars. It was so easy to discuss science with anyone. My thanks also goes to the brilliant people in the ALMF, particularly Aliak-

sandr, Stefan and Manuel for sharing their expertise in microscopy, and in building an imaging enthusiast in me.

Thanks to all the friends that I have made during my PhD at EMBL, and in Heidelberg. I was relieved that they had my back when I needed them, being so far away from home. Thanks to my dear sister and parents for their constant support and their incredible enthusiasm throughout this entire journey.

Last but not least, a big thanks to my cute little Cappuccino and Poulami, the two big surprises that made the end of my PhD life incredibly sweet, ending my stay in Heidelberg on a high note. I cannot thank you both enough for your presence in my life and for all the happiness that you bring along.

Summary

Living systems attain their shape and size through morphogenesis, which spans across several magnitudes of spatial and temporal scales. The pursuit to understand the driving elements that control morphogenesis has primarily focused its attention on the living matter, on the cells and its underlying genetic information. Evidences over the last few centuries has established deeper insights into how cells can self-organize or can be genetically programmed to achieve emergent properties that drive morphogenesis, however, the deeper impact from its internal environment is often ignored or avoided. In case of embryonic development, what starts as a single cell eventually ends up in a multicellular context with several specialized cell types that are crucial to life and its functions, but also builds up an internal niche created by its extracellular matrix in the process. How does an organism build its own native matrix, and how does that integrate with its morphogenesis? In this thesis, I utilize the simple yet complex biology of the sea anemone *Nematostella* vectensis as a model species to investigate the connection between the extracellular matrix and the development of an organism, at the tissue and the organismal scales. In a phase known as the larva-polyp transition, *Nematostella* experiences a shift from an ellipsoidal larva to a tubular polyp featuring four tentacles, post-embryonically. Using immunostaining, generation of endogenous knock-in transgenic lines and photoconversions, I establish the spatiotemporal dynamics of the basement membrane, and focus particularly on collagen IV. Through pharmacological perturbations, I found out that a steady state of collagen IV density across the body axis is crucial for the animal to maintain its organismal morphogenesis. Also, I discovered that the basement membrane is produced by the endoderm and is organized by the muscles. Furthermore, I account for the origins of tissue remodeling that drives the larva-polyp morphogenesis and propose a dominant regime that is modulated through novel muscle-ECM coordination. These findings address the origin of deformations that modulate the larva-polyp morphogenesis, highlighting a key feedback between the active musculature and passive extracellular matrix in a developing organism. I also focus on tissue-specific morphogenesis at the aboral end of the transitioning animal, where a weaker ECM permits the

formation of a secondary pore in a cnidarian, which itself is a debatable topic in evolutionary biology. Using detailed cellular and molecular descriptions, combined with biophysical experiments, I identify key steps controlled by upstream FGF signaling that lead to the development of an aboral pore. My doctoral thesis sheds light on the coordination of the extracellular matrix with the tissue, and how these interactions are important to modulate morphogenesis across largely different spatial scales.

Zusammenfassung

Lebende Systeme erlangen ihre Form und Größe durch Morphogenese, die sich über mehrere Größenordnungen räumlicher und zeitlicher Skalen erstreckt. Das Streben nach dem Verständnis der treibenden Elemente, die die Morphogenese steuern, hat sich bisher in erster Linie auf die lebende Materie, auf die Zellen und die ihnen zugrunde liegende genetische Information konzentriert. In den letzten Jahrhunderten wurden tiefere Erkenntnisse darüber gewonnen, wie Zellen sich selbst organisieren oder genetisch programmiert werden können, um emergente Eigenschaften zu erreichen, die die Morphogenese vorantreiben, wobei jedoch der tiefere Einfluss ihrer Umgebung oft ignoriert oder vermieden wurde. Bei der Embryonalentwicklung entsteht aus einer einzelnen Zelle ein multizellulärer Kontext mit mehreren spezialisierten Zelltypen, die für das Leben und seine Funktionen von entscheidender Bedeutung sind, sich aber auch eine interne Nische aufbauen, die durch ihre extrazelluläre Matrix geschaffen wird. Wie baut ein Organismus seine eigene Matrix auf, und wie ist diese mit seiner Morphogenese verbunden? In dieser Arbeit verwende ich die einfache und doch komplexe Biologie der Seeanemone *Nematostella vectensis* als Modellorganismus, um die Verbindung zwischen der extrazellulären Matrix (EZM) und der Entwicklung eines Organismus auf der Ebene der Gewebe und des Organismus zu untersuchen. In einer Phase, die als Larva-Polyp-Übergang bekannt ist, vollzieht *Nematostella* nach der Embryonalentwicklung einen Übergang von einer ellipsoiden Larve zu einem röhrenförmigen Polypen mit vier Tentakeln. Mit Hilfe von Immunostainings, der Erzeugung von endogenen Knock-in Transgenen und Photokonversionen ermittle ich die räumlich-zeitliche Dynamik der Basalmembran und konzentriere mich dabei besonders auf Kollagen IV. Durch pharmakologische Eingriffe habe ich herausgefunden, dass ein stabiler Zustand der Kollagen-IV-Dichte entlang der Körperachse für die Aufrechterhaltung der organismischen Morphogenese des Tieres entscheidend ist. Außerdem habe ich herausgefunden, dass die Basalmembran vom Endoderm produziert und von den Muskeln organisiert wird. Darüber hinaus erkläre ich den Ursprung des Gewebeumbaus, der die Morphogenese von Larven und Polypen antreibt, und schlage ein dominantes System vor, das durch eine neuartige Muskel-EZM-Koordination moduliert

wird. Diese Erkenntnisse befassen sich mit dem Ursprung der Deformationen, die die Larven-Polypen-Morphogenese modulieren, und zeigen eine wichtige Rückkopplung zwischen der aktiven Muskulatur und der passiven extrazellulären Matrix in einem sich entwickelnden Organismus auf. Ich konzentriere mich auch auf die gewebespezifische Morphogenese am aboralen Ende des Übergangstieres, wo eine schwächere EZM die Bildung einer sekundären Pore in dem Nesseltier ermöglicht, was wiederum ein umstrittenes Thema in der Evolutionsbiologie ist. Anhand detaillierter zellulärer und molekularer Beschreibungen, kombiniert mit biophysikalischen Experimenten, identifiziere ich Schlüsselschritte, die von vorgelagerten FGF-Signalen gesteuert werden und zur Entwicklung einer aboralen Pore führen. Meine Doktorarbeit beleuchtet die Koordination der extrazellulären Matrix mit dem Gewebe und inwiefern diese Interaktionen wichtig sind, um die Morphogenese über verschiedene räumliche Skalen zu modulieren.

Contents

Declaration vii

Acknowledgements ix

Summary xi

Zusammenfassung xiii

Contents xv

List of Figures xix

1 Morphogenesis of biological systems 1

1.1 Morphogenesis through cellular behaviors 2

1.2 Generation of forces in biological systems 3

1.3 Tissue extensions through cell intercalations 4

1.4 Emergence of mechanical plasticity and fluidity in biological systems . 5

1.4.1 Origins of morphogenetic plasticity from the dynamics of actin and myosin 6

2 The extracellular matrix 11

2.1 ECM composition 12

2.2 ECM regulation: synthesis, assembly and degradation 12

2.3 Towards the regulation of morphogenesis 14

2.4 The coupling of ECM and morphogenesis 17

2.4.1 The growing larval wing disc of drosophila is directed by differences in the production of collagen IV and tissue proliferation . 17

2.4.2 The growing egg chamber of drosophila is shaped by a corset of basement membrane 20

2.4.3 Condensation of the ventral nerve cord of drosophila is driven by temporal induction of collagen IV 21

2.4.4 Onset of gastrulation in mouse embryos is coordinated by patterned degradation of the basement membrane . . . 22
2.4.5 Embryonic growth of metacarpal bone in chick reveals a dominant convective flow of ECM driving cells . . . 23
2.4.6 Semicircular canal morphogenesis in zebrafish is driven by hydraulic pressure of hyaluronon . . . 24

3 Cnidarians, extracellular matrix and morphogenesis 27
3.1 Life cycle in cnidarians . . . 28
3.2 ECM in cnidarians . . . 29
3.3 Advantages of *Nematostella* as a model system . . . 30
3.4 Morphogenesis of *Nematostella* . . . 31

4 Aims of the thesis 33

5 The role of basement membrane in organismal morphogenesis 35
5.1 An overview of larva-polyp morphogenesis during early *Nematostella* development . . . 35
5.2 The basement membrane is maintained at a steady state during larva-polyp morphogenesis . . . 36
5.3 The basement membrane gains anisotropic organization driven by underlying muscular architecture . . . 38
5.4 The steady state of basement membrane density is crucial for organismal morphogenesis . . . 40
5.5 Summary and conclusions . . . 45

6 Biogenesis and remodeling of the basement membrane 47
6.1 Endogenous knock-in eGFP::ColIV reveals the tissue-level origin of collagen IV . . . 47
6.2 Muscles and the basement membrane organization during larva-polyp morphogenesis . . . 48
6.3 Dendra2::ColIV reveals the dynamic remodeling of the basement membrane . . . 51
6.4 Summary and conclusions . . . 54

7 The mechanisms of tissue remodeling that drive larva-polyp morphogenesis 55
7.1 Larva-polyp morphogenesis has two underlying remodeling motifs . . . 55

7.2 Perturbation of a stable basement membrane density does not affect tissue thinning . . . 57
7.3 Possible mechanisms that drive larva-polyp morphogenesis beyond 400µm 59
7.3.1 Oriented cell divisions does not drive axial elongation . . . 59
7.3.2 Changes in cell shape does not drive axial elongation . . . 61
7.3.3 Cell rearrangements drive tissue remodeling . . . 61
7.3.4 Cellular volume does not increase during the transition . . . 62
7.3.5 Muscle fibers gain area and intercalate during the transition . . 63
7.3.6 Emergent material properties possibly tune morphogenesis . . . 63
7.4 Summary and conclusions . . . 64

8 Establishment of a secondary body opening in a cnidarian 67
8.1 Primary polyps show sporadic expulsion of fluid from the aboral pole . 67
8.2 Dynamic changes across the germ layers premark the aboral pore formation . . . 69
8.3 A weak local basement membrane premarks the future aboral pore . . 70
8.4 An artificial cavity expansion assay tests the functionality of the aboral pore . . . 73
8.5 The development of the aboral pore is dependent on FGF signaling . . 73
8.6 Summary and conclusions . . . 74

9 Discussions 77
9.1 On the roles of basement membrane in organismal morphogenesis . . . 77
9.2 What is the identity of the aboral pore? . . . 79

10 Materials and methods 81
10.1 Animal husbandry . . . 81
10.2 Fixation and immunostaining . . . 81
10.3 Endogenous eGFP staining . . . 82
10.4 Pharacological treatments . . . 82
10.5 Live imaging with Acquifer and image analysis . . . 83
10.6 Confocal imaging . . . 83
10.7 Dendra2::ColIV photoconversion . . . 83
10.8 shRNA KD . . . 84
10.9 Cavity inflation assay . . . 84

Bibliography 85

List of Figures

1.1 The mechanisms of cellular rearrangements driving tissue scale morphogenesis 4
1.2 Analogy of mechanical phases in between physical and biological materials 9

2.1 The composition of the ECM proteins 13
2.2 Overview of the BM architecture 16
2.3 Examples of ECM dominating morphogenesis across tissues 18

3.1 Phylogenetic position of *Nematostella vectensis* 28
3.2 Life cycle of *Nematostella vectensis* 29
3.3 Muscle system of *Nematostella vectensis* 32

5.1 Larva-polyp morphogenesis of *Nematostella vectensis* 36
5.2 Basement membrane visualization during larva-polyp morphogenesis. . 38
5.3 Basement membrane with its unique stitches 39
5.4 Anisotropic organization of the basement membrane during development 41
5.5 Basement membrane organization is patterned by the emergent musculature 42
5.6 Pharmacological perturbation of basement membrane steady state . . . 43
5.7 Perturbation of basement membrane steady state affects underlying morphodynamics 44

6.1 eGFP::ColIV reveals intracellular collagen IV dynamics 49
6.2 Emergent muscle and collagen IV anisotropy during larva-polyp morphogenesis. 50
6.3 Effect of pharmacological inhibition of basement membrane stabilization on the muscles and collagen IV networks 51
6.4 Dendra2::ColIV reveals dynamics of BM turnover during morphogenesis 52

7.1 Tissue geometry changes underlying larva-polyp morphogenesis 56
7.2 Perturbation of basement membrane stabilization does not affect tissue thinning 58
7.3 Mechanisms driving axial elongation in Nematostella 59
7.4 Cellular motifs of morphogenesis in Nematostella 60
7.5 Muscle fiber morphology and topology during larva-polyp morphogenesis 65
7.6 Tissue remodeling motifs during larva-polyp morphogenesis 66

8.1 Spatial characterization of the aboral pore in *Nematostella vectensis* . . 68
8.2 The dynamics of the germ layers at the aboral end 69
8.3 The dynamic basement membrane at the aboral end during larva-polyp morphogenesis 71
8.4 The aboral view of the basement membrane at the polyp stages 72
8.5 Cavity inflation: a biophysical assay to test the functionality of the aboral pore 72
8.6 $FGFRb^{-/-}$ mutants lack active muscles at the aboral end 74
8.7 $FGFRb^{-/-}$ mutants lack collagen IV degradation at the aboral end . . . 75
8.8 $FGFRb^{-/-}$ mutants lack aboral pore leakage with artificial cavity inflation 76

Chapter 1

Morphogenesis of biological systems

Biological systems acquire their shape and size through an intricate process defined as "morphogenesis". It is defined as a self-organized orchestration of biochemical and physical processes that is driven by specific patterns of deformations precisely regulated over several orders of spatial and temporal scales. The emergent outcome permits the generation of tissues from individual cells and subsequently a "body plan". Several notable examples of morphogenetic events across different animal species harbored the interests of scientists across disciplines over the last centuries to investigate deeper underlying principles. The consistency and reproducibility of emergent shapes observed in morphogenesis implies that embryonic cells generate, perceive, and interpret information to coordinate their behavior. Research spanning the past century has revealed that cells can input information from the environment through interpretation of concentration of specific morphogens or sense their environment for mechanical forces and the local geometric constraints. Upon receiving a stimulus cells can trigger a specific behavior. Active research has hence further focused on deciphering key feedback mechanisms that cells utilize to communicate amongst each other to emergent behaviors.

During embryonic morphogenesis of multicellular organisms, however, there are critical changes taking place within the internal environment of the system. What starts as a fertilized zygote, through successive rounds of cell divisions builds up an internal environment that is initially driven by cell-cell interactions. However, embryos are more than just a bunch of cells. All tissues are built on a network of proteins that are secreted by the cells to its neighborhood, which is appropriately called the extra-

cellular matrix (ECM). The ECM self-organizes to form intricate networks, providing mechanical support and biochemical roles, which permits core biological functions controlling morphogenesis, differentiation and fate specification. The constituents and mechanical properties of the local ECM is also very precise spatiotemporally. The amount of ECM in dry mass is estimated to be of the same order to that of cells, and intuition supports the idea thinking of our human bodies built of both flesh and bone.

The established view of morphogenesis highly credits its coordination on the activities of the cells through their migration, changes in shape, division and death. While on the other hand the ECM is viewed just as a substrate supporting the cells, and any dynamics in the ECM that is observed gets attributed as an effect coming from the cellular activities. How much of this assumption is true? How do developing systems lacking ECM initially accommodate novel cell-matrix interactions, and how does this modulate morphogenesis across spatiotemporal scales particularly? The subsequent investigation forms the backbone of my doctoral thesis.

Over section 1, I introduce the mechanisms that were observed to drive morphogenesis across organisms. Then I introduce the ECM in section 2 and give an overview of morphogenesis across some well-studied systems, posing the duality of cells and ECM as drivers of coordinated morphogenesis. Owing to the emergent tissue complexity, there is a lack of understanding of this feedback across larger spatiotemporal scales. I thus introduce the cnidarians in section 3, particularly our favorite model organism the starlet sea anemone, *Nematostella vectensis*, to understand the biogenesis and roles of the ECM, and particularly demonstrate its importance in coordinating post-embryonic morphogenesis, where an almost spherical larva transforms into an elongated tubular polyp with tentacles. I also address an effective role of the ECM in the formation of a secondary opening in a cnidarian, the notion itself challenges the existing textbook knowledge of body plan evolution across metazoans. Together, I emphasize the role of ECM and propose its equivalency with the cellular components in the pursuit of understanding underlying morphogenetic principles.

1.1 Morphogenesis through cellular behaviors

Morphogenesis encompasses a standardized set of fundamental processes propelled by cell mechanics, collectively contributing to the diverse shapes observed in tissues and organisms. These processes include bending or invagination, generating deformations out of the tissue plane; tissue flow and extension, involving planar expansion and

rotational flows; hollowing, involving internal fluid-filled lumens form within tissues; and tissue branching (Collinet and Lecuit (2021)). Throughout these processes, cells dynamically alter their shapes, undergo division, and rearrange relative to one another. The execution of these events necessitates the application of mechanical forces, such as tension resulting from the contraction of actomyosin networks, cell–cell and cell–substrate adhesion, as well as cell protrusive forces or growth. In each instance, active forces must be intricately organized in both space and time to accurately orient and execute diverse morphogenetic processes. The coordination of mechanical elements and an intricate feedback between deterministic factors and self-organization is paramount for the proper progression of morphogenesis.

1.2 Generation of forces in biological systems

In order to change their shapes, cells require the generation of forces. At the cellular scales, these forces can be active by the hydrolysis of ATP or passive following through energy minimization principles (Rauzi and Lenne (2011)). Active mechanical forces primarily arise from the actomyosin cytoskeleton on a cellular scale and from muscles on tissue scales, while passive forces are generated mostly through stress relaxation and geometric constraints.

The actomyosin cytoskeleton, a vital component of cellular structure, consists of actin filaments cross-linked by myosin II motor protein oligomers. Actin filaments, composed of actin molecules, spontaneously polymerize in vitro with sufficient monomer concentration, exhibiting dynamic assembly and disassembly due to ATP hydrolysis. Nucleation is a crucial step in filament growth, involving the formation of actin dimers and trimers. Polarized actin filaments, with barbed and pointed ends growing at different rates, are facilitated by complexes like Arp2/3 and formin proteins. Arp2/3 forms tree-like networks, while formin initiates straight, unbranched filaments that can be bundled and cross-linked by accessory proteins, influencing cell shape and stiffness.

Organized by myosin motor proteins, actin forms contractile structures, such as those seen in muscles. Skeletal muscle fibers, formed by myocyte fusion, consist of sarcomeres with interleaved actin and myosin filaments. Rapid contraction is triggered by Ca2+ influx, facilitated by accessory proteins like tropomyosin and troponin. Smooth muscles lack troponins and contract through calmodulin-mediated myosin light chain kinase (MLCK) activation. MLCK phosphorylates myosin light chain, initiating contraction. In non-muscle cells, myosin II regulation involves phos-

phorylation by kinases like ROCK and MLCK, while RhoA GTPase activation and Ca2+-dependent MLCK activation contribute to precise actomyosin orchestration. Muscles, exclusive to animals, play key roles in locomotion, defense, feeding, and digestion, with diverse muscle systems derived from the mesoderm. This intricate interplay of cellular components underlies the efficiency and diversity of muscle function across various biological contexts, and together generate active forces across scales. Upon the activation of cell-autonomous forces and external mechanical stimulus, cells and tissues can respond by changing their shape and geometry to perform the required morphogenetic deformation.

1.3 Tissue extensions through cell intercalations

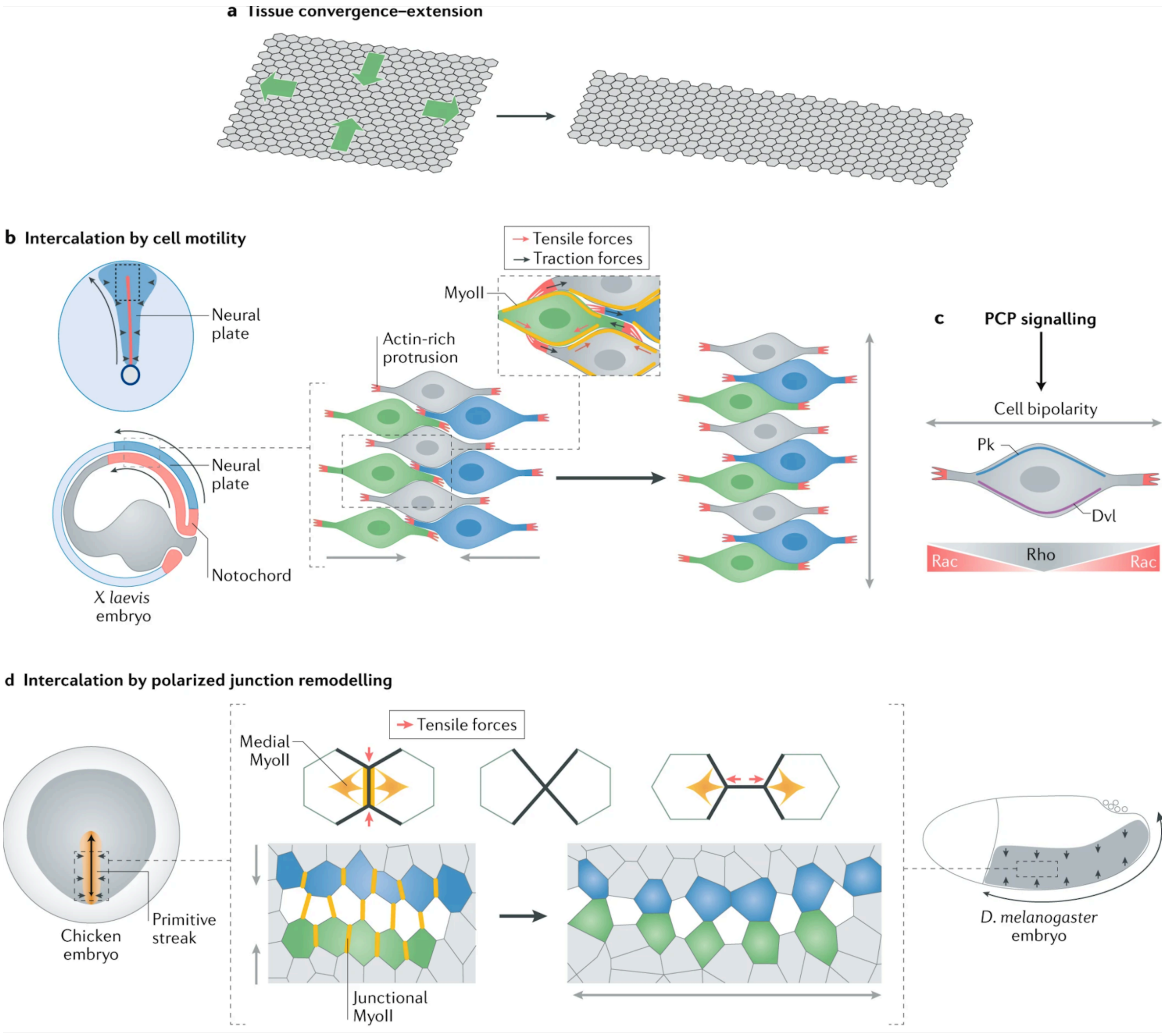

Figure 1.1. The mechanisms of cellular rearrangements driving tissue scale morphogenesis. Cell-rearrangement drive morphogenesis through tissue covergence-extensions. Rearrangements can either be driven by cell motility, or by polarized junctional remodeling. Figure compiled from Collinet and Lecuit (2021).

Cell intercalations, facilitated by convergence-extension movements, is a common driver of tissue extension. Traditionally, two distinct modes of cell intercalation have been recognized in mesenchymal and epithelial cells. However, recent evidence suggests that these modalities can coexist within the same cell population, jointly contributing to the local active forces propelling tissue flow. The first mode involves cell motility, where cells extend polarized actin-rich membrane protrusions and intercalate through movements resembling those of migrating cells. This mode is observed, for instance, in cells of the dorsal mesoderm and the overlying neural plate during gastrulation and neurulation in frog embryos, where cells extend bipolar actin-rich lamellipodia along the medio-lateral axis. In the ascidian notochord and C. elegans embryo, similar polarized membrane protrusions play a role in medio-lateral intercalation. Additionally, during the formation of the dorsal midline in C. elegans, polarized Rac-dependent membrane protrusions at the basolateral side drive the migration and intercalation of cells flanking the midline.

The second mode of cell intercalation involves polarized remodeling of cell–cell contacts through actomyosin contractions. In this mode, cells exchange neighbors while maintaining intercellular adhesion and tissue integrity. This type of intercalation was first characterized in the drosophila germband, where dorsal–ventral junctions shrink, and new antero-posterior junctions form, extending the tissue along the antero-posterior axis. Planar polarized actomyosin contractility at cell–cell junctions and in the medio-apical cortex drives junction remodeling. Similar junction remodeling by actomyosin contractions is observed in vertebrates during processes like primitive streak formation and neural tube closure in chick embryos. Both modes, involving membrane protrusion extension and junction remodeling through actomyosin contractions, complementarily generate local active forces necessary for cell intercalation.

1.4 Emergence of mechanical plasticity and fluidity in biological systems

Whenever a force is applied on a system, either internally or externally, the system reacts by reacting to it, changing its shape and size. The degree of change is termed as deformations. Deformations by default have the logic of causality built into it, where the causative agents are termed the stresses, while the effect generated on the system is termed as the strains. The balances between the active stresses and the generated strains determine the mechanical property of a system. The nature of deformations induced gives an idea of the response of the system. Upon reverting the

active stresses, if the system reverts its deformations by dissipating its strains, the behavior of the system is termed elastic, while if the system cannot dissipate its strain the response is termed plastic. Biological systems finely tune their response across a regime of elasticity to plasticity to perform morphogenesis across broadly different lengthscales and timescales. A deeper understanding of the general mechanism that a system utilizes remains still elusive. At cellular scales, the origins of plasticity are investigated, and across tissue scales, the origins and effects of emergent properties like stiffness and fluidization is investigated. The connections between these properties across scales is a highly researched topic across the physical sciences, and also in the life sciences over the recent years.

1.4.1 Origins of morphogenetic plasticity from the dynamics of actin and myosin

Drosophila gastrulation and germband extension

Time-lapse studies highlighting embryonic cell shape changes often reveal a stepwise progression of events. This characteristic feature was first documented in drosophila during germband extension, where cell intercalation, driven by asymmetric junction shortening, played a crucial role. Similar stepwise events occur in various species, indicating their evolutionary conservation. Prior research has elucidated that contraction and relaxation cycles are linked to the transient formation of cortical actomyosin foci. These foci either constrict the apical area and pull-on junctions or flow in a planar-polarized manner to dorsoventrally oriented junctions, causing their shortening (Rauzi and Lenne (2011)).

A stable actin network, dependent on the formin Frl/Fmnl, is essential for the propagation of pulsatile actomyosin forces in drosophila. Similarly, the maintenance of a sarcomeric-like actomyosin structure oriented perpendicular to the direction of tissue folding, regulated by RhoA and non-muscle myosin II, proves crucial for apical constriction. On the contrary, although microtubules are necessary to facilitate apical constriction during gastrulation, they appear dispensable in other scenarios for promoting plastic cell shape changes. Actin dynamics is thus very important for generating cellular plasticity in the early morphogenetic events of drosophila, emphasizing its sensitivity to various factors, including network architecture, crosslinking, and intricate molecular interactions.

Early morphogenesis of C. elegans embryo

While drosophila morphogenetic events typically involve large, almost flat tissues, the C. elegans embryo, during gastrulation and cell divisions, can be conceptualized as an elongating tube. Its morphogenesis follows a distinct process, incorporating repeated mechanical contractions. Following an initial elongation phase driven by non-pulsatile non-muscle myosin-II (NMY2) forces and circumferentially oriented actin bundles, muscle contractions become crucial for further elongation. Alternate contractions of muscles on each side of the embryo induce tension on dorsal and ventral epidermal cells, triggering biochemical reactions through mechanotransduction (Molnar and Labouesse (2021)).

The periodicity observed in NMY2 pulses in flies and muscle contractions in nematodes raises intriguing questions about the molecular changes accompanying permanent cell deformations. These irreversible changes are proposed to result from a ratchet process, like the unidirectional spinning of a waterwheel against the flow of a water due to asymmetry in spoke orientation. In the context of biology, a ratchet extracting order and work from random fluctuations is conceivable due to the energy consumption by biological objects, such as ATP-driven conformational changes in biological motors, and the inherent asymmetry or polarization of many biological entities. Biological plasticity entails irreversible deformations occurring stepwise, often in response to periodic force inputs like NMYII pulses or muscle contractions, which are also ATP-driven (Lardennois et al. (2019)).

In the context of the second phase of C. elegans elongation, muscle contractions play a crucial role. These contractions induce the bending of actin cables within the epidermis, leading to their severing through villin and gelsolin. The cut and slightly shortened actin cables are subsequently stabilized through a complex involving -spectrin SPC-1, the p21-activated kinase PAK-1, and the atypical formin FHOD-1. Interestingly, the partial molecular dissection of FHOD-1 suggests that its action involves bundling or capping actin filaments rather than promoting their polymerization.

Origins of morphogenetic plasticity from the changes in material properties

Changes in the dynamic material properties of tissues play a crucial role in the regulation of tissue morphogenesis within developing organisms (Lenne and Trivedi (2022)). This arises from primarily from the dynamics of cell-rearrangements, and makes the tissue pliable to morphogenesis. The initiation of zebrafish morphogenesis, partic-

ularly the spread of the blastoderm, is reliant on a rapid and pronounced spatially patterned tissue fluidization. This fluidization of the blastoderm is temporally regulated by the rounding of mitotic cells, which leads to the disassembly of cell–cell contacts during the final stages of cell cleavages (Petridou et al. (2019)). Furthermore, this fluidization process is not uniform throughout the blastoderm but is instead constrained to the central region. This spatial restriction is achieved through the localized activation of non-canonical Wnt signaling within the blastoderm margin. The activation of this signaling pathway enhances cell cohesion in the central blastoderm, thereby counteracting the effects of mitotic rounding on the disassembly of cell contacts. The modulation of fluidity through a transition mediated by the loss of cell cohesion is demonstrated to be a critical regulatory mechanism in zebrafish embryo morphogenesis. Moreover, the changes in adhesion-dependent cell connectivity among cells is directly correlated with the origins of viscosity in tissues through, establishing a link between microscopic and macroscopic properties (Petridou et al. (2021)). This linkage is characterized by a first-order phase transition and its compliance in the control of morphogenetic processes. The intricate interplay between dynamic changes in cell cohesion, tissue fluidization, and signaling pathways highlights the significance of rheological properties in governing the complex and orchestrated events of embryonic development.

The process of solidification in multicellular organisms can be interpreted as the loss of cells capacity to move and rearrange, and this phenomenon is strongly influenced by the actively driven fluctuations that cells can generate. In the case of zebrafish, the gradual solidification of cells is crucial for axis elongation. Unlike in chicks, this solidification process in zebrafish does not involve cell proliferation. Instead, mesenchymal cells originating from the mesodermal progenitor zone, located at the anterior of the animal, progressively lose their ability to rearrange as they migrate into the posterior part known as the PSM (posterior). This transition from a fluid to a solid state resembles a jamming transition, with cells becoming confined as they enter the PSM. The cells within the PSM subsequently form structures called somites, which are precursors to the animal's vertebrae.

To characterize cell-scale mechanical properties magnetically deformable oil droplets were injected into the tail of zebrafish embryos. The stress required was quantified to permanently deform the tissue and observed an increase in the posterior-to-anterior direction, indicating a more solid-like state in the posterior region and progressively solidifying towards the anterior (Mongera et al. (2018)). Additionally, the amplitude of tension fluctuations governing the transitions between solid and

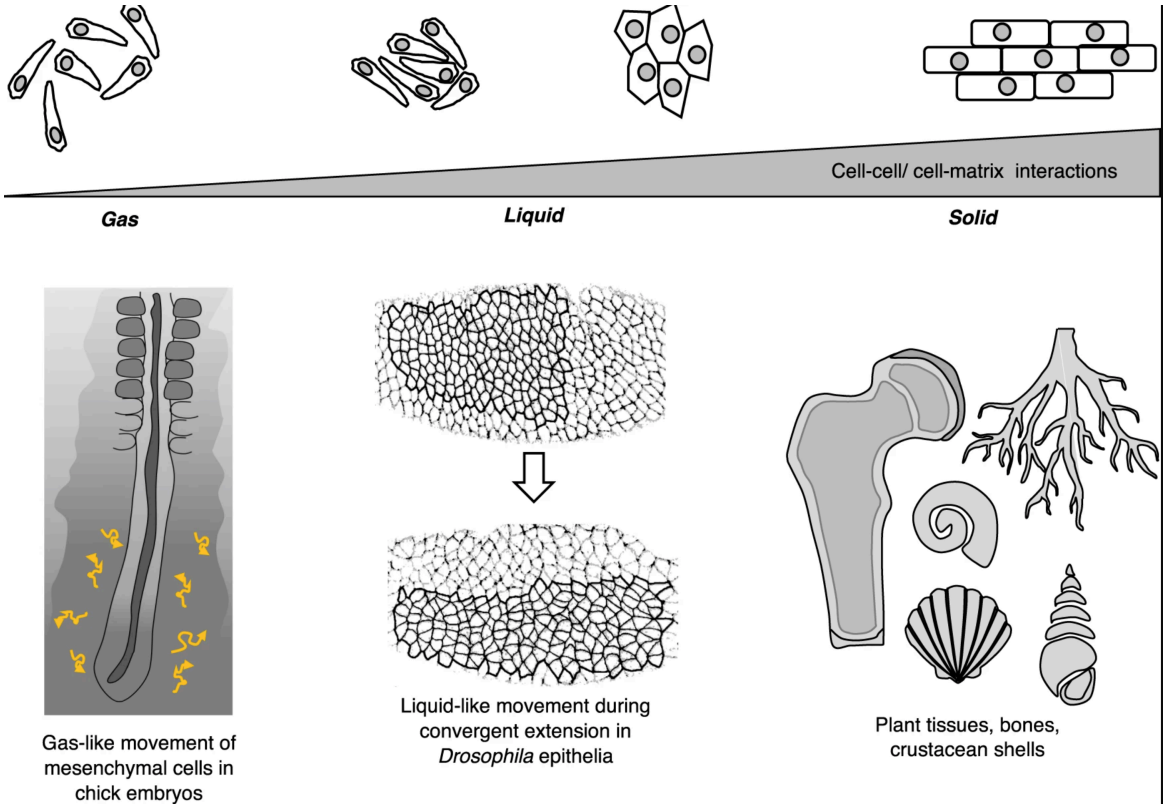

Figure 1.2. Analogy of mechanical phases in between physical and biological materials. Fluid and solid behaviors are equally important to coordinate morphogenesis in biological systems, the importance lies in the fine-tuning of the emergent mechanics. Figure compiled from Lenne and Trivedi (2022).

fluid states appears to be finely tuned to facilitate the shaping of somite boundaries. In this context, the interior of the somite exhibits solid characteristics, while the immediately adjacent tissue remains in a fluid state. These findings align with a dynamic vertex model that considers extracellular spaces and active tensions at cell–cell contacts. Above a critical value of tension fluctuations, the model predicts that the tissue behaves as a fluid. Below this critical value, the tissue can exhibit either fluid or solid behavior, depending on the developmental time. Specifically, if the time required for structure formation is larger (smaller) than the stress relaxation timescale, the tissue behaves as a fluid (solid) (Kim et al. (2021)). This dynamic interplay between cell solidification, tension fluctuations, and developmental timescales sheds light on the intricate mechanics governing tissue behavior during embryonic development.

The interplay of cell-shape changes and cell-rearrangements are precisely coordinated to generate morphogenesis, and the examples described above highlight its overarching importance. However, as mentioned earlier, the biological processes are highly dependent on context, that allows the functional use of similar modes to gen-

erate diversified functions. Cells, in an organismal context, require attachment to its surface in the maintenance of its context, where the interplay of cells and the underlying extracellular matrix becomes crucial. Most widely studied morphogenetic systems lack an environment rich with dynamical cell-ECM interactions, that hold true in the blastoderms of drosophila and zebrafish. Even when the cell-ECM interactions were considered during morphogenesis, the dynamical nature of ECM were ignored. My interests lie in the understanding of how these novel interactions are integrated during morphogenesis, and how they are maintained across larger spatiotemporal scales. In the section 2, I will introduce the ECM, and sample some evidences put forward in the efforts of establishing it as a driver for morphogenesis.

Chapter 2

The extracellular matrix

Prior to the early 1800s, the ”fibers” in connective tissue were believed to be the fundamental building blocks of life, that would arise through spontaneous generation. However, with the identification of cells within connective tissue, the cellular theory gained acceptance as the foundation of life around 1850. It was acknowledged that material outside cells, likely produced by cells, constituted the extracellular matrix (ECM). Over the last century, several components of ECM were identified and characterized through detailed physical, chemical, chemical and cell biological methods, with the focus initially emphasized to understand collagen and elastin structures, and the enthusiasm soon established a vast understanding of the structure of the acellular component that remains associated with the cellular basis of life. However, even half a century before, the ECM was considered as “the styrofoam packing material” of underlying cells and tissues and thus further investigation to understand its biological role in coordinating anything more than a supportive structure was questioned as “why anyone would want to work on that stuff” (Rozario and DeSimone (2010)).

The interests grew with the discovery of ECM receptors, particularly integrins in the mid-1980s, which led to a comprehensive mechanistic comprehension of the physical connections between the intracellular and extracellular domains, which play a role in adhesion, withstand mechanical stress, and enable the two-way transmission of cell signals (Hynes (2004)). Following this observation, the interplay between the cells and the ECM was characterized in various established morphogenetic systems. I will introduce the many components that collectively build up the ECM and some of their direct roles in the coordination of large-scale morphogenesis.

2.1 ECM composition

The ECM, having accompanied the evolution across the tree of life, is often considered to be a principal component in the emergence of multicellularity Özbek et al. (2010). The ECM consists of various molecular families originating from different evolutionary backgrounds Theocharis et al. (2016). These encompass glycosaminoglycans and proteoglycans, collagens, and non-collagenous glycoproteins. Glycosaminoglycans (GAGs) are unbranched linear polymers with repeating disaccharides containing hexosamine and uronic acid. These molecules possess notable physical properties due to the abundance of carboxyl, hydroxyl, and sulfate groups defining individual GAGs like heparan-sulfates. Except for hyaluronic acid (HA), all GAGs are covalently linked to core proteins, forming proteoglycans (PGs) like perlecan. The ECM glycoproteins encompass a diverse range, including collagens, laminins, elastins, tenascins, and fibronectin. Collagens, the most prevalent proteins in the animal kingdom, play a fundamental role in limiting tissue distensibility due to the substantial tensile strengths of collagen fibrils. The collagens have a triple-helical organization, contributing to the distinctive physical properties of these ECM proteins. Collagens are broadly categorized into fibrillar and nonfibrillar forms, capable of assembling into reticular networks and sheets. Non-collagenous glycoproteins in the ECM represent various protein families with diverse origins. Many of these ECM molecules consist of multiple chains, each encoded by distinct genes (e.g., laminin trimer or fibronectin dimer).

The organization, distribution, and density of fibrils and networks of the ECM vary depending on tissue type, its developmental and homeostatic conditions, as well as the direction and magnitude of forces exerted on a given tissue. This can be achieved due to a combination of both cellular and cell-autonomous factors, through guided localized synthesis, assembly and degradation and self-organization.

2.2 ECM regulation: synthesis, assembly and degradation

The biochemistry of ECM is dominated by its remodeling, which is finely tuned by its production, reorganization and subsequent degradation (Bonnans et al. (2014); DeSimone and Mecham (2013)). Signaling and growth factors play a central role in initiating and promoting ECM synthesis. Transforming growth factor-beta (TGF-β) and fibroblast growth factor (FGF) are among the key players that stimulate ECM production by cells. TGF-β, for instance, triggers the activation of fibroblasts, leading

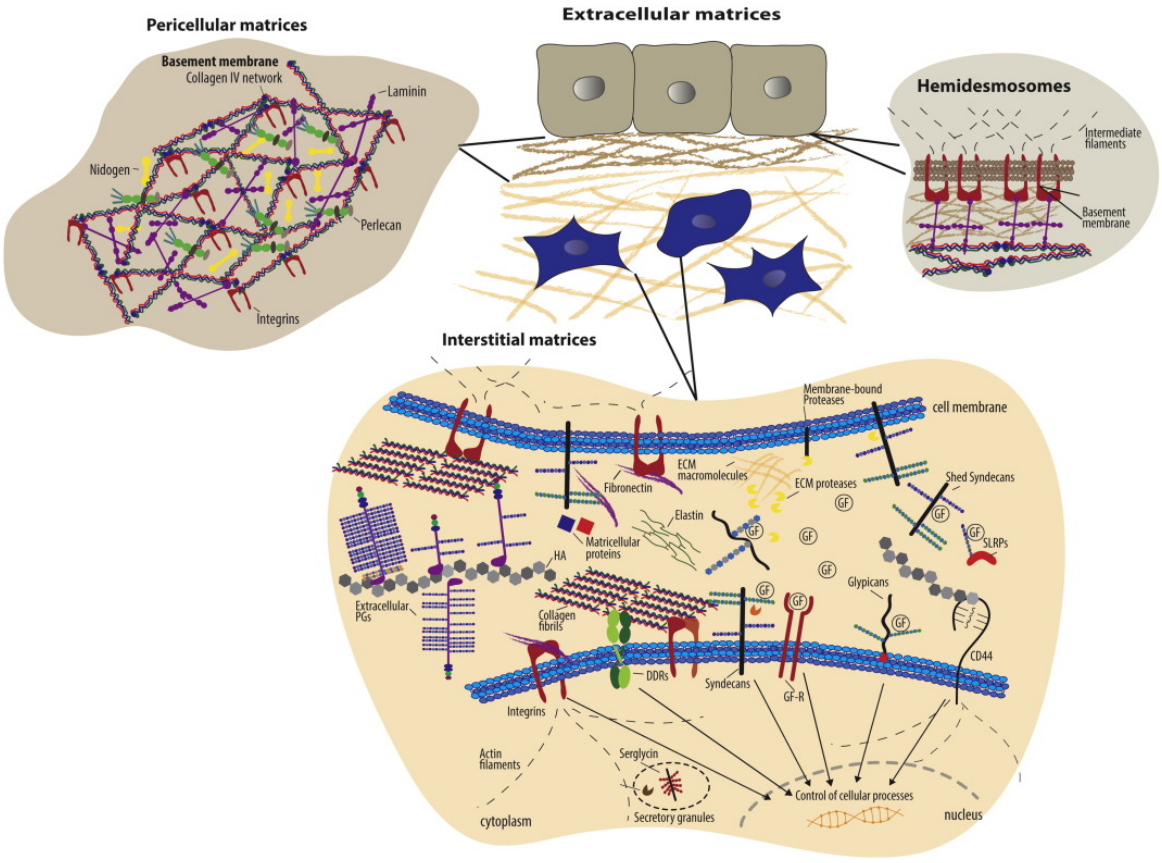

Figure 2.1. The composition of the ECM proteins. The ECM is primarily made of pericellular and interstitial matrices, connected to the cells through the hemidesmosomes. Figure compiled from Theocharis et al. (2016).

to increased collagen synthesis and deposition. FGF stimulates fibroblasts and endothelial cells, promoting ECM protein expression and angiogenesis. The interplay of these growth factors ensures a coordinated response, initiating ECM assembly during development, tissue repair, and various physiological processes. This localization in the multicellular context is determined by upstream signaling activities dictated by Wnt and PCP pathways, hinting at deeper biological cooperation between molecular signaling and ECM for the coordination of regulative morphogenesis.

A crucial process in the biology of ECM proteins is their self-assembly guided by enzymatic activation. Collagens, the predominant ECM protein, undergoes a complex process known as fibrillogenesis. Intracellularly, procollagen molecules are synthesized, modified enzymatically under the activity of prolyl-4-hydroxylases (P4HA) (Gorres and Raines (2010)) and secreted into the extracellular space. Extracellularly, enzymatic cleavage of procollagen through activity of lysyl oxidases (LOX) (Vallet and Ricard-Blum (2019)) expose fibril-forming tropocollagen units, allowing them to self-assemble into staggered fibrils. These fibrils further organize into larger fibers through

lateral association. The precise regulation of collagen assembly is crucial for tissue-specific structural integrity. Laminin assembly is orchestrated through a trimeric structure composed of α, β, γ chains. The trimer self-assembles into a cross-shaped molecule that further polymerizes to form networks. Fibronectin assembly involves a stepwise process. Initially, fibronectin monomers are secreted into the ECM, and a series of self-association events lead to the formation of a soluble dimer. Integrins, cell surface receptors, bind to specific sites on fibronectin, initiating the conversion of the dimer into insoluble fibrils. These fibrils act as adhesive bridges, linking cells to the ECM and facilitating cellular processes. Elastin imparts elasticity to tissues, allowing them to stretch and recoil. Elastin assembly involves a unique process. Precursor molecules, tropoelastins, are secreted into the ECM and crosslinked by enzymes like lysyl oxidase. These crosslinked tropoelastins form insoluble aggregates, which undergo further alignment and association to create elastic fibers.

Every ECM protein requires extensive modifications prior to assembly into an existing network. At the transcriptional level, intricate regulatory networks control the expression of ECM genes. Specific transcription factors, such as Sp1, AP-1, and Smad proteins, bind to promoter regions of ECM genes, initiating or suppressing their transcription. TGF-β, a potent regulator of ECM assembly, activates Smad-dependent signaling pathways, leading to increased expression of collagen and other ECM components. The interplay between these transcription factors ensures precise temporal and spatial control over ECM gene expression during biological processes.

The ECM components are also modulated through enzymatic degradation (Parks and Mecham (2011)). Matrix metalloproteinases (MMPs) and tissue inhibitors of metalloproteinases (TIMPs) constitute a dynamic regulatory mechanism controlling ECM turnover and remodeling. MMPs are zinc-dependent endopeptidases that cleave ECM proteins, facilitating their degradation and turnover. TIMPs, on the other hand, inhibit MMP activity, acting as guardians of ECM integrity. The balance between MMPs and TIMPs is crucial for maintaining the equilibrium between ECM synthesis and degradation. Dysregulation of this balance is implicated in various developmental and pathological conditions.

2.3 Towards the regulation of morphogenesis

Although the structures of ECM proteins and the genetic relationships among encoding genes exhibit wide variability, many share similar functions and common structural motifs. One notable example is the adhesive Arg-Gly-Asp (RGD) sequence located

within a hydrophilic loop of fibronectin, vitronectin, tenascin, and other ECM proteins. RGD sequences are crucial for recognition and binding to various components. Collectively, these distinct ECM molecule groups contribute to extensive functional complexity. The architecture and assembly of ECM in embryonic interstitial spaces may offer the necessary structural integrity to facilitate and, in certain instances, limit cell movements, control the diffusion of morphogens, and provide binding sites for various families of cell surface receptors, including integrins and syndecans. Integrins serve as bridges between cells and the ECM, transmitting signals bidirectionally. Integrins recognize specific ECM proteins, initiating cellular responses that influence ECM synthesis, organization, and remodeling. The activation of intracellular signaling pathways, such as the focal adhesion kinase (FAK) pathway, regulates cellular activities like adhesion, migration, and differentiation, consequently impacting ECM assembly.

The entire ECM architecture can be broadly subdivided into two layers, the interstitial matrix (IM) and the basement membrane (BM). The interstitial matrix forms the bulk of the ECM in tissues. It comprises a diverse array of proteins with fibrillar collagen, particularly types I, II, III, V, XI, XXIV and XXVII (Bella and Hulmes (2017)) being the predominant component. Collagen fibers provide tensile strength and resilience, creating a three-dimensional network that supports cells within the tissue. Other interstitial matrix proteins include elastin, fibronectin, and proteoglycans, each contributing to the unique biomechanical properties of the tissue. The interstitial matrix serves several crucial functions. The dynamic nature of the interstitial matrix allows cells to remodel their microenvironment in response to developmental cues, injury, or physiological demands.

The BM is a specialized ECM structure that underlies epithelial and endothelial tissues, providing a supportive and segregating interface Jayadev and Sherwood (2017). It forms thin dense sheets consisting mainly of laminin, collagen IV, nidogen, and perlecan. Laminin, a glycoprotein, forms a branching network, while collagen IV provides structural stability. Nidogen and perlecan contribute to the linkage and organization of these components. The BM serves as a critical mediator between epithelial or endothelial cells and underlying connective tissues. It provides a physical barrier that separates different tissue compartments and regulates the passage of molecules. Since the BM lies adjacent to the tissue, it has a more imminent role in providing a direct feedback with the immediate tissue architecture (Töpfer (2023)).

The unique physical and hydrodynamic properties of these matrices also in-

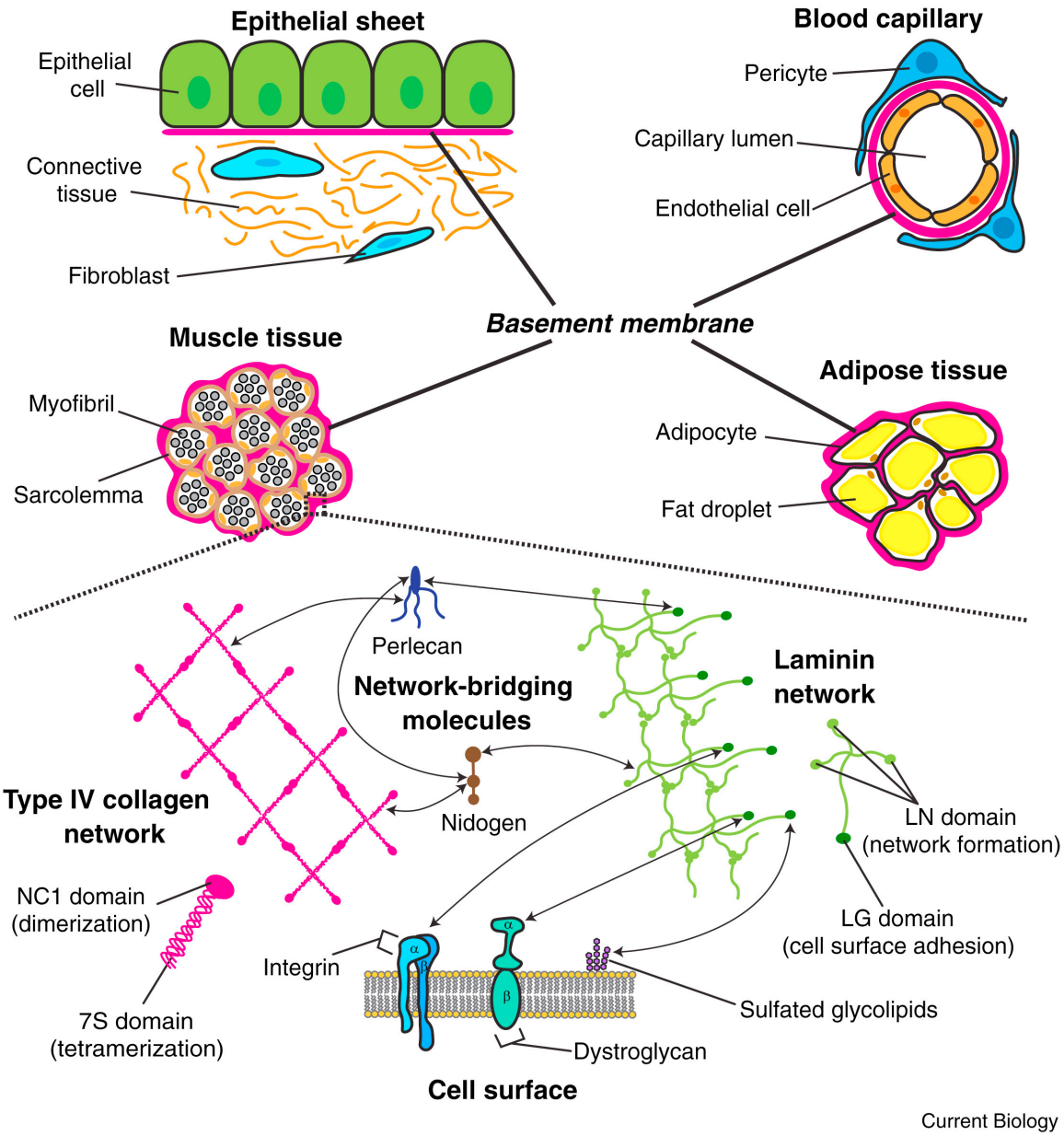

Figure 2.2. Overview of the BM architecture. BM architecture is primarily built with collagen IV and laminin networks, connected by perlecans, nidogens. Figure compiled from Jayadev and Sherwood (2017).

fluence morphogenetic cell behaviors and regulate the diffusion of various secreted growth factors and morphogens. Collagen fibers resist tensile forces, elastin imparts elasticity, and fibronectin facilitates cell adhesion and migration within the tissue. PGs, with their hydrated GAG chains, contribute to tissue compressibility and resistance to compression forces. Hence, a combination of the localized ECM components can be viewed as a morphogenetic language or code interpreted by cells upon contact, imparting a mechanochemical feedback, leading to a regulative role of ECM in the coordination of morphogenesis at an almost equal footing to traditional cellular

drivers. This ”sensing” of embedded information in the ECM by specialized receptors on the cell surface can significantly influence cell behaviors, impacting not only adhesive functions but also cell polarity, migration, and other intracellular signals governing survival, proliferation, and differentiation. Short- and long-range physical forces resulting from morphogenetic movements can additionally modify the availability of cell-interactive and other functional domains within the matrix, regulating response to the extracellular environment.

2.4 The coupling of ECM and morphogenesis

I particularly focus on the roles of specifically collagen IV in the BM, and its possible roles in the coordination of morphogenesis. The emergence of collagen IV networks is highly accredited to the evolution of multicellularity in evolution (Fidler et al. (2017)), hinting at the coordination of epithelial morphogenesis. This has been pursued in many morphogenetic events spanning various model systems. Over the next few sections, I introduce a few different morphogenetic systems, starting with the growing larval wing disc, the egg chamber and the condensation of the central nervous system of the fruitfly drosophila. All these examples exhibit how collagen IV is the dominant driver of morphogenesis across tissue scales in the same organism, which were previously accredited to cellular mechanisms only, and are their mechanisms are extremely context-dependent. I also discuss the role of the BM in coordinating the onset of gastrulation in mouse embryos, exhibiting the dominant role of the ECM across organismal scales. Lastly, I also introduce two additional systems, the embryonic growth of metacarpal bone in chick and the semicircular canal morphogenesis in zebrafish, emphasizing the role of interstitial matrices on morphogenesis, in search of principles that guide the coupling between growing tissues and the ECM on my pursuit to the understanding of the roles of ECM in the organismal morphogenesis of *Nematostella*.

2.4.1 The growing larval wing disc of drosophila is directed by differences in the production of collagen IV and tissue proliferation

The maturation of the larval wing disc of drosophila involves the intricate interplay of two continuous layers of epithelial cells, namely the squamous peripodial epithelium (PPE) at the top, and the pseudostratified disc proper epithelium (DPE) at the bottom. Enveloping both epithelial layers is a continuous BM. In the later stages

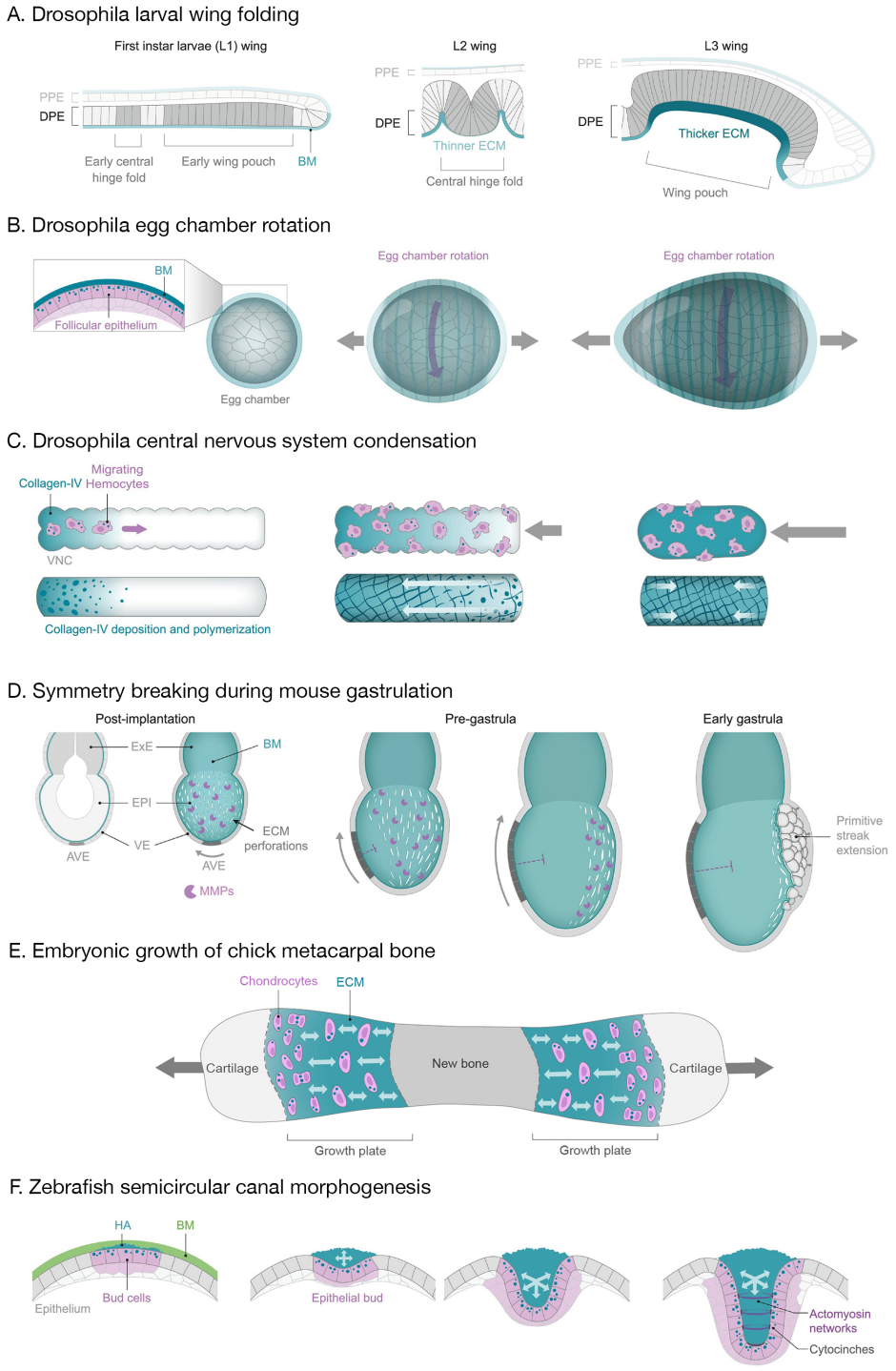

Figure 2.3. Examples of ECM dominating morphogenesis across tissues. Figure compiled from Díaz-de-la Loza and Stramer (2024).

of larval development within the pouch region, a remarkable morphological transformation occurs as the DPE layer bends concavely in relation to the PPE, forming a distinctive dome-like tissue structure (Harmansa et al. (2023)).

Traditionally, explanations for the development of folds within an epithelium have focused on cell-autonomous processes. However, these mechanisms fail to account for the formation of large domes spanning hundreds of cells. While one hypothetical explanation considered was the possibility of differential growth between the PPE and DPE layers, empirical analyses and computational modeling have discredited this notion. Instead, examination of fluorescently-tagged collagen IV revealed a specific increase in thickness in the BM beneath the DPE in the wing disc pouch. Backed by mathematical analysis, it was subsequently proposed that the bending results from a disparity in the production of the ECM and the proliferation of the DPE. Although the force driving the bending originates from the expansion of the epithelial cell layer, it is the spatiotemporally regulated growth of the underlying BM that propels the alteration in tissue shape. Therefore, the central question shifts from mechanisms governing cellular behavior to the control of local ECM dynamics.

The unique growth pattern of the BM underlying the DPE, compared to other regions of the wing and the PPE, presents intriguing questions. Most BM components in the wing disc are believed to originate from a distant source, the larval fat body, which secretes BM components into the hemolymph. This prompts consideration of various non-mutually exclusive possibilities driving the specific growth of the DPE's basement, including integrin receptor activity, reduced local matrix turnover, or increased local BM component crosslinking. Unlike a localized increase in ECM production, these mechanisms seem more plausible in explaining the localized alterations in the BM.

The importance of localized BM alterations extends beyond the wing disc pouch region, as evidenced by a distinct morphogenetic process occurring slightly earlier in larval development in the wing notum and hinge. The formation of creases in these regions involves a reduction in collagen IV within the BM, resulting in increased basal cell area and a decrease in cell membrane tension. Local expression of a matrix metalloprotease (MMP) was found to induce BM degradation, reducing basal tension and generating creases. This suggests a link between BM integrity, tension, and the morphological changes observed.

To understand these bending phenomena, it becomes crucial to explore how the BM is locally disrupted and why BM depletion leads to reduced basal cell tension.

Potential explanations include the role of integrin adhesion in the force generation of the epithelial actomyosin network within the basal region associated with the BM, or the possibility that the BM itself maintains autonomous tension due to intrinsic ECM stress, released upon BM degradation. Insights from previous examinations of BM components and recent preprints suggest that the BM may serve as a long-term store of elastic stresses, contributing to the control of fold formation in the wing disc. These findings align with broader studies indicating that strain mismatches between adjacent tissue layers can result in various mechanical instabilities, such as wrinkles, bends, or folds, depending on the specific nature of the mechanical imbalance. The complex orchestration of ECM dynamics and cell behaviors is thus central to understanding the morphogenesis of the fly's wing disc.

2.4.2 The growing egg chamber of drosophila is shaped by a corset of basement membrane

The drosophila egg chamber comprises 15 nurse cells and one oocyte encircled by a simple epithelium. The egg chamber undergoes a gradual size increase and concurrent morphological transformation from a circular to an elliptical form. This alteration in shape is attributed to an anisotropic expansion toward the anterior and posterior poles, induced by the expanded volume of nurse cells and the oocyte within the chamber. Despite presuming isotropic growth in these cells, the mechanism through which the chamber transitions from circular to elliptical geometry precisely was not completely understood. From the point of view of the cells, the actomyosin network of follicular epithelial cells contributes to the elongation process (Qin et al. (2017)), however, a crucial factor propelling anisotropic growth is the surrounding BM enveloping the egg chamber (Haigo and Bilder (2011)). Simultaneous with the egg chamber's expansion, follicular epithelial cells collectively migrate using the BM as a substrate, depositing fibrils oriented perpendicularly to the antero-posterior axis. Furthermore, spatial variations in the fibrillar properties, characterized by their mechanical anisotropy, are observed across the egg chamber, with the BM at the poles exhibiting greater softness compared the center (Crest et al. (2017); Töpfer et al. (2022)). Consequently, the BM functions as a corset, directing egg expansion towards the poles and resulting in an elliptically shaped egg chamber.

Subsequent investigation revealed that achieving the correct organ shape does not necessitate alterations in the cell shape or the occurrence of oriented cell division. Rather, a significant factor in shaping the organ involves the reorientation of elongated cells specifically at the anterior region of the follicle. This polarized reorientation

is meticulously regulated by mechanical signals originating from the patterned BM. These mechanical cues are effectively transduced by the Src tyrosine kinase, leading to modifications in the trafficking of junctional E-cadherin (Chen et al. (2019)).

The molecular mechanisms responsible for mechanical anisotropy of the BM around the developing egg chamber still remain unknown. Although an increase in collagen IV levels is noted within the BM at the chambers center compared to the polar regions, this does not appear to be linked to local differences in collagen transcription. Several potential mechanisms, including anisotropic ECM deposition, component turnover, or crosslinking, could account for this gradient in BM mechanical properties. Recent research also suggests that the mechanics of the developing BM are under intricate spatial control: polar cells, specialized cells at the egg chamber's poles, sense local and distant BM properties to precisely modify the ECM's structure and mechanics (Ku et al. (2023)). This feedback between cells and ECM likely enables fine-tuning of the morphogenetic process.

2.4.3 Condensation of the ventral nerve cord of drosophila is driven by temporal induction of collagen IV

The ventral nerve cord (VNC) in drosophila is an elongated tubular structure connected to the brain, housing a central bundle of axons enveloped by glial cells and a BM that encases the entire tissue. During embryonic development, a significant reduction in the length of the VNC occurs, progressing from the posterior to the anterior direction. Although it is established that this process involves ECM producing cells, specifically hemocytes, and BM components like collagen IV and laminin, the precise role of ECM in this morphogenic event has been unclear (Borchiellini et al. (1996); Matsubayashi et al. (2017); Olofsson and Page (2005); Sanchez-Sanchez et al. (2017)).

Recent investigations challenge the conventional understanding, revealing that the activity of cells within the VNC, including glia and neurons, is not crucial for initiating VNC morphogenesis. Inhibiting cellular functions, such as using dominant negative GTPases, myosin inhibition, or even eliminating surrounding cells, has minimal impact on the initial stages of the process (Karkali et al. (2022); Serna-Morales et al. (2023)). In stark contrast, disruption of ECM components, particularly collagen IV, or hindering the distribution of these components within the embryo results in severe morphogenetic defects in the VNC from the outset (Serna-Morales et al. (2023)).

Live imaging techniques have unveiled that, preceding VNC morphogenesis, the embryo contains minimal collagen IV. Concurrent with the initiation of VNC condensation, there is an exponential increase in the expression and assembly of collagen IV around the tissue. Mathematical modeling proposes that the morphodynamics of this process can be elucidated by a sudden anisotropic increase in surface tension, which was experimentally validated through atomic force microscopy during collagen IV induction. Timelapse imaging of glial cells and collagen IV dynamics during the initial assembly of the BM displayed a viscous flow of ECM on the tissue surface, characterized as convective, akin to the coherent ECM motion. Importantly, this convective ECM motion was found to be independent of glial remodeling and hypothesized to be propelled by anisotropic stresses resulting from a transient gradient of collagen IV deposition on the tissue surface. Moreover, subtle disruptions in collagen IV polymerization, achieved through dominant negative mutant collagen IV transgenes, proved sufficient to alter the overall rate of VNC morphogenesis. This underscores the significance of de novo ECM network production in generating forces and convective movements that actively shape developing tissues.

The convective motion of ECM has already been reported underlying tissue flow in chick embryos and hydra, the exact mechanisms, however, are still unclear. The assembly of polymer networks inherently generates stresses, and this study strongly suggests that the formation of an ECM network contributes significantly to the mechanical forces driving tissue development.

2.4.4 Onset of gastrulation in mouse embryos is coordinated by patterned degradation of the basement membrane

In the initial stages of mouse embryo development, a structured egg cylinder comprises the internal epiblast and outer visceral endoderm, delineated by a BM. During the pre-gastrulation phase, these embryos undergo an initial asymmetric expansion along the proximo-distal axis. Subsequently, on the posterior side of the embryo gastrulation unfolds, wherein the primitive streak, a localized thickening of ectoderm cells, extends distally. Recent research emphasizes the significant role played by anisotropic BM alterations in orchestrating these developmental processes (Kyprianou et al. (2020)). Within the egg cylinder, spatially oriented perforations in the BM are induced by MMPs and initially surround the epiblast. The elliptical shape of these BM holes aligns with the growth axis of the embryo. This alignment is proposed to result from the predominant direction of embryo growth along the proximo-distal axis, generating anisotropic stresses that weaken the BM. Intriguingly, experiments involving

enzymatic removal of the BM using collagenase led to alterations in the growth axis, resulting in rounder embryos. This suggests that mechanical asymmetries within the BM network might actively contribute to asymmetric embryo growth.

In subsequent stages of development, the perforations become directed toward the posterior side of the embryo due to the inhibition of MMPs induced by Nodal signaling in the anterior region. MMP-induced BM perforation, coupled with tension associated with tissue growth, weakens the BM on the posterior side. This, in turn, is believed to support the anterior extension of the primitive streak and facilitate the process of gastrulation. While some upstream signals triggering asymmetric BM dissolution in pre-gastrulation stage embryos are known like Nodal, there is speculation regarding potential feedback mechanisms akin to those observed in the fly egg chamber. These putative mechanisms could enable the developing embryo to finely regulate BM properties, as excessive or insufficient degradation would likely have detrimental consequences.

Similar to previous examples in developmental biology, where forces driving asymmetric embryo expansion and branching morphogenesis are attributed to the internal pressure exerted by growing cells, it becomes apparent that the patterned, localized alterations in the ECM play a pivotal role in inducing anisotropic changes in tissue shape. This intricate interplay between cellular dynamics and ECM remodeling underscores the complexity of embryonic development and highlights the importance of understanding the regulatory mechanisms governing these processes.

2.4.5 Embryonic growth of metacarpal bone in chick reveals a dominant convective flow of ECM driving cells

The elongation of long bones primarily occurs at the growth plate, a cartilaginous structure that progressively expands along a proximo-distal axis before undergoing ossification. Chondrocytes, embedded within the developing growth plate cartilage, play a pivotal role by depositing an interstitial ECM into the intercellular space. Live imaging of the developing embryonic chick growth plate, where chondrocytes were retrovirally tagged with GFP, enabled the characterization of the dynamics of growth plate expansion (Li et al. (2015)). Contrary to previous proposals suggesting convergent-extension-driven cellular rearrangements, the live imaging results demonstrated that all cellular displacements occurred along a proximo-distal axis. Furthermore, the rate and orientation of chondrocyte cell divisions did not account for the observed homogeneous cellular displacements. Quantifying the increase in cell volume

revealed anisotropic expansion of chondrocytes, aligning with the direction of growth plate elongation. This suggested that asymmetric cellular growth played a role, but the complete explanation required further investigation. Notably, the increase in the volume of the surrounding ECM was more than double that of the cells, indicating that the expansion of the growth plate is predominantly driven by the asymmetric production and deposition of matrix.

However, the mechanism behind the anisotropic expansion of the cartilaginous ECM remained unclear. Since chondrocytes are entirely embedded in the ECM, assembling the matrix network predominantly along a proximo-distal axis implies the need for specialized mechanisms. Previous studies have highlighted polarized secretory mechanisms controlling ECM deposition in other systems. For instance, in the drosophila egg chamber, follicular epithelial cells deposit BM components basally through Rab-mediated trafficking, crucial for proper tissue morphogenesis (Isabella and Horne-Badovinac (2016)). Interestingly, there is involvement of planar polarity signals in chondrocyte organization (Gao et al. (2011)), leading to speculation that a similar directional bias in ECM assembly within the growth plate might be influenced by these signals. The underlying molecular mechanisms orchestrating the directional bias in ECM assembly remain a subject of further exploration. The potential involvement of planar polarity signals and lessons from other systems with polarized secretory mechanisms add layers of complexity to the understanding of growth plate dynamics.

2.4.6 Semicircular canal morphogenesis in zebrafish is driven by hydraulic pressure of hyaluronon

The semicircular canals within the inner ear emerge through invaginations of the otic epithelium, ultimately fusing to establish the intricate canal architecture. A recent study in zebrafish (munjal2021extracellular) challenged existing explanations for initial bud formation, ruling out factors such as localized epithelial proliferation, epithelial buckling, or cellular rearrangements. Instead, their findings highlighted a crucial role for the ECM.

Investigations into hyaluronan synthesis enzymes during bud formation revealed that these enzymes are locally produced by the bud cells, leading to the creation of a dense hyaluronic acid (HA)-rich ECM network within the bud. This unique HA-rich matrix induces osmotic swelling of the ECM, causing the developing bud to expand. The zebrafish otic bud expands in an anisotropic manner, challenging a sim-

plistic explanation based solely on osmotic pressure, which would result in isotropic bud expansion.

The anisotropy observed in the zebrafish otic bud is attributed to a remarkable mechanism involving cells circumferentially extending protrusive membrane tethers, referred to as 'cytocinches,' around the bud. These cytocinches act as constraints, counteracting isotropic osmotic pressure and leading to oriented bud extension. This dynamic highlights a role reversal in cell/ECM interactions compared to other morphogenetic processes, such as the anisotropic growth of the fly egg chamber. In the case of the egg chamber, isotropic pressure from cellular growth within the chamber is sculpted by an anisotropic ECM Crest et al. (2017)). Conversely, the asymmetric expansion of the otic bud is driven by isotropic osmotic swelling of the ECM, subsequently shaped by protrusive structures originating from the epithelial cells.

A recent preprint further suggests that HA-driven swelling of the ECM may be a widespread phenomenon during morphogenesis. For instance, in the developing chick presomitic mesoderm, coupled with tissue confinement, HA production is hypothesized to generate pushing forces that contribute to the posterior elongation of the embryo (michaut2022activity). This expanding body of research emphasizes the multifaceted and context-dependent roles played by the ECM in orchestrating diverse morphogenetic processes during embryonic development.

With the examples described, we can appreciate the feedback between the ECM and morphogenesis, and in particular the role of collagen IV in its coordination. Importantly, all of these morphogenetic processes underscore the critical importance of understanding ECM dynamics. We summarized that this feedback is initiated through the spatiotemporal control of ECM composition, where the finely tuned dynamics of ECM from both ends through synthesis and degradation plays a key role in the underlying downstream morphogenetic mechanisms. Adding to the dynamics, an interesting event of convective flow of ECM across morphogenetic systems asks deeper questions in the decoupling of cellular and cell-autonomous drivers. Another key mechanism is the emergent mechanical constraints, like the cytocinches in zebrafish inner ear and the ECM corset in the drosophila egg chamber, against expansion forces. Most often, the stresses generated are isotropic, while the constraints mechanically guide anisotropic strains that break the symmetry of the system, driving morphogenesis. The investigation, however, is focused on either early embryonic development or at the scale of organs. Over developmental time, with the maturation of the underlying ECM, it is important to understand how this feedback is continuously maintained,

across larger spatiotemporal scales. This becomes tricky to investigate, owing to the increase in tissue complexities across bilaterian model systems. I hence introduce the cnidarians in the following section.

Chapter 3

Cnidarians, extracellular matrix and morphogenesis

Cnidarians, a diverse group primarily inhabiting marine environments, includes corals, sea anemones, hydroids and jellyfishes. The two main subdivisions within this phylum are anthozoans, including sea anemones and corals, and medusozoans, comprising jellyfish and hydroids. Anthozoans predominantly adopt a sessile lifestyle, forming polyps, while medusozoans typically undergo both polyp and free-swimming medusa stages in their life cycle. These organisms are diploblastic, originating from two germ layers, namely ectoderm and endoderm, and they all exhibit a single opening that serves as a gateway for the animals to interact with the environment. A distinctive feature of this phylum is the presence of specialized stinging cells, called cnidocytes or nematocytes, employed for both capturing prey and defense mechanisms. The phylogenetic proximity of cnidarians as the sister group to bilaterians renders them invaluable for investigating the evolutionary aspects of bilaterians. However, beyond evolutionary studies, cnidarians serve as essential subjects for research in diverse fields such as ecology, regeneration, and morphogenesis, as evidenced by various scientific studies (Fritz et al. (2013); Ikmi et al. (2020); Martindale et al. (2004); Pukhlyakova et al. (2019); Stokkermans et al. (2022)). Their unique biological characteristics make cnidarians valuable models for advancing our understanding across a spectrum of scientific disciplines.

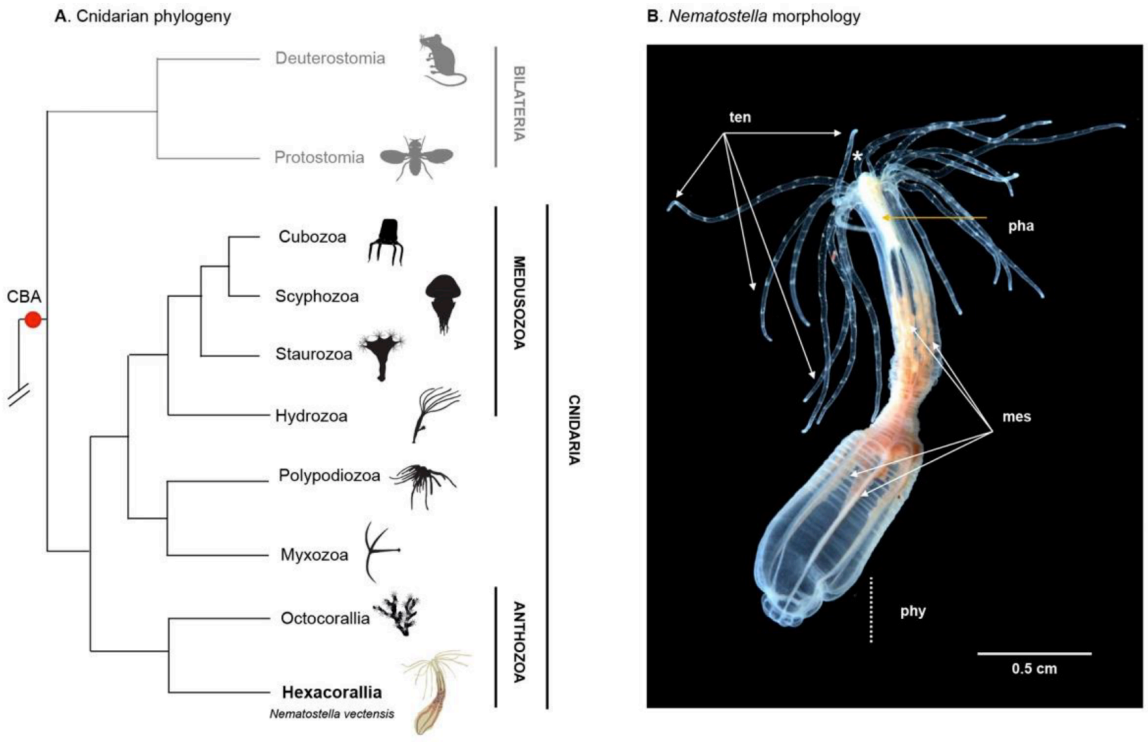

Figure 3.1. Phylogenetic position of *Nematostella vectensis*. (Left) *Nematostella* belong to the cnidarians, the sister group of bilaterians. *Nematostella* is characterized by two germ layers, ectoderm and endoderm sandwiching a layer of ECM, called the mesoglea. (Right) Body plan of an adult *Nematostella* consists of a body column and tentacles around the oral pole.

3.1 Life cycle in cnidarians

The life cycle of cnidarians unfolds through a series of distinct phenotypic stages. Initially, gastrulation gives rise to two-layered planula larvae, which, after a free-swimming phase, settle and undergo metamorphosis to transform into benthic polyps equipped with oral tentacles. This polyp stage represents the final form in anthozoans, while medusozoan species of the Scyphozoa and Cubuzoa classes develop into another sexually mature form, the medusa or jellyfish, through asexual propagation by the benthic polyp. In Hydrozoa, the medusa stage is absent, but polyps exhibit both sexual and asexual reproduction, particularly through lateral budding. The triggers for metamorphosis vary among cnidarian species but typically involve external stimuli.

In the case of *Nematostella vectensis*, the life cycle consists of a sexual phase where the males and the females produce gametes to the external environment. There also exist an asexual reproductive cycle, where the animals can propagate by binary fission.

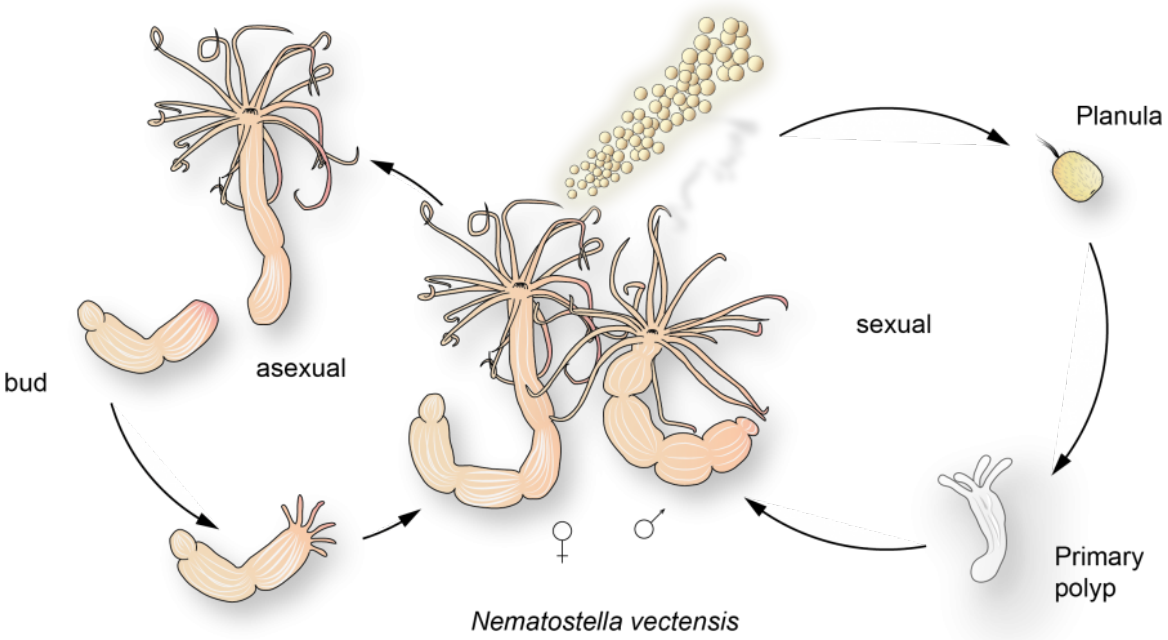

Figure 3.2. Life cycle of *Nematostella vectensis*. *Nematostella* has two distinct reproductive cycle, either through asexual budding or through sexual cycle. I have focussed on the the transition between the swimming planula to primary polyp. Figure compiled from https://thenode.biologists.com/a-day-in-the-life-of-a-cnidarian-lab/lablife/.

3.2 ECM in cnidarians

Cnidarians can be ideal model systems to investigate the ECM due to their simplified geometry. The ECM, referred to as the mesoglea, remains sandwiched between their two germ layers. Importantly, the mesoglea can be mostly or entirely cell-free, facilitating the extraction of pure ECM material in substantial quantities for downstream molecular survey (Tucker, Richard. et al. (2011)). The hydrozoan freshwater polyp Hydra and the anthozoan starlet sea anemone *Nematostella vectensis* are the most studied cnidarian model systems. Extensive morphological and molecular analyses of various aspects of ECM biology have been conducted in both species (Sarras et al. (1994); Zhang et al. (2002); Özbek et al. (2010)).

In Hydra, the mesoglea has been molecularly investigated for many years, with individual components identified through biochemistry, cloning, and bioinformatic analysis. Despite using mass spectrometry to analyze isolated, cell-free Hydra mesoglea samples, the molecular composition revealed an unexpectedly low number

of ECM proteins compared to other animals, suggesting a small repertoire of ECM proteins .

The accessibility of the mesoglea has enabled researchers to address functional questions that would be challenging to answer in more complex animals. For instance, studies have explored the connection between cell migration and mesoglea dynamics, as well as the interdependence of Wnt signaling with mesoglea composition and physical properties. MMPs also play a crucial role in Hydra's developmental processes, including foot epithelia differentiation, foot regeneration, ECM turnover, and Wnt cleavage.

In the starlet sea anemone *Nematostella*, the structure of the mesoglea during development has been investigated, revealing variations in thickness and morphology depending on the body region. However, the earliest timepoint is way beyond its embryonic developmental stages, and its biogenesis is poorly understood. Despite the simplicity of their basic body structure, cnidarians exhibit striking parallels between the mesoglea and the complex ECM of vertebrates. Comparative genetic analyses have revealed that cnidarians possess all fundamental components of an animal ECM, including structural proteins like collagens, cell-matrix adhesion factors like laminins, and ECM remodeling factors like MMPs. Throughout evolution, the core ECM proteins has undergone expansions, modifications, and losses in different animal lineages (Tucker and Adams (2014)). Even in seemingly simple cnidarians, the ECM plays a pivotal role in crucial processes, highlighting its far-reaching implications for understanding ECM protein functions across the entire animal kingdom.

3.3 Advantages of *Nematostella* as a model system

As mentioned earlier, the starlet sea anemone *Nematostella vectensis* has some advantages that could be leveraged to focus on the interaction of ECM with morphogenesis. As a model organism itself, it has some remarkable highlights. It is very easy to maintain them in a lab throughout their entire life cycle. The genome has been sequenced, and advanced molecular editing is accessible using TALENs, CRISPR/Cas9, mRNA overexpression, morpholino and shRNA mediated knockdowns through microinjections (He et al. (2018); Ikmi et al. (2014); Paix et al. (2023)). Even though they are evolutionary distant from the established bilaterian model organisms, key molecular regulators and pathways are preserved, allowing addressing interesting biological questions that are inaccessible otherwise due to tissue complexity. The entire embryogenesis takes place outside of an enclosed environment, and the developmental

states are relatively translucent, allowing access to imaging, fixed in toto as well as live in certain contexts. Visualization of proteins and mRNA of interest is accessible through immunostaining and in situ hybridization.

3.4 Morphogenesis of *Nematostella*

As a cnidarian, the anatomy of *Nematostella* consists of the two germ layers of ectoderm and endoderm, which sandwiches the mesoglea. Initially, the fertilized eggs create a hollow blastula after repeated rounds of cell divisions and compactification. The blastula gastrulates via invagination, defining the germ layers and the future oral pole is defined at the blastopore lip. Post gastrulation, the embryo transforms into a larva and starts to swim around to explore its niche, before finally settling down and subsequent morphogenesis into a polyp with 4 tentacles. The primary body axis is patterned by patterned domains of Wnt ligands, while BMP patterns a secondary axis (Layden et al. (2016)).

Post-embryonically, *Nematostella* starts to develop its muscular system, which comprises both longitudinal and circular muscles, each characterized by distinct morphology, localization, and gene expression patterns (Jahnel et al. (2014); Sebé-Pedrós et al. (2018)). In the body column, longitudinal muscles are situated within the mesenteries and can be further categorized into parietal muscles, found towards the distal part of the mesenteries, and retractor muscles, located more proximally (Jahnel et al. (2014)). Circular muscles run perpendicular to the longitudinal muscles, bridging the spaces between different mesenteries. Both types of muscles in the body column consist of myoepithelial cells (Jahnel et al. (2014)).

As *Nematostella* develops into a juvenile polyp, parietal and retractor muscles become folded, maintaining connections to the epithelium through thin cytoplasmic bridges. In contrast, circular muscle cells retain a shorter and wider connection between basal myofilaments and the apical epithelial component (Jahnel et al. (2014)). Together, these longitudinal and circular muscles enable contractions, leading to peristaltic movements.

Similar to other sea anemones, tubular-shaped body column forms a hydrostatic skeleton supported by internal fluid pressure. Muscle contractions regulate the shape of the body column by modulating its diameter and length. Circular muscles control the diameter, and longitudinal muscles alter the length of the body column (Jahnel et al., 2014). Muscle contractions fall into two types: isotonic, changing

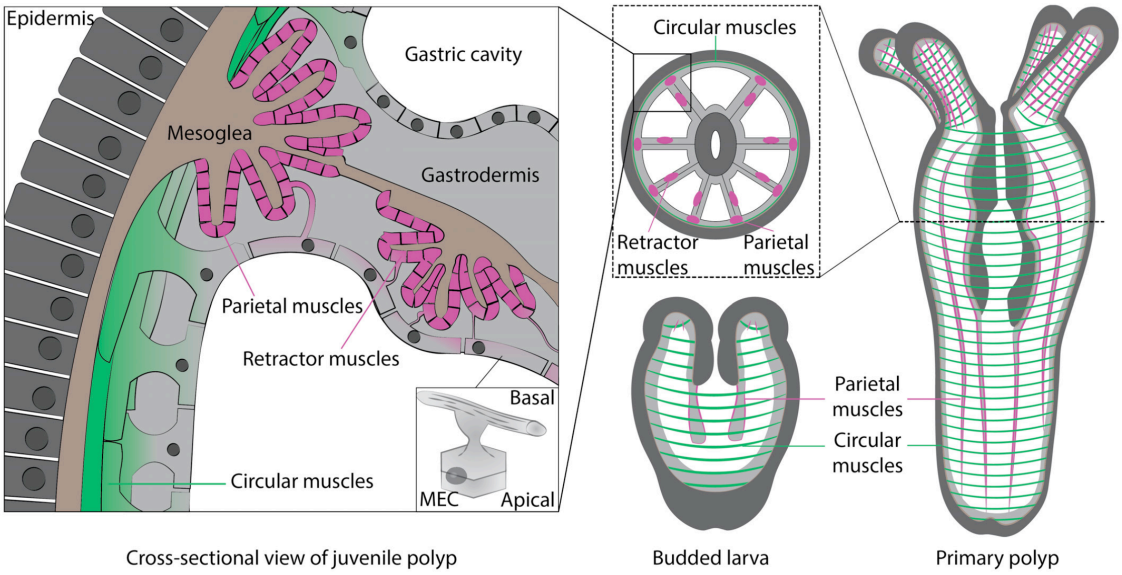

Figure 3.3. Muscle system of *Nematostella vectensis*. The endoderm houses the muscular machinery of *Nematostella*. The endoderm contains the myoepithelial cells, with two orthogonal fibers. The muscular system contains 3 sets of muscles, the retractor, parital and circular muscles. Figure compiled from the thesis of Dr Anniek Stokkermans.

muscle length, and isometric, maintaining a constant length. The interplay between these two muscle types and the different longitudinal and circular muscles collectively shapes and regulates the body column of *Nematostella*.

The larva-polyp morphogenesis is characterized by cycles of hydraulically driven stresses that drive axial elongation. The hydraulic pressure is driven by expansion of cavity regulated by muscular organization and contraction (Stokkermans et al. (2022)). It is not known how and when the mesoglea is established post-embryonically, and how it supports this metamorphosis. The subsequent investigation lies at the heart of the aims of my thesis.

Chapter 4

Aims of the thesis

Visualization of the basement membrane markers of *Nematostella vectensis*

The first objective of my PhD project is to visualize the ECM in *Nematostella*. I will focus on the basement membrane (BM) proteins, and keep collagen IV in focus owing to its established roles in morphogenesis. I would start with immunostaining for collagen IV and laminin to see if there are any differences in between this two major networks, and later utilize the established molecular toolkit to generate knock-in transgenic lines expressing endogenously tagged collagen IV. I would plan to initially conjugate with eGFP to confirm and then with Dendra2, a photoconvertible protein, to unlock the dynamics.

Basement membrane biogenesis and dynamics in the larva-polyp morphogenesis of *Nematostella vectensis*

Once I have established tools to visualize collagen IV, I will use it to characterize the spatiotemporal patterns of its expression during the larva-polyp morphogenesis. I will report the dynamics of the emerging collagen IV networks.

Basement membrane and tissue interactions during larva-polyp morphogenesis

I will complement the interactions of collagen IV with the muscular system and the epithelia to identify key mechanisms that permits the coordination of larva-polyp morphogenesis.

The roles of the basement membrane across local and global scales of morphogenesis

Through appropriately designed perturbations and subsequent molecular characterizations, I plan to comment on the roles played by the basement membrane across different lengthscales within the context of larva-polyp morphogenesis.

Chapter 5

The role of basement membrane in organismal morphogenesis

5.1 An overview of larva-polyp morphogenesis during early *Nematostella* development

As discussed in section 3, I have focused my research to understand the morphogenetic processes that drive the necessary changes throughout the larva to polyp transformation. With the work of past doctoral student Dr. Anniek Stokkermans, *Nematostella* development can be tracked and followed with advanced image analysis using a wide-field microscopy setup (Stokkermans et al. (2022)). This is acquired using a high throughput screening microscope developed by Acquifer. Individual animal development (Figure 5.1 A) can be tracked across multiple animals through long timelapses, at time intervals that can range in between seconds to hours to days. This allowed me to visualize and characterize the larva-polyp morphogenesis with great details across organismal scales, and across large populations to observe underlying trends (Figure 5.1 B, left). One key metric that I have often used throughout to characterize morphogenesis is through the changes in the oral-aboral distance that I have labeled as the body length, which linearly increases over time from around 250µm to around 750µm during larva-polyp transition. This holds true across a population scale, and gave me the opportunity to characterize the body length of a growing animal as a metric of its developmental time. I have used the aspect ratio of the animal (the ratio between the body length and body width) as a metric of its emergent shape and the computed volume (cylindrical approximation from a 2D cross-section) as a metric of its emergent size to construct its morphospace, where individual and population of

animals track linear trajectories as they develop in time (Figure 5.1 B, right).

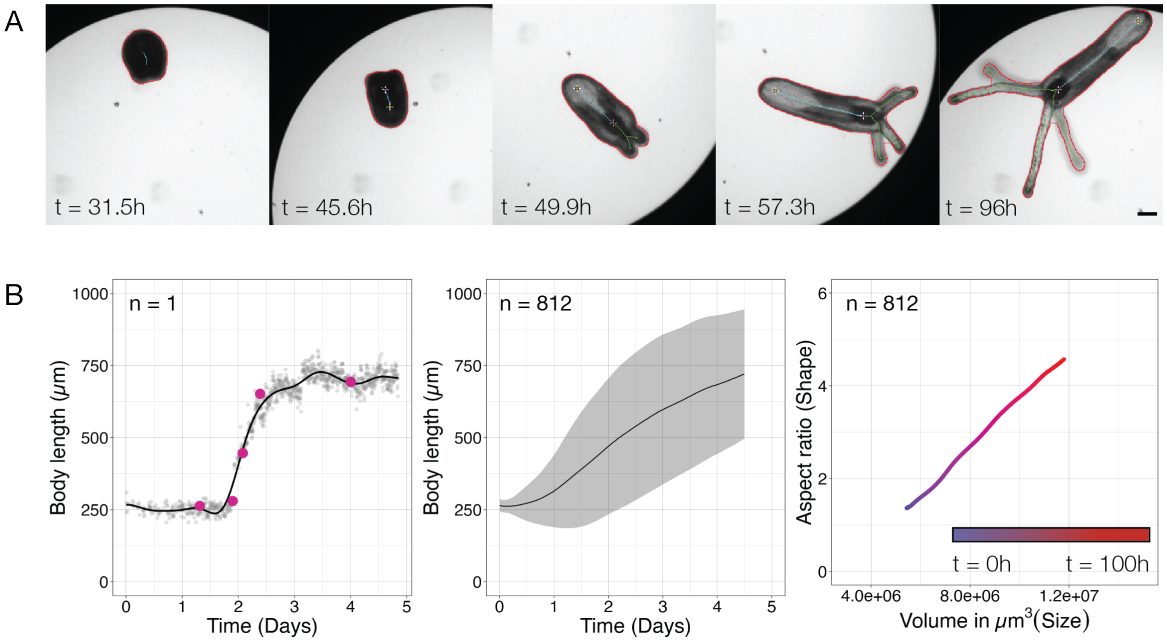

Figure 5.1. Larva-polyp morphogenesis of *Nematostella vectensis*. A. Snapshots during live imaging of a larva under metamorphosis in the Acquifer system at 27°C. The hours represent time from the start of acquisition, at the swimming larva stage. Scale bar: 50µm. B. (Left) Segmentation of body length over days during morphogenesis, with the points depicting stages represented in panel A. (Center) The body length over days in a large population of developing animals. (Right) The morphospace of a developing animal, shape represented by the aspect ratio of the body, size represented by the computed volume. The profile represents the average change of shape and size across animals, color coded by time (in hours).

5.2 The basement membrane is maintained at a steady state during larva-polyp morphogenesis

I wanted to understand the dynamics of the basement membrane (BM), particularly if there were any spatiotemporal dynamics that underlie larva-polyp morphogenesis. I wanted to first visualize the dominant BM components, and I focused on laminin and collagen IV since these proteins lay the foundation of BM across the tree of life. For the former, I kindly received a custom-made antibody against laminin-γ from Gideon Bergheim of COS Heidelberg, and for the latter I received a JK2 antibody from Dr Haruko Tomono of Shigei Medical Research Institute in Japan. The monoclonal JK2 antibody recognizes the NC1 domain of collagen IV scaffolds and has been widely used

to characterize the collagen IV networks across metazoans (Boudko et al. (2023); Fidler et al. (2014); Shimizu et al. (2008)). I performed immunostaining with these two antibodies in animals across larva-polyp morphogenesis to observe the spatial dynamics of the BM across developmental time. I observed the cross-section using confocal microscopy, and the results revealed a very strong signal sandwiched in between both the germ layers and almost nothing within the germ layers after reaching the larval stage (Figure 5.2 A). Before reaching the larval stages, I observed intercellular signal for both the proteins across both the germ layers during the embryonic stages, only a bright localization of collagen IV was sandwiched in between the germ layers. I concluded that prior to the larval stages, the BM proteins is produced by both the ectoderm and the endoderm and is then trafficked into the emerging mesoglea. Hence I next focused on the intensity of the immunofluorescence signal and wanted to see if there were any underlying spatiotemporal patterns. To do that, I have quantified the fluorescence intensities of both the BM markers along the oral-aboral axis. Surprisingly, I found out that it does not vary much spatially within the mesoglea of an individual animal. This allowed me to report an average intensity with its calculated standard deviation for both the proteins for every single animal. This metric would roughly approximate the relative density of the proteins within the developing mesoglea. I compared this reported intensity across different developmental stages, and could report the normalized intensities and its errors for both the proteins against the maximum observable. I next plotted the normalized intensity against the body length of the animal. Assuming the intensity of the proteins reflect directly to its density, this analysis revealed a regulatory mechanism of the BM, whereby there is an increase of relative density of both collagen IV and laminin in the beginning of larva-polyp morphogenesis until the animal reaches about 400µm (Figure 5.2 B). Elongation of the body column after 400µm appeared to have a stable local concentration of both collagen IV and laminin. The immunostaining results also revealed another interesting metric regarding the relative timescales of ECM establishment. For both collagen IV and laminin, the average density goes up from 200µm to 400µm at different speeds. This can be observed from the different slopes for both the proteins at this temporal regime. Surprisingly, collagen IV seemed to reach its effective stable state around 350µm, which is earlier than laminin at around 400µm in comparison (Figure 5.2 B). Combined with the observation that the laminin localization within the BM follows after collagen IV, this contradicts the biogenesis of the basement membrane that was observed during regeneration ((Jr)).

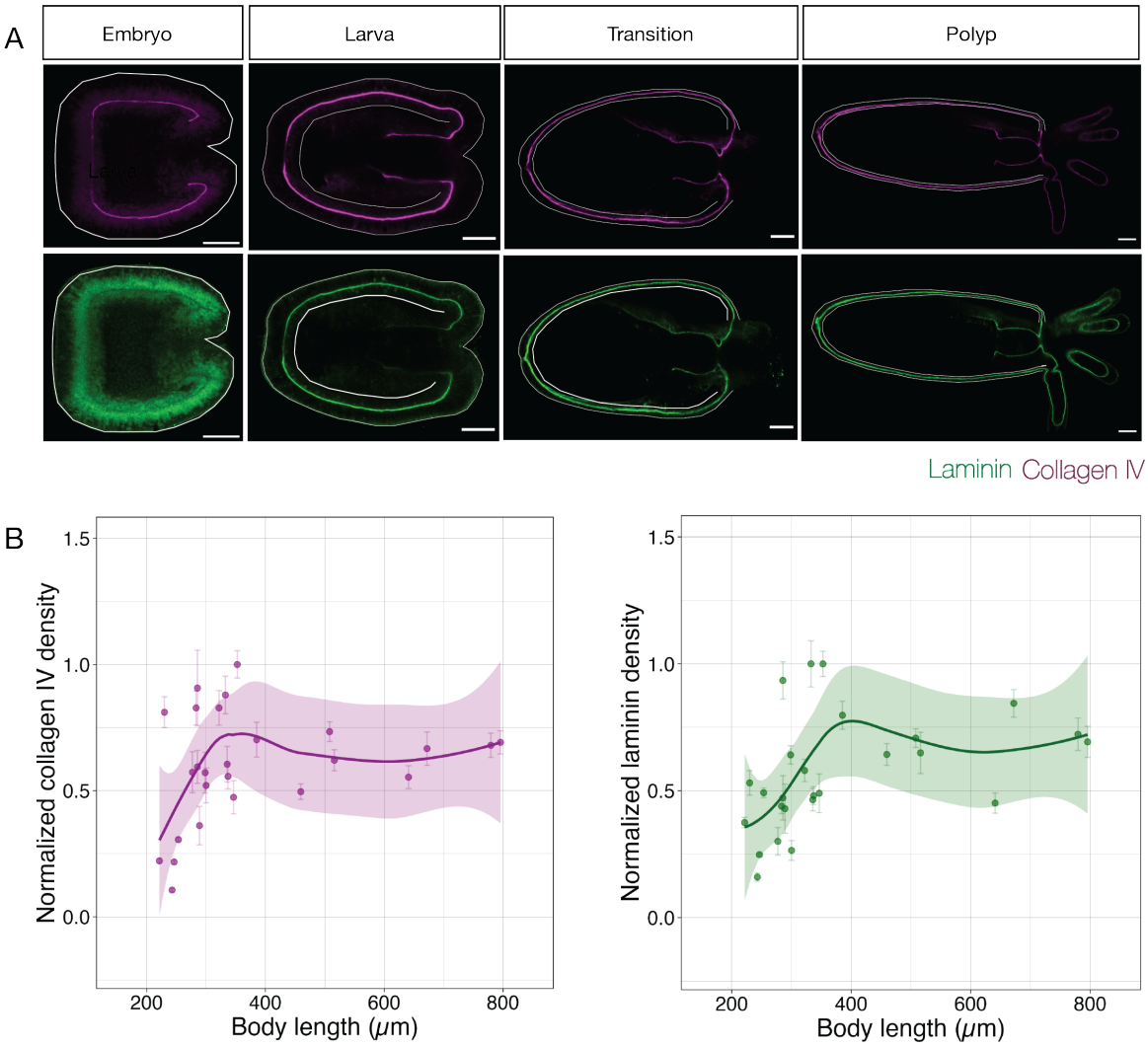

Figure 5.2. Basement membrane visualization during larva-polyp morphogenesis. A. Cross-sectional view across the oral plane of immunostaining against basement membrane markers collagen IV and laminin, across different developmental stages. Scale bar: 50µm. B. Normalized densities of collagen IV (left) and laminin (right) plotted against body length.

5.3 The basement membrane gains anisotropic organization driven by underlying muscular architecture

Next, I focused on the spatial organization of both protein networks underlying the germ layers. To obtain that, I observed the maximum intensity projections of the Z-stacks across developmental stages. This revealed the order of the structural organization of both collagen IV and laminin along the surface (Figure 5.4 A). I observed a temporal order in between the collagen IV and laminin networks during their

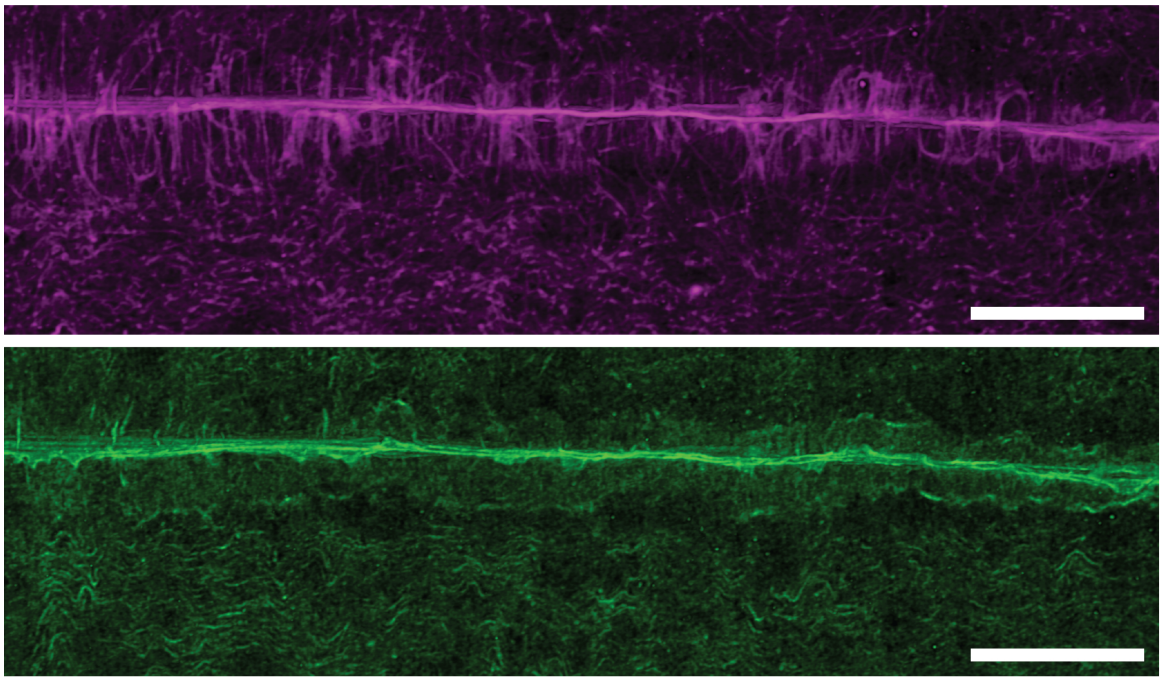

Figure 5.3. Basement membrane with its unique stitches. Collagen IV and laminin immunostaining exhibiting stitches on the boundaries and wavy organization on the segments. Collagen IV primarily marks the stitches, while laminin remains more organized on the segments.

assembly, where firstly collagen IV networks are established prior to laminin networks(Figure 5.4 A), which corresponds to the data obtained from the cross-sectional densities (Figure 4.2B). This is very distinct in the embryonic stages, where there is a huge marked difference between both the networks. There were also parallel lines observed along the oral-aboral axis in both the protein networks (Figure 5.4 C), which makes the immunofluorescence signal deviate from isotropic at the embryonic stages to anisotropic during larva-polyp transition. The emergent anisotropy observed in the alignment of the fibers seems to align to the patterned anisotropy that is generated by the segmentation of the endoderm (He et al., 2018). The endoderm in *Nematostella* is segmented sequentially into 8 segments and produces invaginated boundaries where the neighboring segments connect (Figure 5.4 B). I focused on these boundaries with high resolution confocal microscopy (Figure 5.4 C) and the images showed a striking pattern in particularly the collagen IV networks, whereby I observed filaments crossing over the segments, which I aptly named “stitches”. These stitches were primarily rich in collagen IV, while the laminin was much more organized within the segments (Figure 5.3). The BM of *Nematostella* has structural modifications that allow its relative body flexibility (Tucker, Richard. et al. (2011)), and the wavy organization can

come from crimping of the BM (Liu et al. (2014)) during successive rounds of muscle contractions.

The segmented endoderm also generates the emergent muscular architecture during the larva-polyp morphogenesis, which produces longitudinal muscles along the oral-aboral axis and circular muscles perpendicularly. These muscle fibers lie adjacent to the basal side of the endoderm, which faces the BM. To test whether there is a link between the organizations of BM and muscular networks during development, I generated previously characterized shRNA mediated knockdowns targeting genes that affect muscle organization (Figure 5.5) (Stokkermans et al. (2022)). For BMP2/4 shRNA knockdown, the endoderm is not segmented and longitudinal muscles are not differentiated. In this context, I did not detect any collagen IV stitches. For the Tbx20 shRNA knockdown, there are ectopically induced defects in the local organization of the muscles. Here, BM markers show defects in their stitching patterns, where the defects in muscle alignment generates similar defects in the collagen IV stitches. This observation hinted towards a deeper control of local BM organization by the muscular architecture. This result echoes observations made in other organisms, like drosophila (Chu and Hayashi (2021)), C elegans (Labouesse (2012)), zebrafish (Jessen (2015)) and planarians (Chan et al. (2021)), where the muscles and the localized ECM is connected during development.

5.4 The steady state of basement membrane density is crucial for organismal morphogenesis

The early phase of elongation is characterized by a marked increase in the intensity profile of the basement membrane components, leading to a steady state of intensity irrespective of continuous body elongation. ECM proteins are extremely dynamic in nature, where the underlying dynamic is controlled by its production, its remodeling and its subsequent degradation. To maintain constant axial elongation, this steady state is achieved under non-equilibrium, with imbalance in between production and degradation rates. I wanted to know the effect on morphogenesis if these rates are modulated. To achieve this, I perturbed inhibition of recruitment of new fibrils into the existing network and also through inhibition of degradation of existing fibrils within the network. I targeted these perturbations through pharmacological inhibitions of post translational modulators (Figure 5.6 A). I inhibited the recruitment of collagen IV by preventing its polymerization with the application of 50µM of 2,2'-bipyridine (BPY), a well-known inhibitor of prolyl-4-hydroxylase (P4HA). P4HA prevents colla-

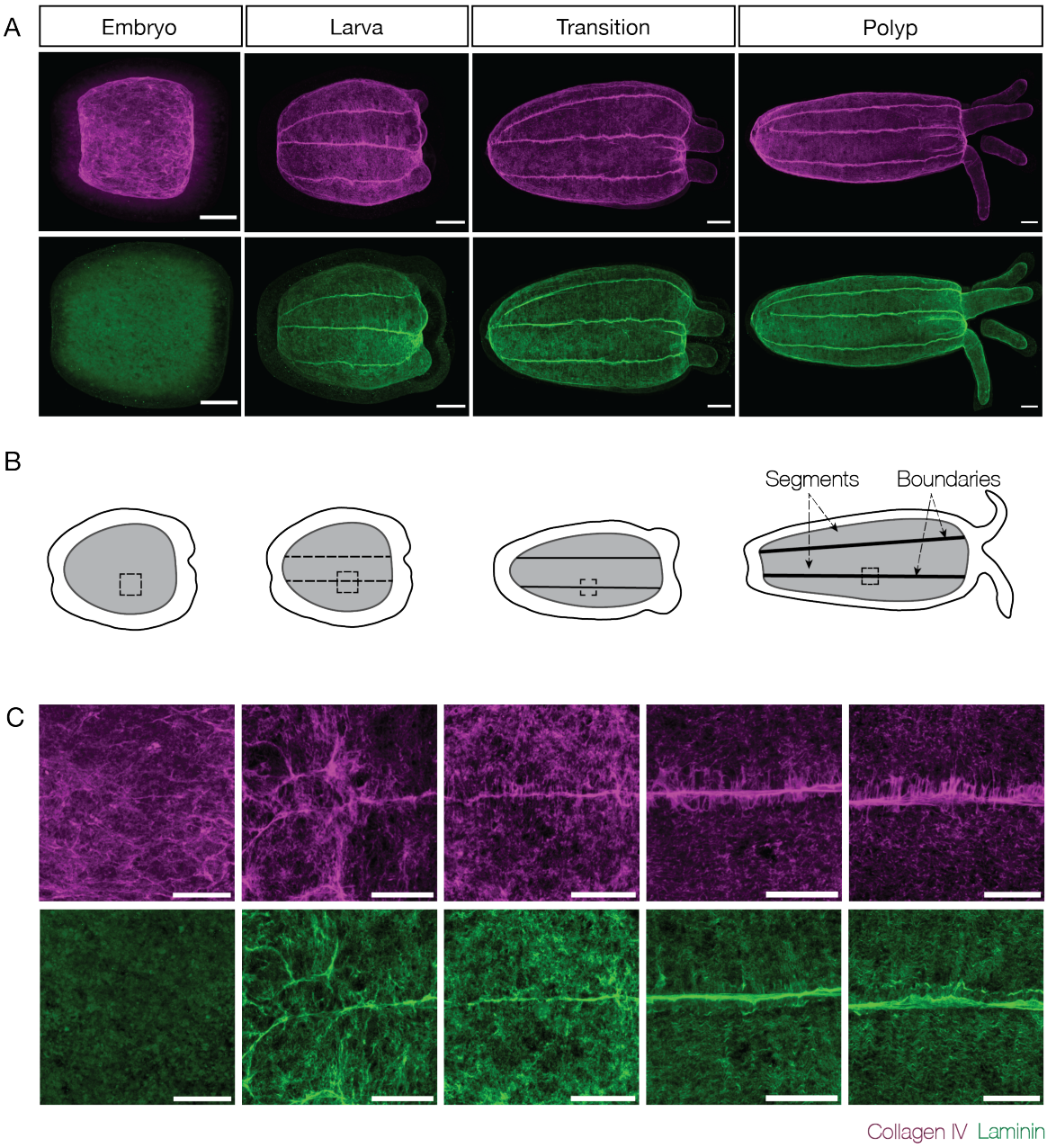

Figure 5.4. Anisotropic organization of the basement membrane during development. A. Maximum intensity projection from immunostaining of BM markers to represent the surface organization, across developmental stages. Scale bar: 50µm. B. Representation of the endodermal organization, zones demarkated by segments and boundaries. C. Zoom-in images of surfaces at the boundaries during development, depicting emergent anistropy in BM networks. Scale bar: 20µm.

gen cross-linking (Gorres and Raines (2010)), primarily across fibrillar type 1, but it is reported to affect the stability of collagen IV networks as well (Adachi et al. (2005); Holster et al. (2007)) and also is reported to weaken tissue stiffness in hydra (Naik et al. (2020)). On the other end, I inhibited the degradation of collagen IV with the

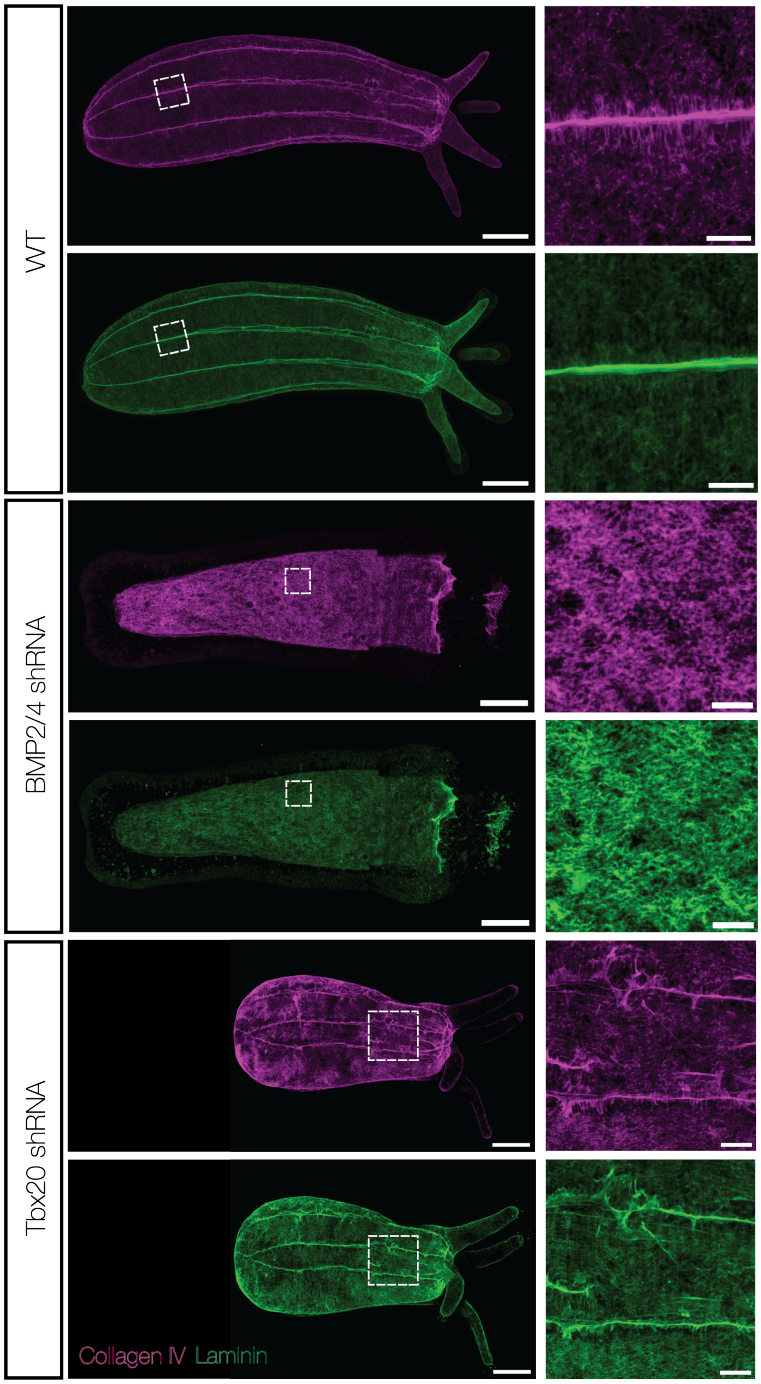

Figure 5.5. Basement membrane organization is patterned by the emergent musculature. Maximum intensity projections of BM markers for control and mutants that affect muscle organization. Scale bars: 50µm (zoomed out), 20µm (zoomed in).

application of 50µM GM6001, which is a well-known MMP inhibitor that prevents collagen IV degradation (Kato et al. (2006); Misko et al. (2002)) and increases the stiffness of the network (Bordeleau et al. (2017); Martin-Martin et al. (2011)).

An advantage of pharmacological inhibition is its temporal control of adminis-

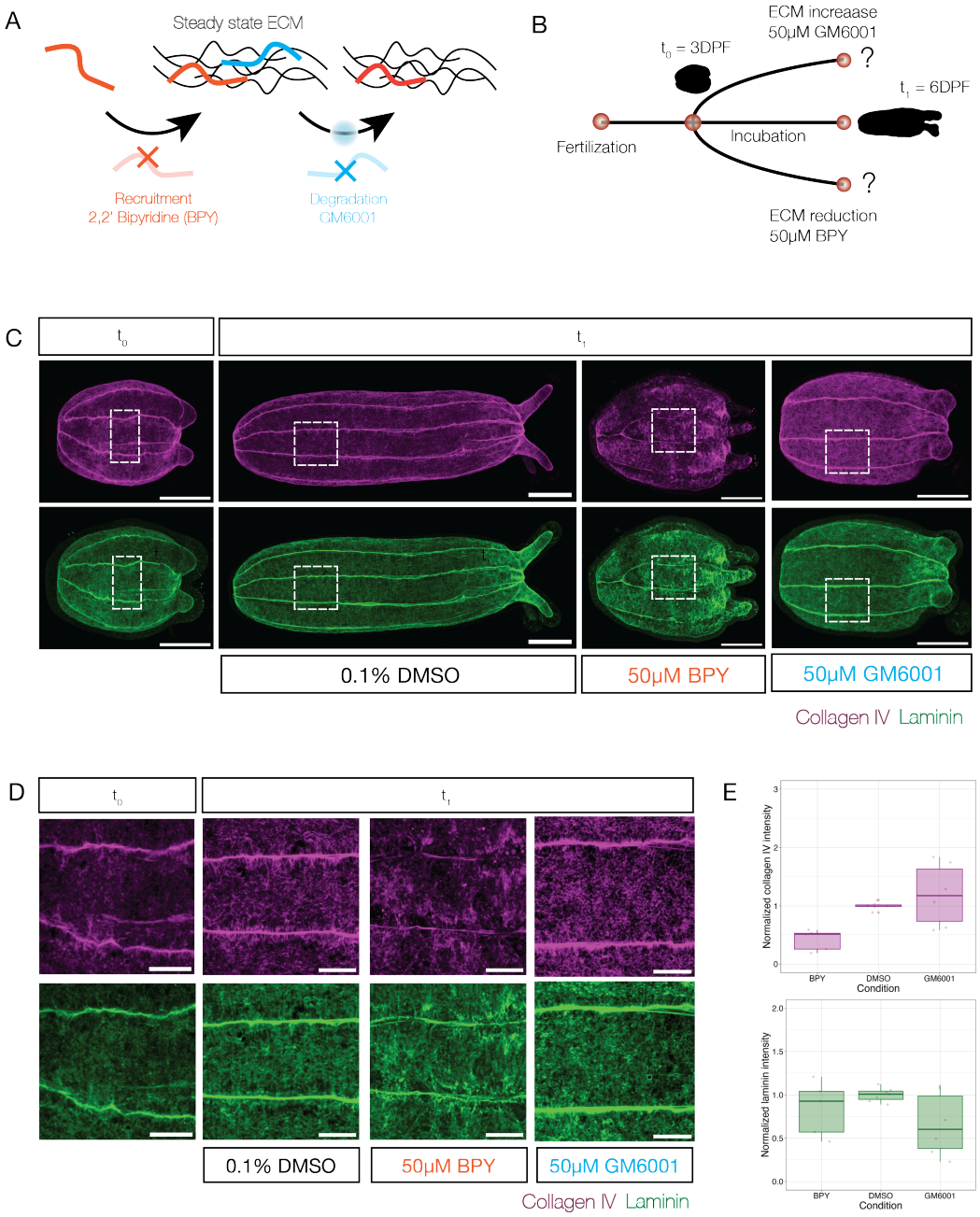

Figure 5.6. Pharmacological perturbation of basement membrane steady state. A. Steady state ECM can be affected by perturbing recruitment and degradation. B. Experimental plan for the perturbation of BM stabilization. C. Maximum intensity projection of immunostaining with BM markers at the start and end of the treatment, for controls and phenotypes. Scale bar: 50µm. D. Zoomed insets from panel C. Scale bar: 20µm. E. Quantification of normalized intensities of BM markers between control and phenotypes

tration. I kept fertilized eggs at 27°C for 3 days post fertilization (t_0) to let them reach their swimming larval forms, following which I incubated the larva in the respective drugs for 3 additional days (t_f), by the end of which the controls reach primary polyp

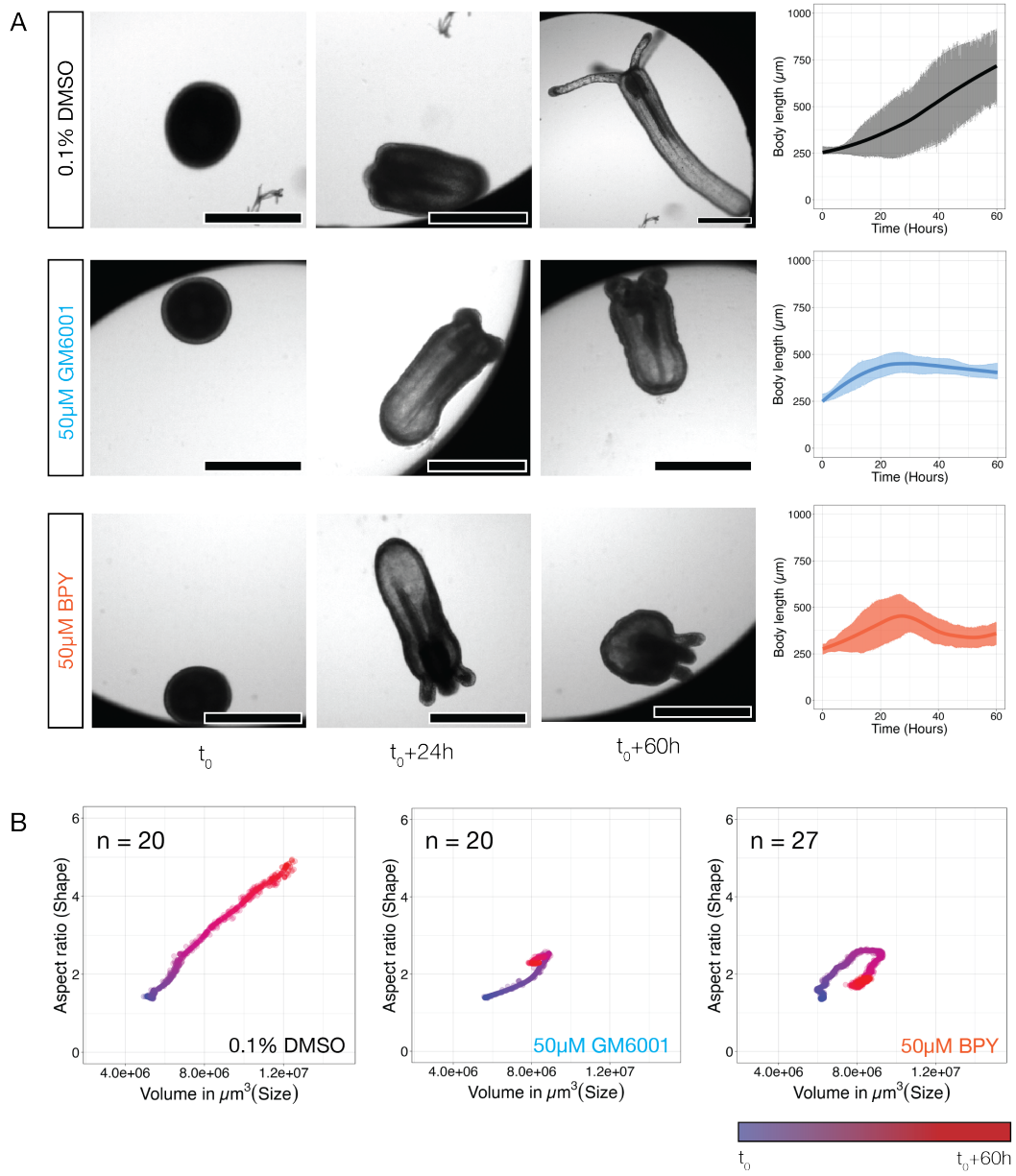

Figure 5.7. Perturbation of basement membrane steady state affects underlying morphodynamics. A. (Left) Snapshots from live imaging with Acquifer with larva-polyp morphogenesis under pharmacological perturbation. Scale bar: 100µm. (Right) Quantifications of body length with time for controls and treatments across multiple animals. B. Morphospace construction under pharmacological perturbations.

stages (Figure 5.6 B). There was a clear morphogenetic defect in either cases, where I saw a robust phenotype (Figure 5.6 C, 5.6 D). Both drugs produced a phenotype with smaller body length, and upon immunostaining with BM markers exhibited preferential defects in the intensity profiles of collagen IV networks compared to laminin (Figure 5.6 E). The results confirm that the drugs administered had an expected modification of intensity profiles in the BM networks. This affects morphogenesis at the

organismal scale, as observed in the body length of the phenotypes.

I was then interested in understanding the mechanisms that underlie the generation of emergent shapes in the phenotypes. I performed live imaging of *Nematostella* larva under the perturbations and tracked their changes in shape and size over time through live imaging with the Acquifer system (Figure 5.7A). For the controls, the animals grew linearly and became polyps. However, the animals with stiffer BM arrest their growth at around 500µm within 24 hours from the start of the treatment and maintain its shape and size, while the animals with softer BM arrest their growth around 500µm within 24 hours as well but collapses back to its initial starting length, around 300µm (Figure 5.7A). I generated plots for the control and the treatments to see how the animal map their respective morphospaces, denoted by their changes in shape and size (Figure 5.7B). I then plotted the changes of size and shape of animals from both the control and the treatments in their respective morphospace. Control animals exhibited a linear growth, animals with stiffer BM exhibited a stable state where they halt their morphogenesis, while animals with stiffer BM exhibited a reversal of their direction of morphogenesis. Interestingly, the slopes produced in the morphospace by the animals in their first 24 hours also trace the effects of their possible changes in tissue mechanical properties: animals with stiffer BM managed to grow their size faster than their shape while this dynamic was reversed in animals with softer BM (Figure 5.7B).

5.5 Summary and conclusions

Nematostella larvae undergo a major transformation to metamorphose into a polyp with four tentacles. How the mesoglea fits into this morphogenetic regime was previously unknown, since the earliest known evidence in the literature was in the juvenile polyps (Tucker, Richard. et al. (2011)). Through immunostaining of core basement membrane markers, I investigated the spatiotemporal order of the basement membrane establishment. I found out that both collagen IV and laminin networks are established early on during larva-polyp morphogenesis. The early phase of elongation is characterized by a significant increase in the intensity profile of BM components. This phase then transitions into a period where, despite ongoing body elongation, the intensity profile of BM constituents remains relatively constant. Furthermore, these networks revealed an anisotropic organization that is patterned by the underlying muscular organization. I also found that collagen IV exhibit stitch-like patterns on the boundaries of the segments. I perturbed the steady state of the BM networks by

affecting recruitment and degradation of the new and old fibrils within the network, and both affected the global geometry during morphogenesis. Through live imaging, I could also report on how the dynamics of morphogenesis is affected, as animals from both the drug phenotypes grow to 500µm before they exhibit a pronounced effect in their morphogenetic trajectory.

These observations led me to hypothesize a strong role of BM on the morphogenetic control during larva-polyp transformation. The organismal control of larva-polyp morphogenesis is controlled by the muscular hydraulics acting against increasing cavity pressure, which increases its internal stresses. The strains generated on the body wall generates the required deformation for morphogenesis. Mechanical properties of the body wall might be dominated by the mechanical properties of the sandwiched BM (), and hence the animals require the maintenance of a stable BM that permits a balanced increase in its shape and size. Making the BM stiffer halts morphogenesis, while making it softer might dissipate the driven stresses.

The immunostaining only allowed visualization of the mesogleal BM. To maintain a stable density of BM concentration across development, there needs to be constant production, which needs to be accounted for. In section 6, I introduce a new method to resolve this issue and highlighted on the biogenesis of the BM. Since the muscles control the spatial organization of the underlying BM, I also focus on the interactions between the muscles and the BM.

Chapter 6

Biogenesis and remodeling of the basement membrane

6.1 Endogenous knock-in eGFP::ColIV reveals the tissue-level origin of collagen IV

Through immunostaining of collagen IV and laminin, I uncovered a mechanism that highlights the importance of maintaining a stable basement membrane density to coordinate larva-polyp morphogenesis of *Nematostella*. The immunostaining only revealed the extracellular BM, however a balance between production and degradation rates is required to maintain a steady state. I decided to focus particularly on collagen IV. To unlock the true dynamics that underlie the biogenesis of the BM, I decided to use the advanced genetics of the model system to address the missing intracellular production. In collaboration with Dr Alexandre Paix, a CRISPR-Cas9 guided endogenously fused eGFP::ColIV transgenic line was generated with a more robust protocol (Paix et al. (2023)). eGFP was tagged to a coding exon after the signal peptide domains, which prevents cleavages from splicing events, keeping in mind that collagen IV, like most ECM proteins, are heavily modified post-translationally (Figure 6.1 A).

The endogenous eGFP::ColIV expression gave me the first direct evidence of early collagen IV biogenesis, whereby I located a weak signal inside the invaginating blastopore lip during gastrulation. The first strong expression is located already at gastrula stages, when the germ layers are distinctly defined. I observed that collagen IV is asymmetrically produced only within the endodermal cells filled with eGFP::ColIV puncta, while the ectoderm was devoid of any signal (Figure 6.1 B). Next, I looked

at the distribution of eGFP::ColIV signal across animals spanning across larva-polyp morphogenesis, and throughout the intracellular collagen IV was localized within the endoderm and the developing mesoglea (Figure 6.1 C). To quantify and analyze, I focused at the cross-section and integrated the signal over a region orthogonal to the oral-aboral axis. Normalized across the area, this provided me a metric of collagen IV intensity across the ectoderm, endoderm and mesoglea as a profile plot against the cross-sectional position, represented on the right (Figure 6.1 D).

I then performed the same analysis across different developmental stages and normalized by the reported maximum intensity. From each profile plot, I can take the area under the curve to report a germ layer specific local intensity of collagen IV across all layers, plotted over body length as a proxy of developmental time. The results revealed a differential dynamic across the different layers (Figure 6.1 E), whereby the ectoderm displayed background autofluorescence, the endoderm displayed an increase of collagen IV intensity before the animal gains a body length of 400µm and slowly reduces to a constant rate, while the mesoglea maintains a steady local concentration of collagen IV beyond 400µm. My results accounted for the missing collagen IV by endodermal production, enabling the maintenance of steady state within the mesoglea.

6.2 Muscles and the basement membrane organization during larva-polyp morphogenesis

The traditional protocols that are used to visualize the ECM proteins often require steps that include ethanol, which prevented the co-staining with phalloidin that permits the visualization of the cellular structures, particularly the muscle fibers. Since the BM organization is controlled by the developing muscles, I wanted to visualize the link in between the developing muscular system and the BM simultaneously. The endogenous eGFP::ColIV allowed parallel staining with phalloidin (Figure 6.2). Over the body segments, the collagen IV networks start highly organized orthogonally to the developing circular muscles in a wavy organization. On the segment boundaries, I found the colocalization of the collagen IV stitches over circular muscles across neighboring segments. This also validated the presence of collagen IV stitches that were identified with the immunostaining, as non-technical artifacts. The stitches also start to appear across development as more circular muscles are differentiated. This led me to hypothesize that the collagen IV stitches might provide a physical mechanism to connect muscles across segments, allowing the coordination of muscle contractility across the animal.

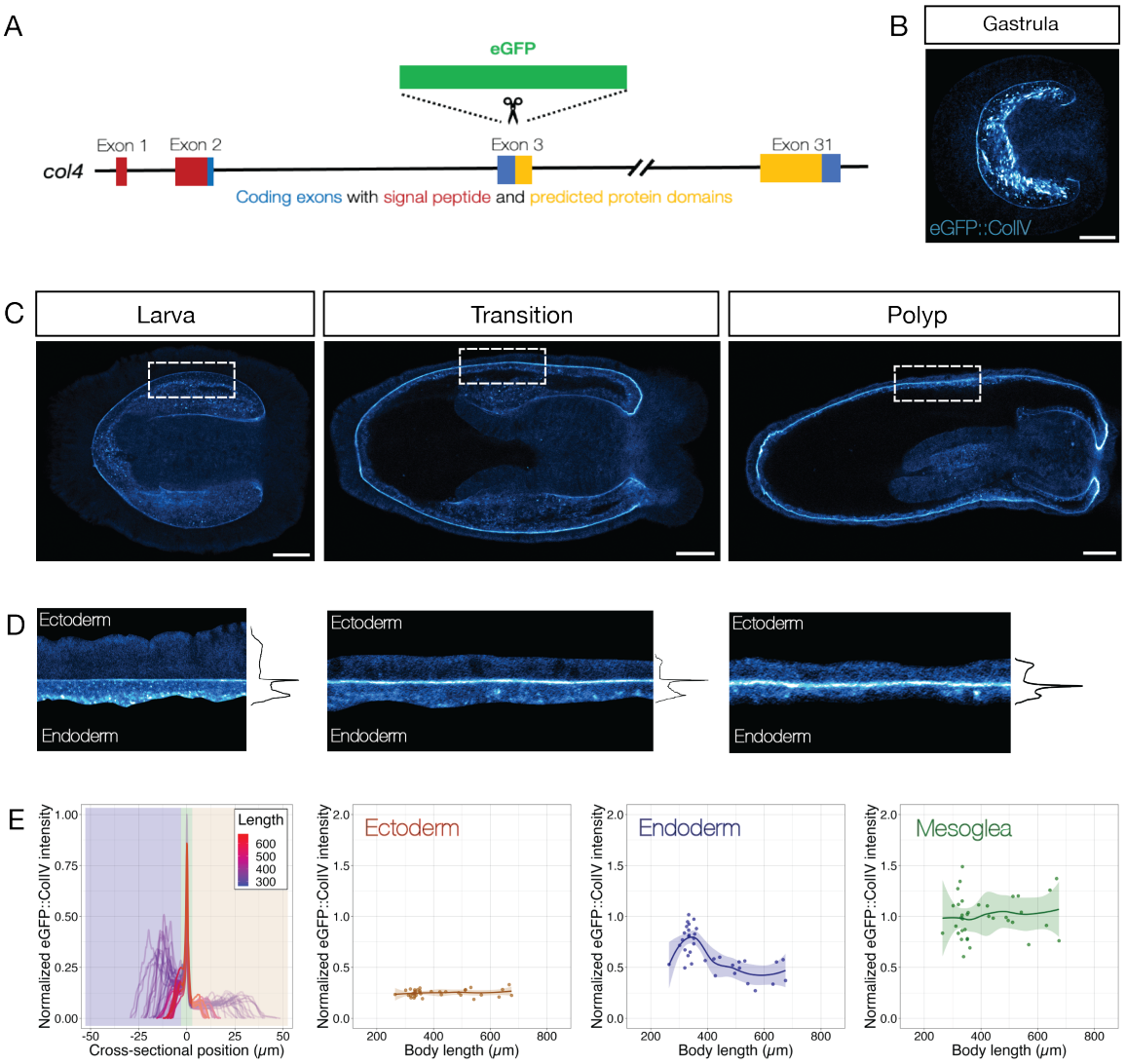

Figure 6.1. eGFP::ColIV reveals intracellular collagen IV dynamics. A. Knock-in design for eGFP::ColIV transgenic line. B. Endogenous eGFP::ColIV in early gastrula. Scale bar: 50µm. C. Cross-sectional view across oral plane for endogenous eGFP::ColIV, across larva-polyp morphogenesis. Scale bar: 50µm. D. Cropped profiles from panel C representing lateral cross-sections centered at the mesoglea. The upper side represents the ectoderm, while the lower side represents the endoderm. The insets are followed by an average intensity projection profile along the mesogleal coordinate. E. (Left) Quantification of normalized endogenous eGFP::ColIV intensity across the cross-sectional position centered along multiple animals (n = 36), The plot color code represents the body length, while the box colors represent the layer. The sum of the signal within the individual layers is further separated into the remaining panels.

Endogenous eGFP::ColIV also confirms the observations from immunostaining when the collagen IV steady state is perturbed. eGFP::ColIV signal intensity was

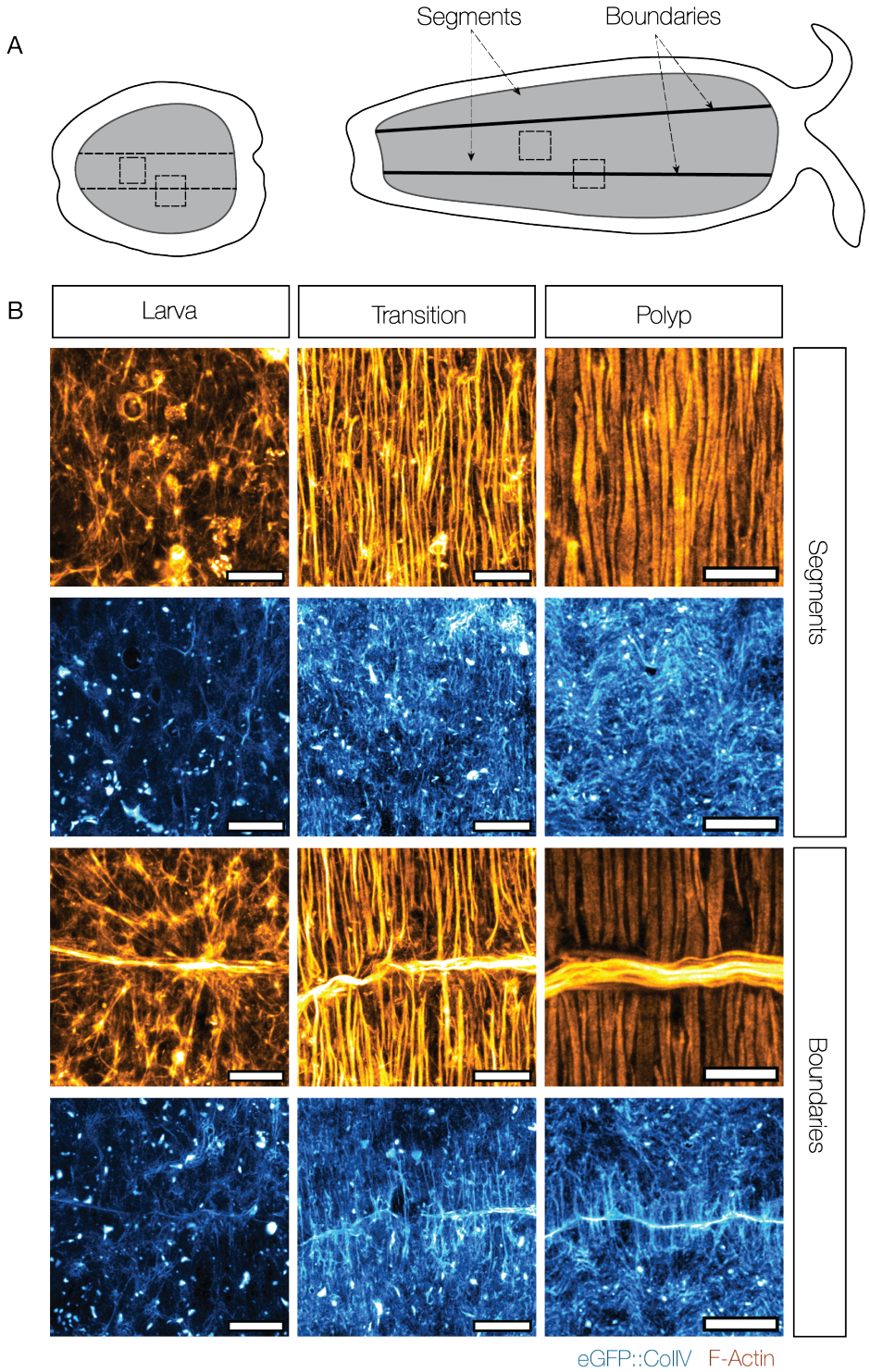

Figure 6.2. Emergent muscle and collagen IV anisotropy during larva-polyp morphogenesis. A. Cartoon depicting the segment and the boundaries of the endoderm. B. Co-staining of F-actin (Phalloidin) and endogenous eGFP::ColIV along the segments and the boundaries during development. Scale bar: 20µm.

upregulated with a higher number of stitches when the BM is stiffened and down-regulated with lesser number of stitches when the BM is softened (Figure 6.3). The

treatment did not affect the orthogonality of the muscular organization, but affected the differentiation of individual fibers.

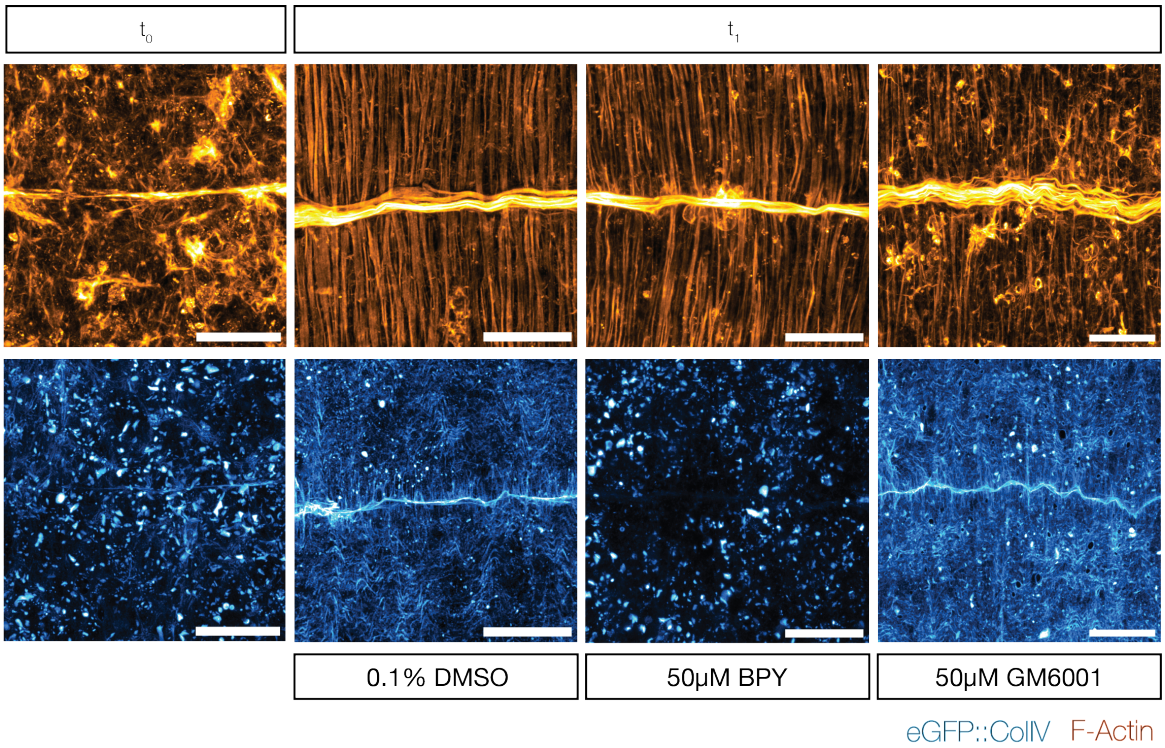

Figure 6.3. Effect of pharmacological inhibition of basement membrane stabilization on the muscles and collagen IV networks. Co-staining of F-actin (Phalloidin) and endogenous eGFP::ColIV along the boundaries for control and treatments. Scale bar: 20µm.

6.3 Dendra2::ColIV reveals the dynamic remodeling of the basement membrane

Through endogenous eGFP::ColIV characterization, I unlocked the production and the steady state of the collagen IV during larva-polyp morphogenesis. I wanted to further understand the other mechanisms that controls the dynamics of this network. One key mechanism is through remodeling, where an existing network can be reorganized without further fibril deposition or degradation. The larva-polyp morphogenesis involves a 3-fold increase in body length, and I wanted to understand how the collagen IV networks are modified during this transition. To reveal this dynamic, I collaborated with Dr Alexandre Paix to generate another transgenic line, where collagen IV was endogenously tagged with a photoconvertible protein, Dendra2, which expresses green fluorescence under native state and can be converted to red with UV exposure.

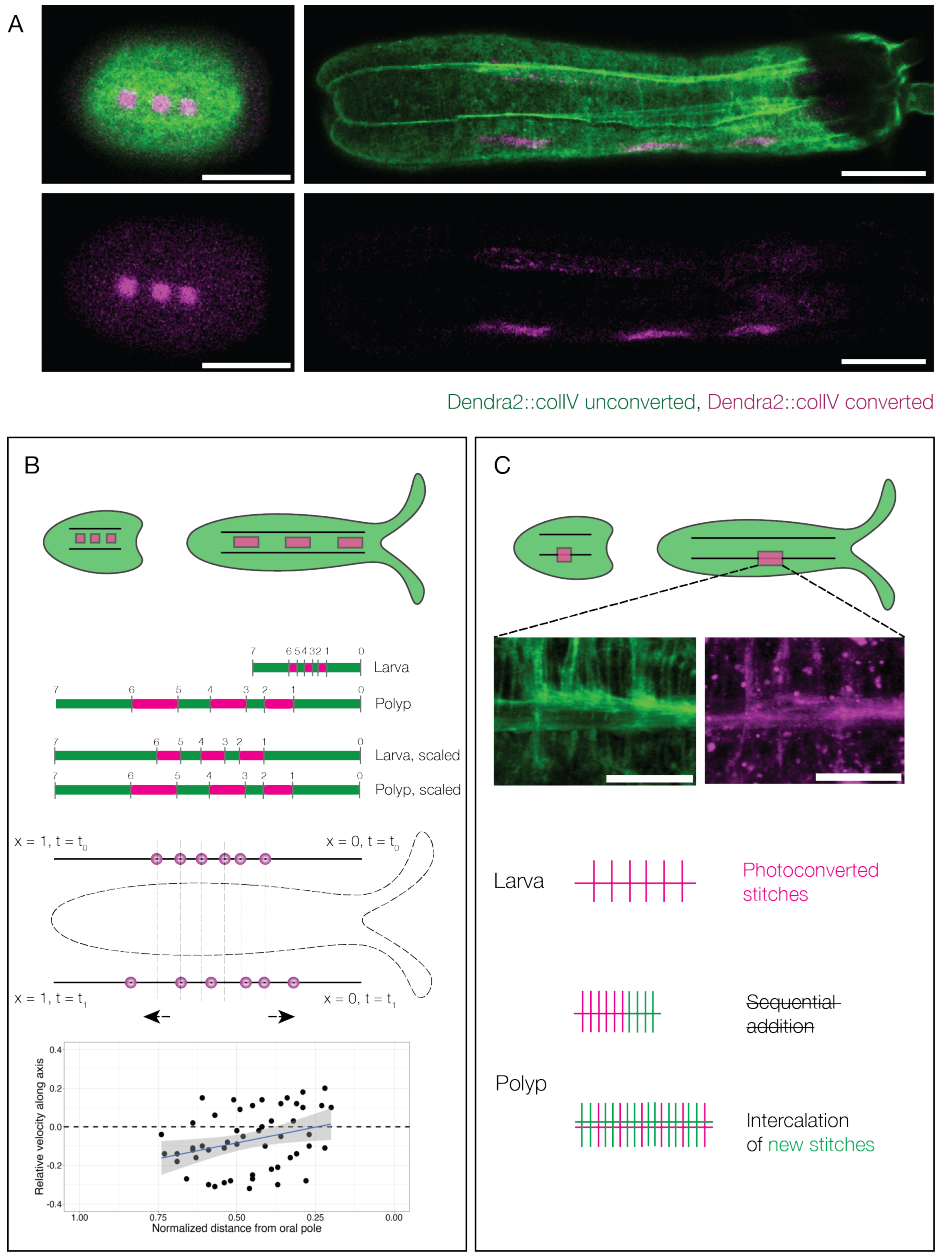

Figure 6.4. Dendra2::ColIV reveals dynamics of BM turnover during morphogenesis. A. UV photoconversion of clones and their subsequent tracking during morphogenesis. Scale bar: 100µm. B. Tracking of clones and their relative velocities across the oral-aboral axis during larva-polyp morphogenesis. C. Intercalation of new collagen IV stitches during morphogenesis. Scale: 10µm.

The dynamics reported for collagen IV is highly regulated by the local tissue, since it involves additional molecular actors that either add or degrade from the existing network. Depending on the local context, the turnover can vary largely across timescales. My experimental design was controlled by photoconverting patches of native Dendra2::ColIV along the oral-aboral axis of the animal, and following the clones along developmental time. An estimate of degradation can be inferred from the loss of

the photoconverted red signal within a clone, while an estimate of production can be inferred from the amount of new green signal coming up within an existing clone compared to the background. The larva-polyp transition takes 3 days when the animals are incubated at 27°C. The ideal experiment would require the photoconversion and imaging of the clones over 3 days. Since the metamorphosis require the motility of the animal and is halted with immobilization, it was impossible to track the clone at a finer time resolution. I hence tracked the photoconverted clones when the animals completed metamorphosis (Figure 6.4 A). I found out that the converted red signal persists over 3 days, and the clone shape is modified since the animal has increased its length almost 3 times. The green signal in between the red clones were found to be invariant to the background, which meant that the production rate of collagen IV was much higher than its degradation.

To understand how the animal elongation remodels its entire collagen IV network during organismal morphogenesis, I traced the clones in a rescaled coordinate system, where 0 indicated the oral end and 1 indicated the aboral end. Normally, I made on an average 3 clones per animal along the oral-aboral axis on the body segments, which gave me initial location of 7 points (Figure 6.4 B). I can track how much these initial points have moved across space during larva-polyp morphogenesis, by calculating the relative shift of the final locations against the initial locations post metamorphosis. This gave me a metric of velocity of collagen IV, a positive value indicating that the clone has migrated towards the oral end, while a negative value indicates that the clone has migrated towards the aboral end during the larva-polyp morphogenesis (Figure 6.4 B). Data from multiple animals were pooled together (n = 6) to build statistics and see any emergent axis specific pattern. Next, all the velocities were plotted across all the animals with their calculated velocity on the y-axis. On the x-axis, I plotted the location of the clones initially (Figure 6.4 B). My observations revealed that there is a bidirectional migration of collagen IV during larva-polyp morphogenesis, where collagen IV close to the oral end tends to migrates towards the oral side while that towards the aboral end does the opposite. An empirical normalized distance of 0.25 from the oral pole (corresponding to 75µm in a 300µm long larva) is reported to be the point of inflection, which means if a clone is converted at a length 50µm from the oral pole it is expected to move towards the oral pole, if it is converted 150µm from the oral pole it is expected to move towards the aboral pole, while if it is converted at 75µm from the oral pole it is not expected to move in either direction. This experiment and analysis explored a convective dynamics of the emergent dynamic collagen IV network organization during development, much

similar to examples of ECM in embryonic chick metacarpal bone (Li et al. (2015)) and hydra (Aufschnaiter et al. (2011)). Dendra2::ColIV also unlocked the dynamics that controls the addition of new stitches at the boundary. The clonal analysis of Dendra2::ColIV across body segments revealed dilution of the local collagen IV network across morphogenesis, which holds true for boundaries as well. Tracking photoconverted clones on the boundaries revealed addition of new green stitches in between converted stitches (Figure 6.4 C), making new collagen IV stitches intercalated in between existing stitches.

6.4 Summary and conclusions

I characterized the dynamics of collagen IV assembly by analyzing endogenous expression of eGFP::ColIV across axial space and developmental time. The results also revealed a deeper mechanism of the connection of the emergent BM networks with the endoderm. The endoderm produces the BM, while the muscles, housed by the endoderm, organize the local BM density and anisotropy. eGFP::ColIV intensity inside the mesoglea does not increase initially as observed during immunostaining, which can be further checked by including animals from earlier developmental time points in the analysis pipeline. One other possible explanation might be that the bright puncta interfere with the signal inside the mesoglea. Dendra2::ColIV revealed the convective dynamics of the BM, where the turnover is visualized through an intercalation of new BM fibrils, both in segments and in the boundaries. A novel mechanism of ECM remodeling through a bidirectional flow towards the animal extremities was demonstrated through the tracking of individual photoconverted clones across development.

In 7, I investigate the mechanisms of tissue remodeling that drives larva-polyp morphogenesis. I then provide arguments for and against the dominant mechanisms that permits the animal to coordinate its growth, and propose a working model that adds more information into the mechanisms that underlie the strain dynamics from muscular hydraulics.

Chapter 7

The mechanisms of tissue remodeling that drive larva-polyp morphogenesis

7.1 Larva-polyp morphogenesis has two underlying remodeling motifs

To understand the mechanisms that drive the tissue deformations to control larva-polyp morphogenesis, I decided to measure the macroscopic changes across the different developmental stages (Figure 7.1 A). The pertinent morphometric parameters that was important to extract were the body length (excluding the tentacles), the body width (average thickness along the oral-aboral axis) and particularly the lateral thicknesses along both the germ layers (Figure 7.1 B). Given the axial symmetry of the system, these parameters were accessible through a cross-section across the oral plane of the animal (Figure 7.1 A). I built a Python-ImageJ based pipeline to extract the relevant metrics, and plotted them primarily against the body length to build a map of morphogenetic changes. The data was pooled across many animals (n = 82) to track morphogenesis sequentially, the body length being used as a proxy for developmental time. This strategy allowed me to stage the larva-polyp morphogenesis as a continuous metric, instead of discrete phenotypic stages that was highly affected by observational bias.

The first interesting observation was the change of lateral tissue thickness over the increasing body length (Figure 7.1 C). The animals at their larval stages

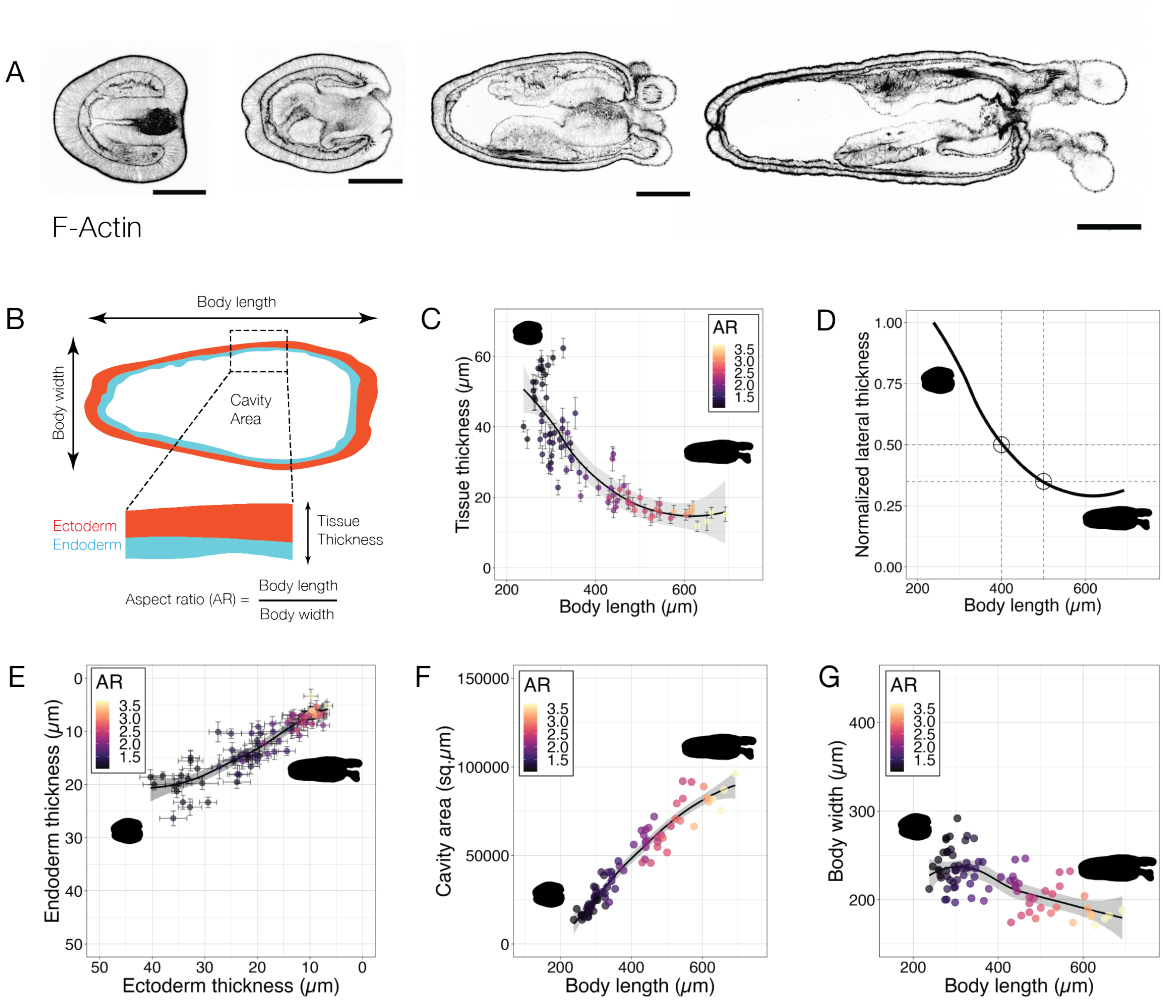

Figure 7.1. Tissue geometry changes underlying larva-polyp morphogenesis. A. F-Actin (Phalloidin) staining across cross-section of the oral plane during larva-polyp morphogenesis. Scale bar: 100µm. B. Segmented body without tentacles and the morphometric parameters extracted. C. Map of lateral tissue thickness across body length. D. Plot of normalized lateral tissue thickness and body length. E. Map of ectoderm and endoderm thicknesses across development. F. Map of cavity area over body length. G. Body width and body length changes over development.

start from a body length of around 250µm with a lateral thickness of approximately 50µm and, through morphogenesis, eventually become polyps having body lengths of around 700µm with a lateral thickness of approximately 15µm. The process was also uncovered as non-linear exhibiting two distinct modes. To understand that, I normalized the lateral thickness to the initial starting thickness (Figure 7.1 D). I found out that the lateral tissue is already thinned to 50% linearly from 50µm to 25µm by the time the body length reaches from 250 µm to 400µm. Afterwards, the tissue is further reduced from 25µm to 15µm while the body length changes from 400µm to 700µm. The gain in body length cannot be explained through lateral thinning beyond

500µm since there is almost no changes in tissue thickness. I concluded that the entire larva-polyp morphogenesis has at least two elongation patterns, one that is highly by lateral tissue thinning between 250µm to 400µm and followed up by a regime of slower tissue thinning that eventually requires further mechanisms.

To figure out how the germ layers individually change their thickness, I next plotted the thickness of the individual layers as the animals underwent morphogenesis (Figure 7.1 E). The effect of lateral tissue thinning was highly pronounced as the animals linearly thinned down their germ layers, with an initial ectoderm thickness around 40µm and endoderm thickness around 20µm to a final ectoderm thickness around 10µm and endoderm thickness around 5µm. The linearity underlying the thinning process was very interesting since both the germ layers thinned down at the same rate, with which I concluded that the tissue layers are coupled and highly coordinated throughout larva-polyp morphogenesis.

There was a linear increase of the cavity area as the animals gained their length, as the cavity area increased almost 7 times (Figure 7.1 F). The increase in the cavity size is the dominant driver of larva-polyp morphogenesis, which increases the size of the animal. Through measurements with optimal coherence microscopy (OCM) (Stokkermans et al. (2022)), it is known that the cavity volume changes 9 folds while the tissue volume changes 1.5 folds during larva-polyp morphogenesis. My analysis extended this measurement in finer details across the entire transition and uncovered the underlying linearity. The larva-polyp morphogenesis is also primarily driven by a constant increase in body length (2.8 times) while the body width reduced slightly (0.8 times) (Figure 7.1 G).

7.2 Perturbation of a stable basement membrane density does not affect tissue thinning

I decided to check how the drugs that affect the of the basement membrane affect the morphometric parameters that I have characterized along larva-polyp morphogenesis. This would allow the investigation of the effects of the drugs on tissue remodeling. I performed the same pharmacological treatment as described in section (Figure 7.2 A) and performed phalloidin staining. There was a definite phenotype in the body length that agrees to what I have already reported, and I also plotted along with changes in the body width (Figure 7.2 B, 7.2 C). Next, I plotted both these dimensions along with the trend that I previously fitted during development. The control conditions

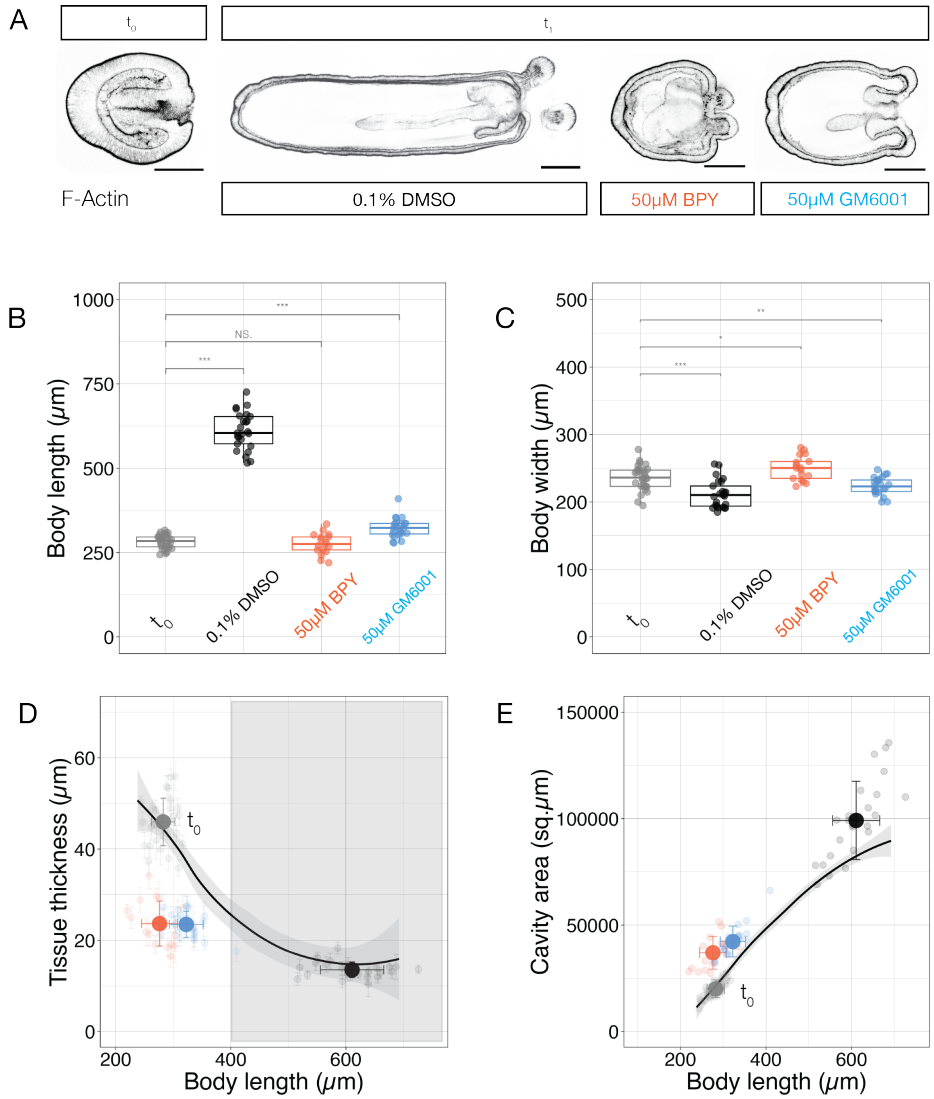

Figure 7.2. Perturbation of basement membrane stabilization does not affect tissue thinning. A. F-Actin (Phalloidin) staining of controls and phenotypes under pharmacological perturbations targeting BM stabilization. Scale bar: 100µm. B-C. Change of morphometric parameters (body length (B) and body width (C)) between control and phenotypes. D-E. Change of morphometric parameters (tissue thickness and cavity area) over body length between control and phenotypes.

nicely followed the trajectory laid during development, while the drug phenotypes remained locked close to the starting point t0. The cavity area of the phenotypes also remained close to t0, indicating no increase in cavity size increase to drive growth (Figure 7.2 D). Then I looked at the changes in tissue thickness in both control and perturbed conditions, and surprisingly the perturbations do not affect the thinning process completely, as in both conditions the tissue thins down from 50µm at t0 to 25µm at tf, but not completely to 15µm as in the controls (Figure 7.2 E). I concluded that the perturbation of basement membrane does not affect the first larva-polyp

morphogenetic motif, that is driven by tissue thinning, but rather affect the motif that follows up.

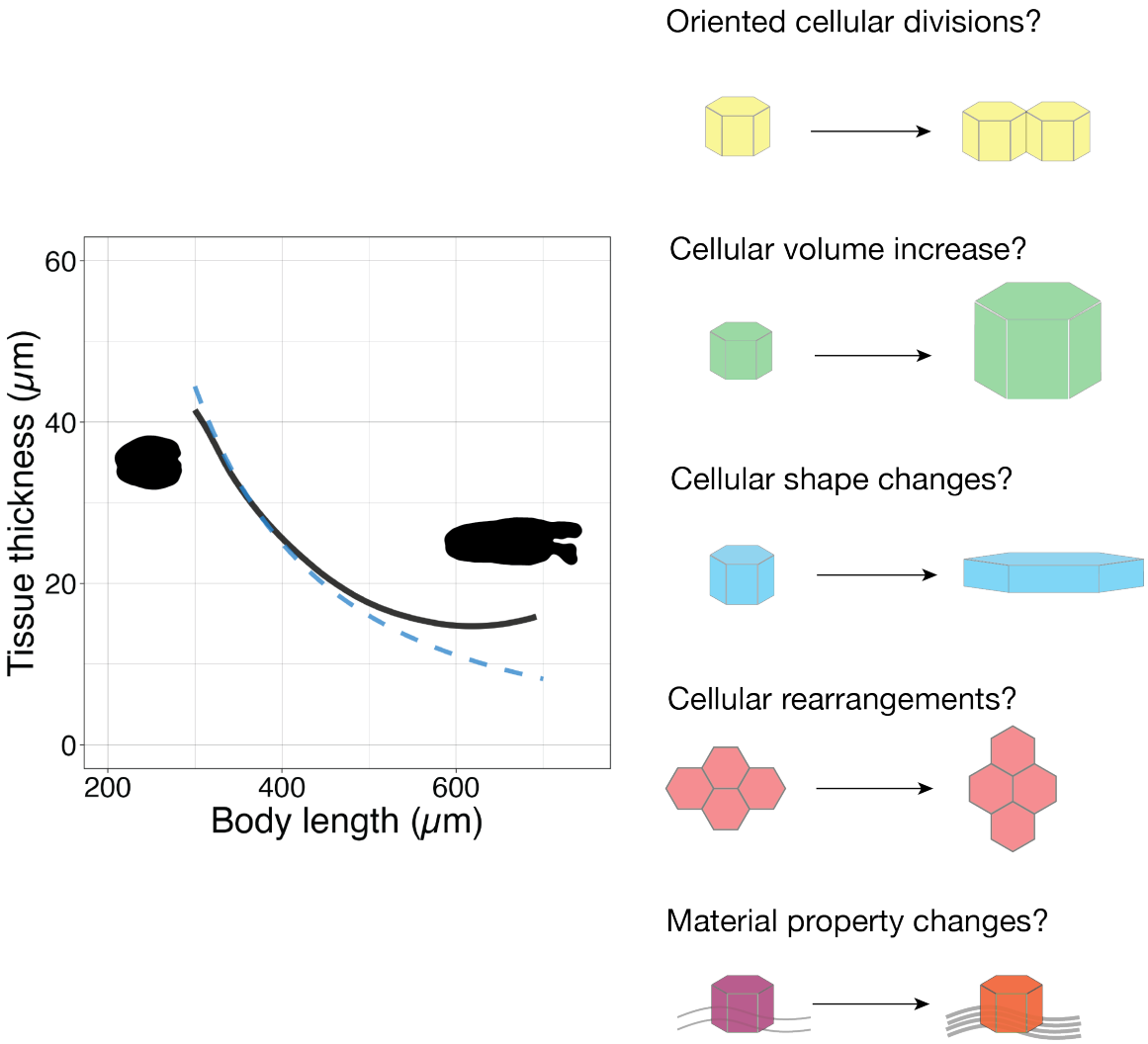

Figure 7.3. Mechanisms driving axial elongation in Nematostella. (Left) Normalized lateral thickness over body length during larva-polyp morphogenesis. The black line is the observed trend, while the red dashed line represents a toy model for tissue thinning driven axial elongation. (Right) Key mechanisms driving tissue morphogenesis.

7.3 Possible mechanisms that drive larva-polyp morphogenesis beyond 400µm

7.3.1 Oriented cell divisions does not drive axial elongation

One key mechanism that drives anisotropy in tissue growth is through directional preference of cellular divisions, where a dominant direction prepatterned by underlying

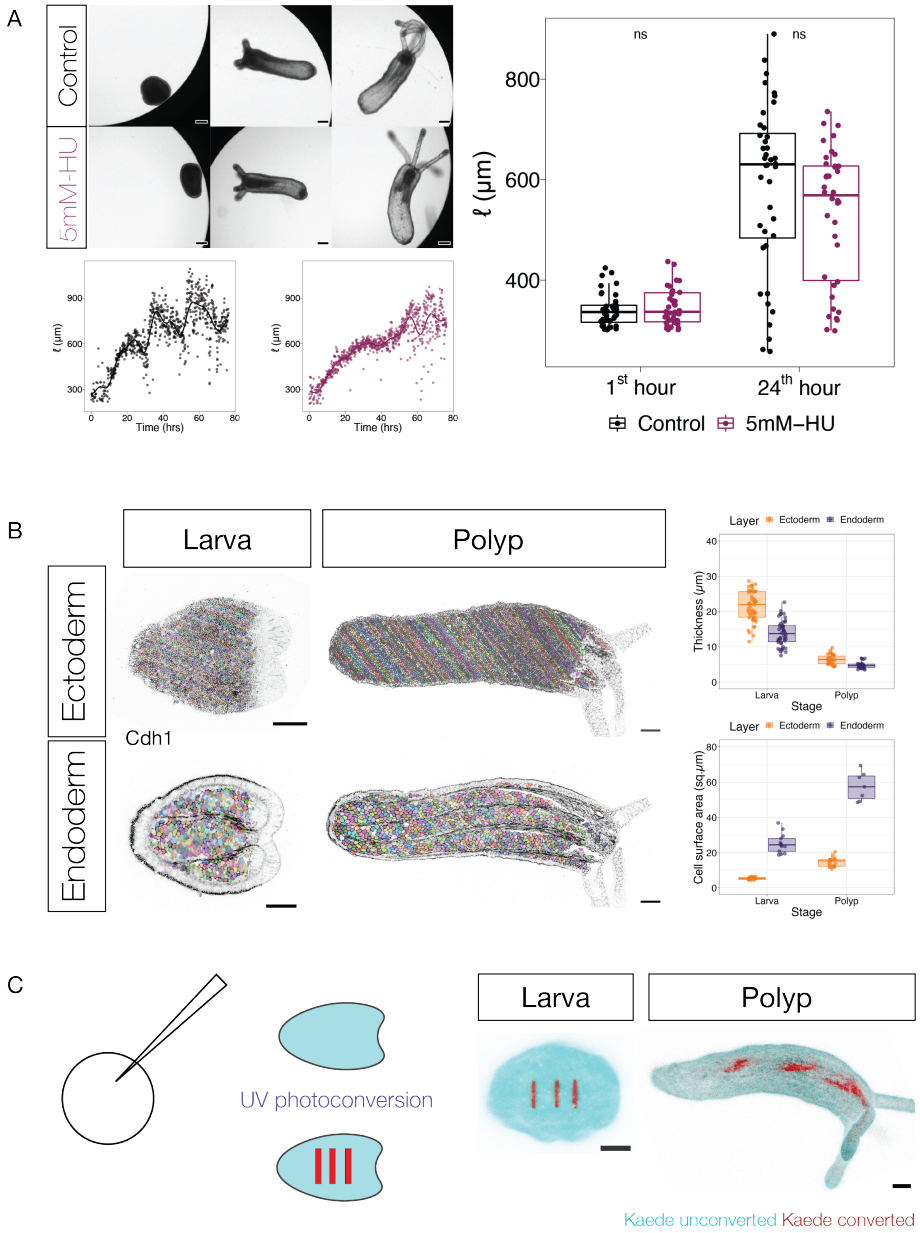

Figure 7.4. Cellular motifs of morphogenesis in Nematostella Oriented cell divisions does not drive larva-polyp morphogenesis. (Left) Snapshots during live imaging while inhibition of cell divisions with 5mM hydroxyurea. Scale bar: 50µm. (Right) Body length does not significantly change with 5mM HU treatment. B. Epithelial volume of the cells do not significantly change during larva-polyp morphogenesis. (Left) Cdh1 staining and segmentation of cells across germ layers. Scale bar: 50µm. (Right) Cell thickness and cell surface area changes in between larva and polyp stages. C. Larva-polyp morphogenesis is dominantly driven by cell rearrangements. (Left) mRNA injection to express ubiquitous Kaede and subsequent photoconversion. (Right) Tissue remodeling visualized using photoconverted clones. Scale bar: 50µm.

signaling cascades prefer cells to divide in a certain direction allowing tissue growth polarity. During the initial stages of larval development, cell divisions exhibiting a directional preference were noted (Fritz et al. (2013)). Anniek has already ruled this factor out; budding larvae during larva-polyp morphogenesis were treated with 5 mM hydroxyurea (HU), resulting in a notable decline in the number of actively dividing cells arrestinbg cells in their M phase. This reduction persisted even after 24 hours of exposure to 5 mM HU. Despite the reduced cell divisions, the animals continued to elongate and generate polyps, hinting other drivers at play during the transition.

7.3.2 Changes in cell shape does not drive axial elongation

Changes in cell shape also cannot completely explain the driving mechanism to drive morphogenesis beyond 500µm, as the tissue stops thinning with further increase in body length. To test this, I constructed a toy model, where I assumed an epithelial cell that elongates through elongation. Under the assumption that the cells do not change volume in the process, the dynamics between its length (L) and thickness (ω) will be constrained by a differential equation

$$2\omega dL + Ld\omega = 0 \tag{7.1}$$

The solution to this differential equation yields

$$\omega(L) = \frac{\kappa}{L^2} \tag{7.2}$$

Fitting from observed data (Figure 6.1C) gives me a numeric value of κ. Plotting this equation alongside the observed data trend clearly shows that the tissue thinning cannot completely explain axial elongation beyond 400µm (Figure 7.3 left).

7.3.3 Cell rearrangements drive tissue remodeling

A dominant mechanism that drives tissue remodeling is through cellular intercalations, and this is a dominant effector controlling larva-polyp morphogenesis. Anniek established photoconversion of injected mRNA that encodes Kaede to track tissue rearrangements. Kaede ubiquitously express green fluorescence that can be photoconverted to red upon exposure with UV rays. Specific regions of interest could be photoconverted during the larval stages and can be later tracked at the polyp stages to check for tissue rearrangements (Figure 7.4 C). This experiment yielded a dominant mechanism of tissue remodeling through rearrangements. This was tested also in animals with shRNA mediated KD targeting muscle organization (Stokkermans et al. (2022)), which affects the emergent tissue geometry. The rate of rearrangement can

be observed by the change in aspect ratio of the clones. In BMP2/4 KD, animals grow longer and show larger axial rearrangement with increase in the aspect ratio of the clones, while in the Tbx20 KD, the animals grow in width instead and show an inverse trend with a decrease in aspect ratio of the clones.

7.3.4 Cellular volume does not increase during the transition

Metric	Stage	Layer	Value
Thickness (µm)	Larva	Ectoderm	21.47 ± 4.3
		Endoderm	13.87 ± 3.59
	Polyp	Ectoderm	6.39 ± 1.37
		Endoderm	4.73 ± 0.9
Area (sq. µm)	Larva	Ectoderm	5.36 ± 0.62
		Endoderm	25.28 ± 5.52
	Polyp	Ectoderm	14.81 ± 2.61
		Endoderm	57.69 ± 8.08
Volume (cu. µm)	Larva	Ectoderm	115.05 ± 26.62
		Endoderm	350.68 ± 118.7
	Polyp	Ectoderm	94.58 ± 26.31
		Endoderm	272.92 ± 64.53

Table 7.1. Properties of single cells across germ layers during larva-polyp morphogenesis.

Another important mechanism that might be a key is changes in cellular volume. To measure that, I analyzed the data collected by Anniek, where she performed Cdh1 immunostainings in larva and polyp stages and segmented single cells across both germ layers to measure their surface area and thickness (Figure 7.4 B). I computed the volume of the cells by simply comparing the epithelial cells as regular polygons, multiplying their reported thickness with their surface area (7.1). The thickness of the tissue was reported to drop to 0.3 times across both epithelial layers during morphogenesis, while the apical surface area increased 2.76 and 2.28 times across both layers. The computed volume of individual cells remains close to 0.8 times between larva and polyp stages, under the assumptions that ignored the cellular morphology. Changes in the muscle fibers could not be accounted under this assumption. Changes in epithelial cell volume thus could also not be directly credited to control larva-polyp morphogenesis.

7.3.5 Muscle fibers gain area and intercalate during the transition

The muscle fibers, when labelled through phalloidin, are packed extremely dense to understand the changes acquired within individual morphologies during development. It is not known if the circular muscles are confined within one segment, or span across neighboring segments. In order to perform muscle contractions across the body, the muscle fibers need to be coupled across the segments, either by themselves protruding across the segments or physically linked through crosslinks. To visualize the morphologies of individual muscle cells and the topology of both of their fibers, I used the mosaic expression of a transgenic eGFP::Snail line, as Snail is expressed primarily across the endodermal cells that houses the muscles (Figure 7.5 A). I observed that the muscle fibers are indeed confined within the same segment, and can have three distinct topologies, where they can remain in between the boundaries, can remain adjacent to one of the boundaries or remains adjacent to both boundaries. I quantified the area covered by segmented muscle fibers (Figure 7.5 B) across 89 cells among 10 larva and across 60 cells across 9 polyps, and found that the muscle fiber areas increase by 1.5 times during larva-polyp morphogenesis. I also quantified the proportion of the adjacency of muscle fibers to their boundaries by grouping them across their topologies (Figure 7.5 B). I found that during larva-polyp morphogenesis the muscle fibers never cross their segments, and progressively become more adjacent to their boundaries, with almost no muscle fibers detected to be non-adjacent to their boundaries. In summary, the muscle fibers grow and intercalate during larva-polyp morphogenesis, aligning its fibers close to the segment boundaries. A physical link amongst muscle fibers in between neighboring segments might be established by collagen IV stitches, since they overlap (Fig 6.2). The effect of the perturbation of the stable BM density on the muscle morphologies remain yet to be verified.

7.3.6 Emergent material properties possibly tune morphogenesis

During larva-polyp morphogenesis, the dominant mechanism of tissue remodeling is through rearrangements of the epithelial cells. To move, the cells need to move on the underlying BM. The mechanical properties of the BM thus can become a crucial factor to determine the proper rearrangements necessary for morphogenesis. The BM stiffness is a crucial contributor to the emergent tissue mechanics, often accounting with a stiffness coeffecient recorded at 250-500 kPa compared to 12 kPa measured in muscle cells (Guimarães et al. (2020); Van Helvert et al. (2018)). With the pharmaco-

logical treatments, I was able to perturb the organization and the density of the BM, which definitely would affect the emergent mechanics. The effect of these drugs on the cellular rearrangements needs to be verified. For a stiffer BM, I would expect to see less changes in the aspect ratio of the photoconverted Kaede clones, while in the the case of a softer BM, I would expect to see an opposite effect, possibly mimicking the observations from the shRNA KD of Tbx20 (Stokkermans et al. (2022)). The results obtained from the Kaede photoconversion during this pharmacological treatment possibly will highlight on the effective fluidity of the tissue, a metric that is measured and proven important for axial elongation in biological systems.

7.4 Summary and conclusions

The larva-polyp morphogenesis is biophysically driven by muscular hydraulics, where the muscular organization and contractions drive organismal growth against the increasing cavity pressure. This generates stresses across the tissues, and through my findings I accounted for the dynamics of the generated strains that are necessary to drive deformations across the tissues. The metamorphosis is driven across different motifs, dominated by tissue thinning to drive elongation between 250µm to 400µm. Post 400µm, morphogenesis is not driven by either oriented cell divisions, tissue thinning or an increase of cellular volume, but rather by cellular rearrangements in the epithelia. This is supported by a finely-tuned BM density, which together effectively control the a fine-tuned tissue fluidization that modulate larva-polyp morphogenesis.

The BM may also help the muscles to coordinate larva-polyp morphogenesis across the organismal scale, by allowing them to connect across different endodermal segments through the presence of stitches on segment boundaries. The muscle fibers themselves grow in size and intercalate during development. The role of the BM on the dynamics of the muscle fibers needs to be further investigated. In conclusion, the results guide to the understanding of modulation of larva-polyp morphogenesis at the organismal scale (Fig 7.6), where I link cell-autonomous factors and the role of the ECM working harmoniously to drive the deformations.

Sections **??** build up a story of an intimate role of the basement membrane in the larva-polyp morphogenesis of *Nematostella*. I propose the maintenance of a stable ECM density across the body axis as a key mechanism that modulates morphogenesis at the organismal scale. However, upon close observation, an alert reader can notice that the BM does not exist everywhere within the body column of the developing *Nematostella*, as early as the larval stages 5.2. This mystery continues to section

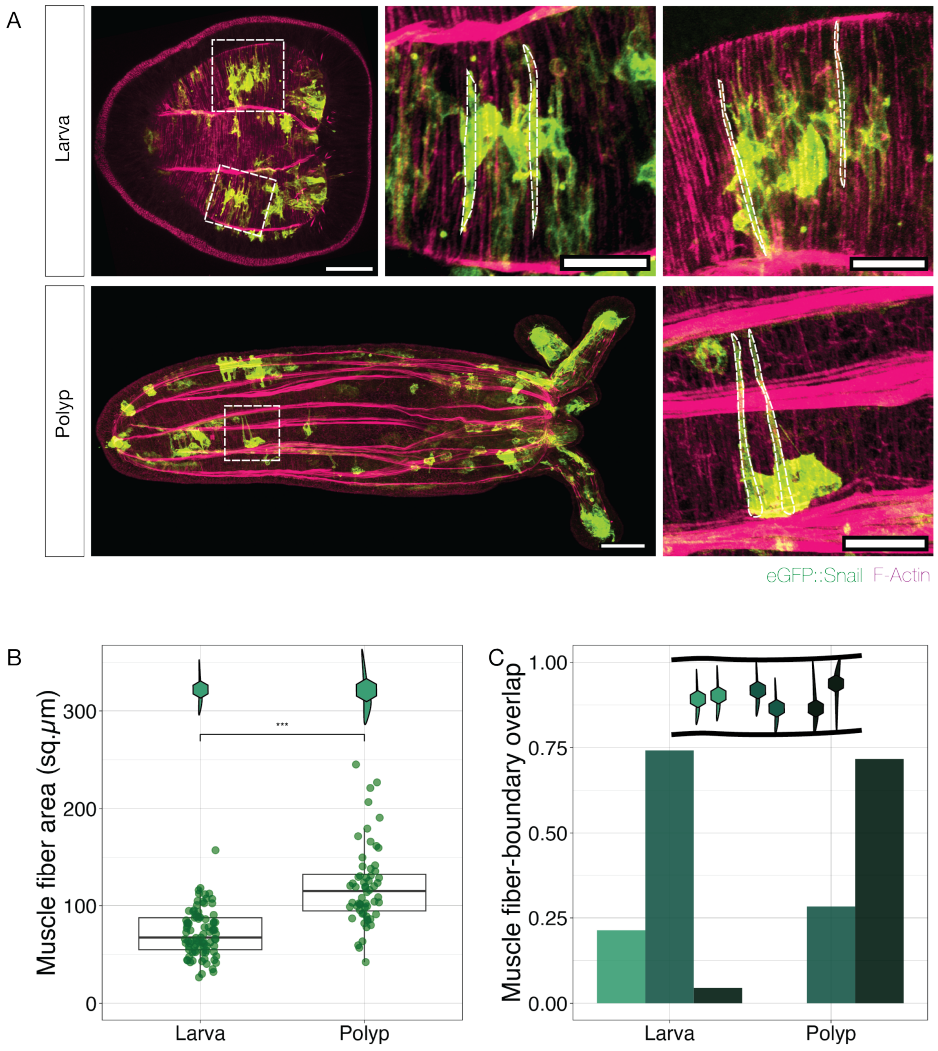

Figure 7.5. Muscle fiber morphology and topology during larva-polyp morphogenesis. A. Mosaic expression of eGFP::Snail along with F-actin (Phalloidin) in larva and polyp stages. Zoomed insets show highlighted fibers. Scale bars: 50µm (zoomed out), 10µm (zoomed in). B. (Left) Quantification of area of muscle fibers between larva and polyp stages. (Right) Quantification of muscle fiber-boundary adjacency between larva and polyp stages.

8, where I introduce another morphogenetic event that the BM is responsible in its coordination.

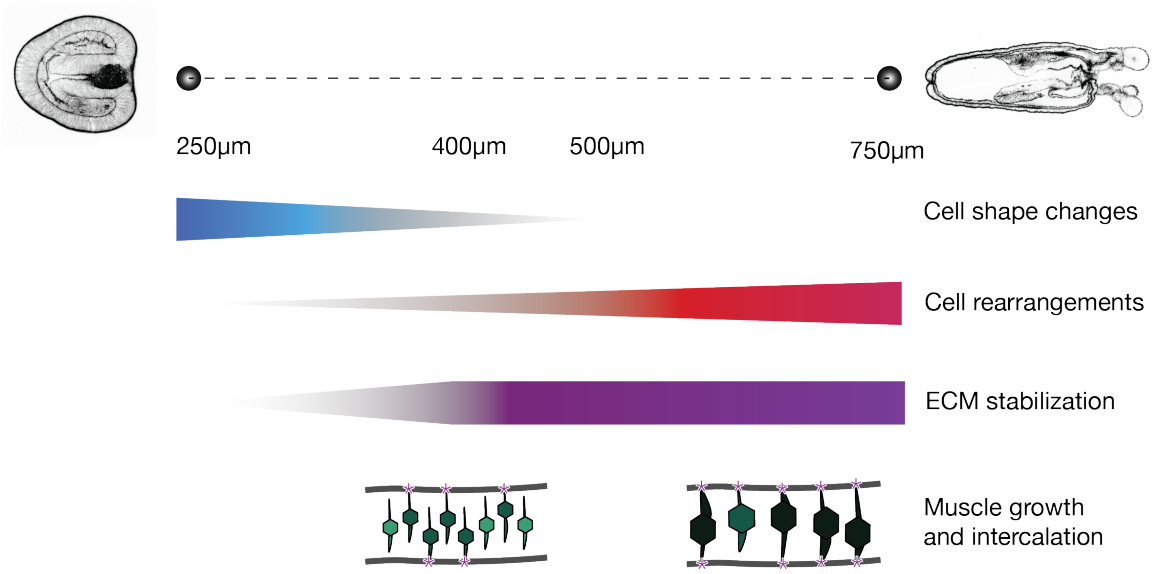

Figure 7.6. Tissue remodeling motifs during larva-polyp morphogenesis. Deformations during larva-polyp morphogenesis is initially driven by tissue thinning, and is followed by cellular rearrangements. Muscle-ECM interactions only affect the regime controlled by cell rearrangements.

Chapter 8

Establishment of a secondary body opening in a cnidarian

The origin of digestive openings is a highly debatable topic in metazoan evolution (Hejnol and Martindale (2009)). A common hypothesis postulates that early animals had a digestive cavity with one main gastric opening used for both feeding and defecation. This scenario is based on the ”sac-like” body shape of ctenophores and cnidarians that seemingly lacks a ”through-gut” system with distinct mouth and anus functions. However, emerging evidence in these early-branching metazoans points to the existence of another opening opposite to the oral pole (Presnell et al. (2016); Shimizu et al. (2007)), but the developmental mechanisms underlying the formation of this cryptic pore are still unknown. As seen in Figure 5.2, there is a discontinuity of the presumptive mesoglea at the aboral pole, as early as in the larval stages. I decided to follow this observation and investigate the dynamics of tissue remodeling at this aboral end during larva-polyp morphogenesis.

8.1 Primary polyps show sporadic expulsion of fluid from the aboral pole

In *Nematostella*, the gastrulation site leads to the formation of the future oral pore (Technau (2020)), forming the feeding mouth of the future polyp (Figure 8.1A). During live imaging with the Acquifer, I often observe that *Nematostella* primary polyps occasionally expel fluid from the aboral extremity (Figure 1B). This suggests the presence of an aperture at the aboral end. Since fluid leakage was not continuous, I hypothesized that the structure underlying this leakage could switch between intact

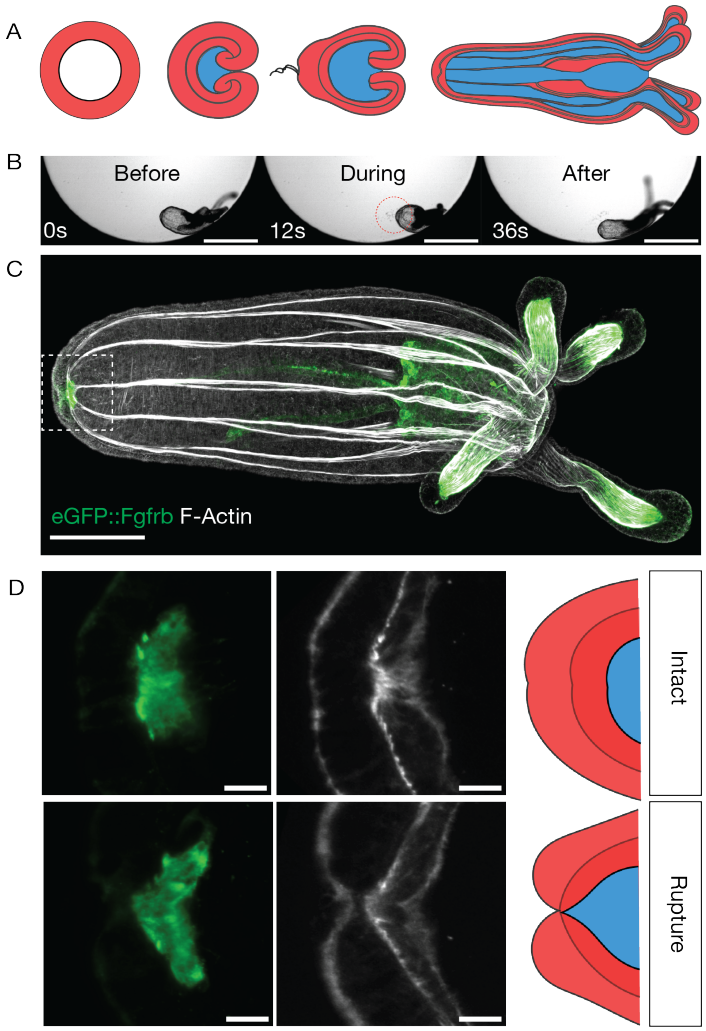

Figure 8.1. Spatial characterization of the aboral pore in *Nematostella vectensis*. A. Representation of the body plan of *Nematostella*. B. Snapshots during live imaging of polyps using Acquifer microscope. *Nematostella* polyps exhibit sporadic expulsion from the aboral end. Scale bar: 1mm. C. Transgenic eGFP::Fgfrb polyp imaged using confocal microscope. eGFP::Fgfrb is only expressed at the aboral pole, inside the pharynx and the mesenteries anf in the tentacle tips. D. (Left) Zoomed-in image at the aboral end. The aboral can exist in two states, intact or ruptured. Scale bar: 10µm. (Right) Schematic of the morphology of the aboral end configurations.

and ruptured states. To explore this possibility, I analyzed the epithelial architecture of the aboral pole using the eGFP::Fgrfrb transgenic line that already marks the aboral end along with the pharynx, mesesnteries and tentacle tips (Ikmi et al. (2020)) (Figure 8.1B). We found that the aboral pole can exist in two configurations, where it can have an intact epithelial architecture or a striking loss of epithelial integrity (Figure 8.1C,D). Interestingly, the site of this tissue rupture always overlapped with

high expressions of eGFP::Fgfrb, suggesting a link between the location of fluid leakage and this developmental signaling.

8.2 Dynamic changes across the germ layers pre-mark the aboral pore formation

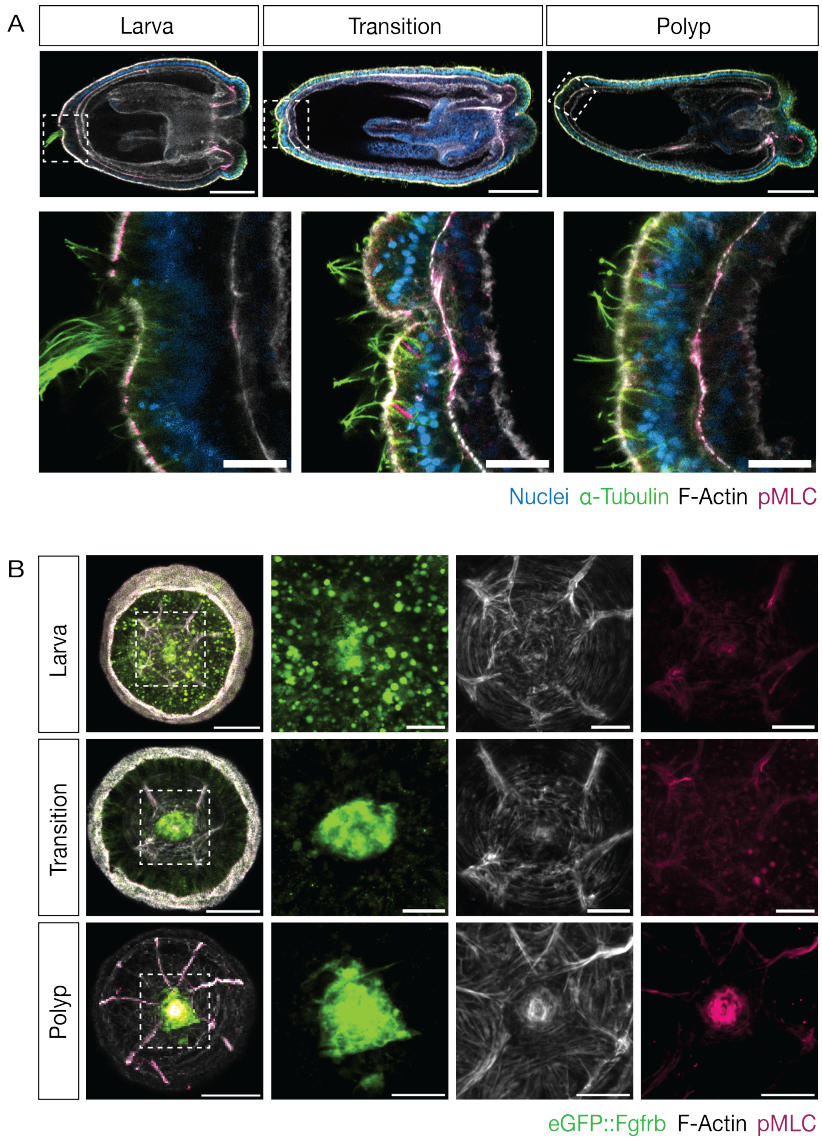

Figure 8.2. The dynamics of the germ layers at the aboral end. A. Loss of epithelial integrity is marked at the ectoderm when the animal loses its apical tuft. However, the epithelia can recover. Scale: 50µm (zoomed-out), 10µm (zoomed insets). B. Aboral view exhibits the gain of organization within the endoderm. Fgfrb expression is upregulated at the aboral end, which is followed up by the circularization of the muscles. Post metamorphosis, a tight ring of muscles are phosphorylated at the aboral end.

To characterize the embryonic origin of this presumptive aboral pore, I next tracked the cellular and molecular changes taking place during development, at the aboral end. It is already known that this region is premarked by a loss of basal cell-cell contacts with downregulation of Cdh3 (Pukhlyakova et al. (2019)). One mechanism that could drive the formation of the aboral pore might be the loss of epithelial integrity when the larva loses a thick bundle of cilia at the aboral end, its apical organ (Sinigaglia et al. (2015)). The loss of apical organ causes the ectoderm to rupture temporarily, but the tissue can heal afterwards (Figure 8.2A). A single polyp can show aboral leakage multiple times, and post metamorphosis from a larva, which suggests that the formation of the aboral pore requires a much more active mechanism than the disruption of ectodermal integrity through the shedding of the apical organ.

Next, I focused on the endoderm. I performed immunostaining in eGFP::Fgfrb animals, looking for expression of eGFP::Fgfrb in combination with the muscular architecture and also performed immunostaining for phosphorylated myosin light chain (pMLC) that enables the visualization of active muscles. I found a temporal coordination in between Fgfrb upregulation, muscle fiber alignment and its activity. Fgfrb starts to upregulate during larva-polyp transition within the endoderm, which is followed up by the circularization of the muscles at the aboral end. Post-morphogenesis, a tight set of circularized muscles exhibit a high pMLC signal, sitting at the base of the Fgfrb+ rosette cells (Figure 8.2B). This special structure represents like an active muscular valve sitting within the endoderm. Taken together, the germ layers are heavily modified at the aboral end during larva-polyp morphogenesis.

8.3 A weak local basement membrane premarks the future aboral pore

To form a functional pore across germ layers, the basement membrane also needs to be coordinated at the aboral end. I next tried to understand the role of cell-matrix contacts across development at the aboral end. Using immunostaining against both basement membrane markers collagen IV and laminin, I found out that there is localized destabilization of the matrix close to the aboral end, which is already established at early larval stages and is maintained throughout morphogenesis (Figure 8.3). However, I also report an interesting dynamic between laminin and collagen IV networks at the aboral end, where from later transition onwards collagen IV remains destabilized while the laminin starts to upregulate locally (Figure 8.4). This complements a similar strategy that dictates a weaker cell-cell adhesion at the aboral end through

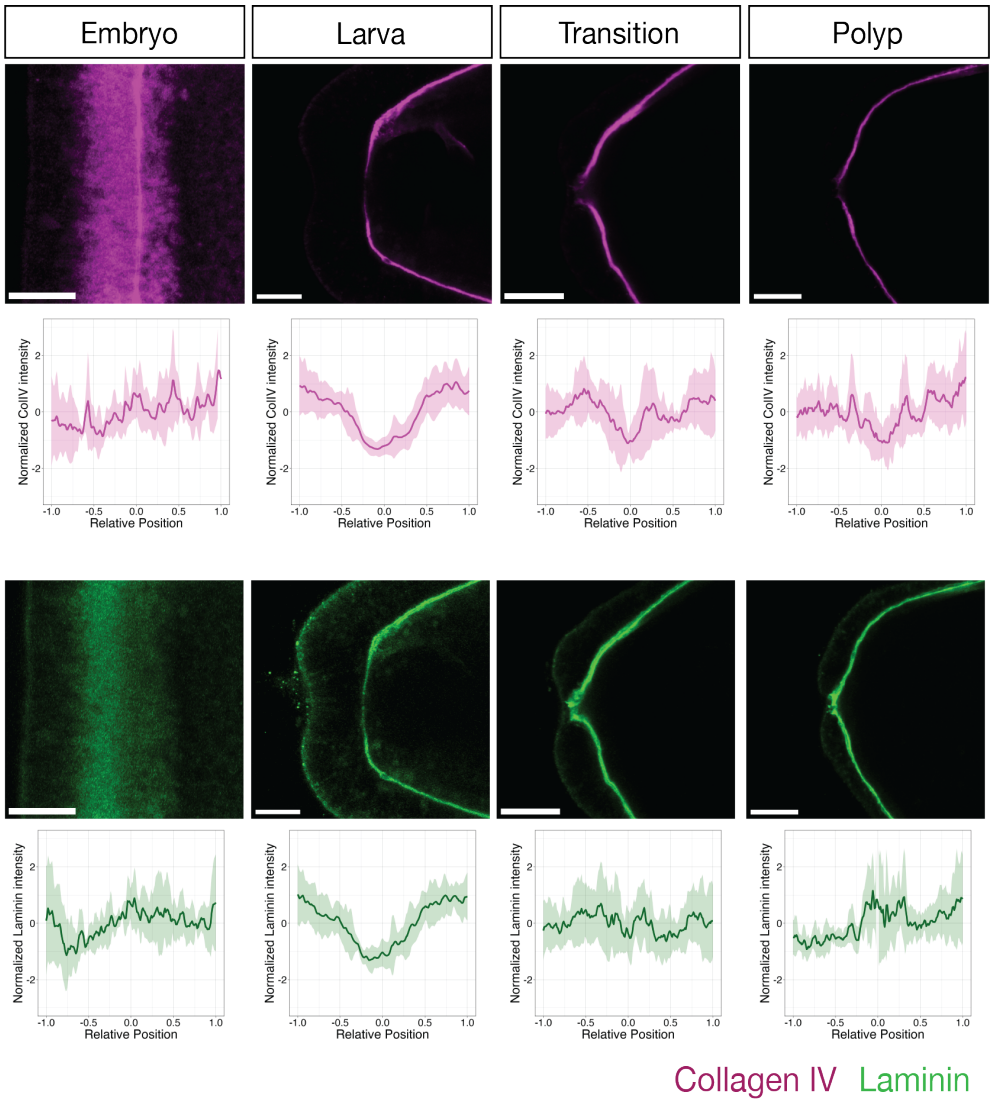

Figure 8.3. The dynamic basement membrane at the aboral end during larva-polyp morphogenesis. Immunostaining of basement membrane markers collagen IV and laminin during larva-polyp morphogenesis at the aboral end during development. The intensities of the standardized signal plotted relatively to the position of the aboral end (n=5 for each stage). Scale bar: 20µm.

local downregulation of Cdh3 while Cdh1 is maintained (Pukhlyakova et al. (2019)). The aboral end of *Nematostella* thus is marked by weaker cell-cell and cell-matrix connections, priming it for a future opening.

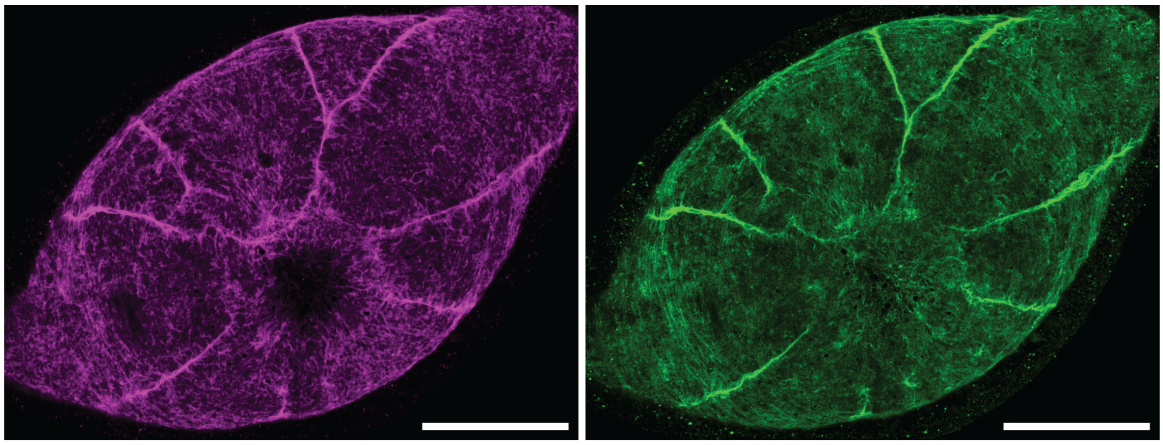

Figure 8.4. The aboral view of the basement membrane at the polyp stages. The differences in between collagen IV and laminin networks at the aboral end is clear in this representation. Scale bar: 50µm.

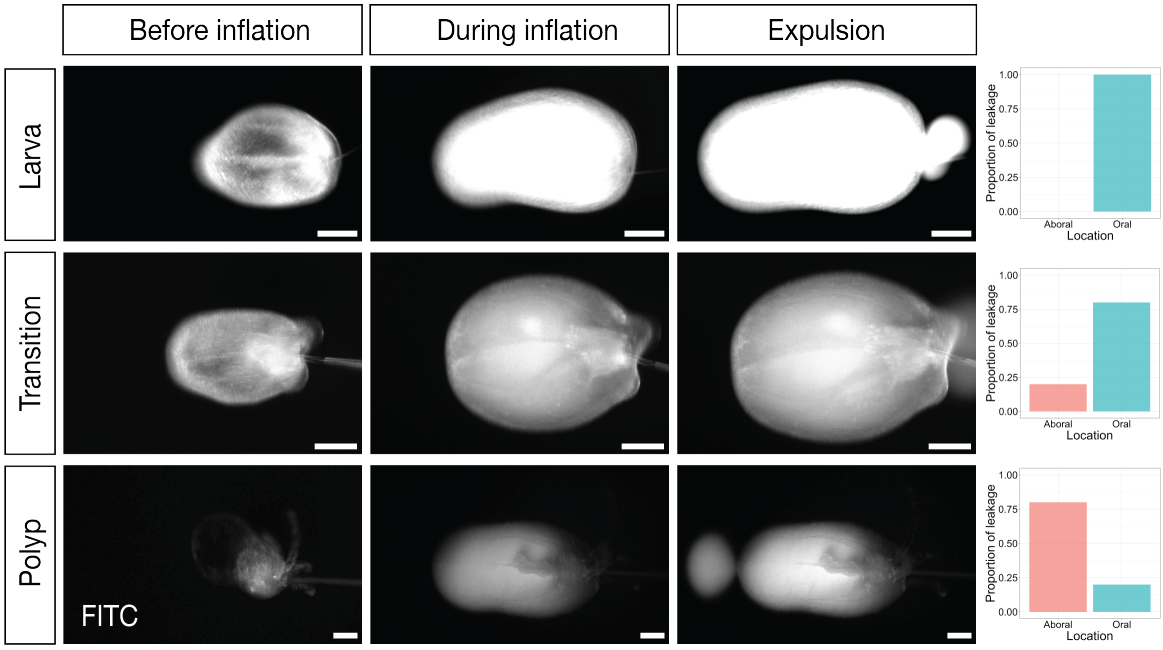

Figure 8.5. Cavity inflation: a biophysical assay to test the functionality of the aboral pore. Animals undergoing artificial cavity inflation with seawater labeled with FITC. Scale bar: 100µm. Quantification of leakage location across development. n = 6 in each case.

8.4 An artificial cavity expansion assay tests the functionality of the aboral pore

During axial elongation along larva-polyp morphogenesis, the body wall of the animal gets thinner. It is intuitive to understand that formation of a pore is easier in thinner tissue in contrast to its thicker counterpart. To understand the role of cavity pressure on pore formation, I established a mechanical assay to inflate the gastrovascular cavity of *Nematostella* during development to check what happens when the excess cavity pressure induces expulsion of seawater. I insert a capillary through the mouth and pump seawater mixed with 1:100 dilution of FITC to check from where the seawater gets expelled. I found out that during development, until the animal completes its metamorphosis, there is almost no expulsion of seawater from the aboral end and instead the animal uses its mouth. From polyp stages onwards, *Nematostella* uses its aboral end mostly to neutralize the excess cavity pressure, even though the mouth controls the influx of seawater inside the cavity. I infer that *Nematostella* indeed forms a functional mechanosensitive organ that has a primary function of neutralizing excess cavity pressure, that is functional post larva-polyp morphogenesis.

8.5 The development of the aboral pore is dependent on FGF signaling

I finally tried to test if the aboral pore formation is molecularly orchestrated by FGF signaling, since it is locally marked by high Fgfrb upregulation. In order to directly test the effect of FGF signaling on aboral pore formation, I used a previously characterized $Fgfrb^{-/-}$ mutant (Ikmi et al. (2020)). Apart from the obvious phenotype displaying a shorter body length with rounded tentacles, I report that the mutants lack an existence of an aboral pore by characterising the presence of all the markers characterized. The mutants lack phosphorylation of the muscles at the aboral end (Figure 8.6). The lack of muscle phosphorylation will inhibit the formation of the mechanosensitive valve. FGF signaling also affects basement membrane remodeling, where I observed no localized degradation of collagen IV at the aboral end (Figure 8.6). The lack of weak cell-ECM contacts at the aboral end will possibly not allow the maintenance of a ruptured state. The final test was performed by the cavity inflation assay, where unlike the siblings, the mutants failed to open its aboral pore to neutralize excess cavity pressure (Figure 8.8). I conclude that the formation of a secondary body opening at the aboral end requires the active role of FGF signaling mediated

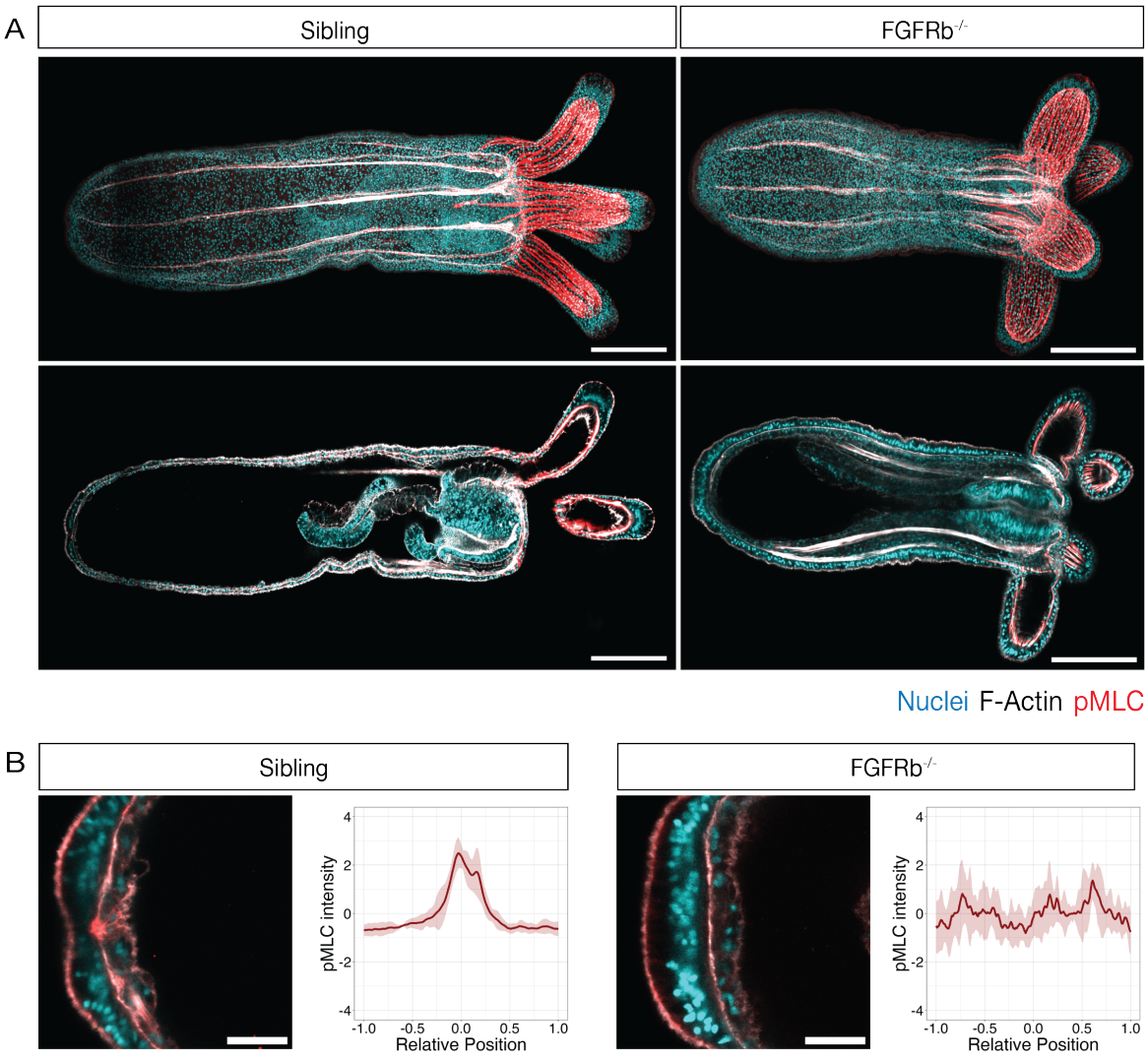

Figure 8.6. FGFRb$^{-/-}$ mutants lack active muscles at the aboral end compared to siblings. A. FGFRb$^{-/-}$ mutants show difference in body size with rounded tentacles. Scale bar: 100µm. B. Lack of pMLC upregulation in FGFRb$^{-/-}$ compared to siblings. Scale bar: 20µm.

through its receptor Fgfrb, perturbing which affects the downstream processes that helps establishing an active organ instead of just a local rupture.

8.6 Summary and conclusions

I have tried to understand molecularly how a secondary body opening is established in the cnidarian *Nematostella* at the opposite end of the mouth that is patterned by gastrulation. Using detailed cellular and molecular descriptions, combined with biophysical experiments, I identify key steps that lead to the development of an aboral pore during larva-polyp morphogenesis. First, a localized remodeling of collagen IV

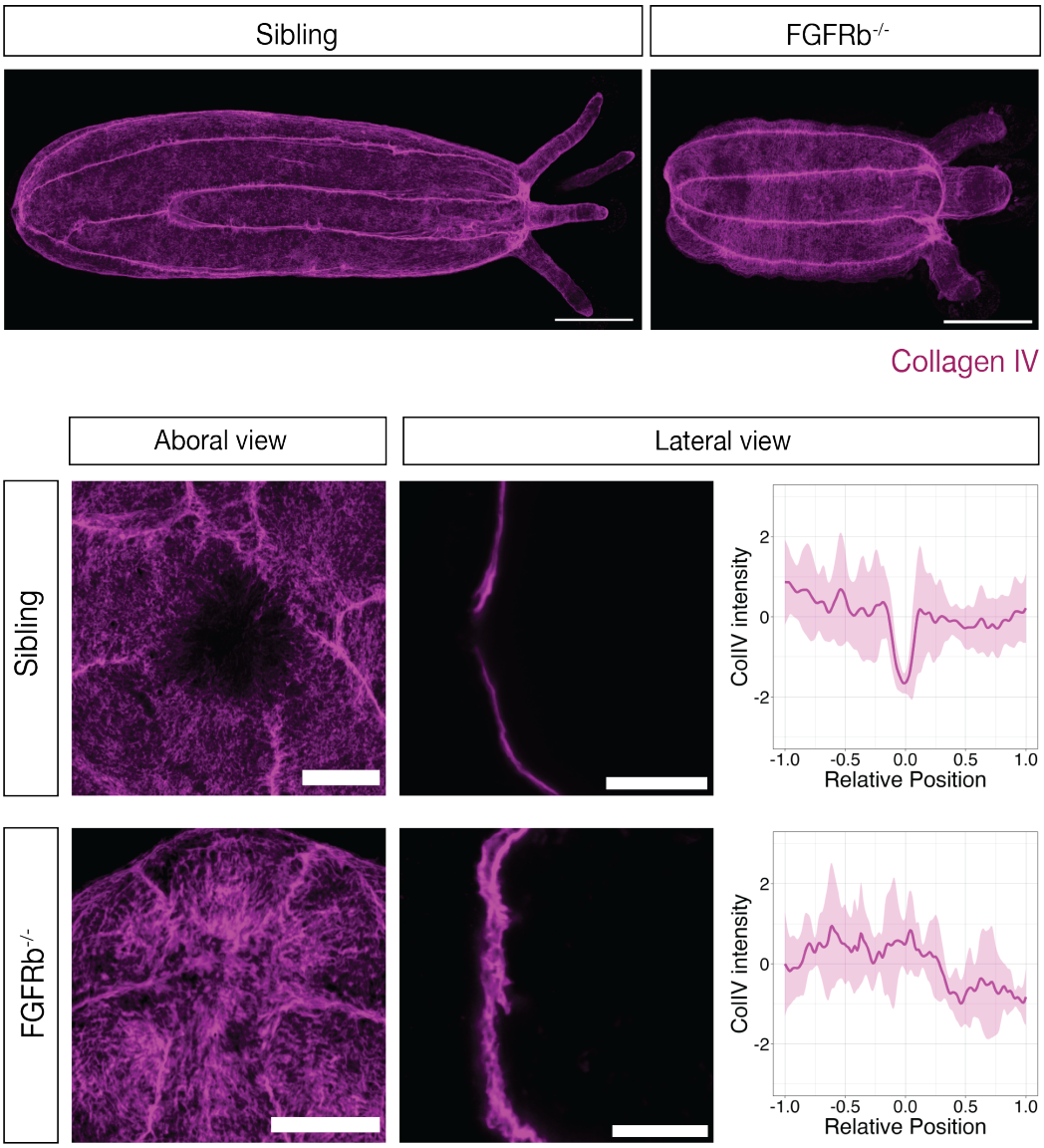

Figure 8.7. FGFRb$^{-/-}$ mutants lack collagen IV degradation at the aboral end compared to siblings. (Top) Collagen IV organization remains unperturbed in the mutants across the body axis, with characteristic patterns on the segments and the boundaries. Scale bar: 100µm. (Bottom left) The difference is clear at the aboral end with the aboral view, where there is a lack of degradation compared to siblings. Scale bar: 20µm. (Bottom right) The lateral view and the quantifications. Scale bar: 20µm.

and Cadherin 3 in early development pre-marks the future site of the aboral pore, preparing for a weak spot. During larva-polyp morphogenesis, select endodermal cells adopt a funnel-shaped muscular organization with a high phospho-myosin enrichment at the tip of the aboral pole. In parallel, the aboral ectodermal layer undergoes dynamic gain and loss of epithelial integrity, that allows the maintenance of ruptured and intact states simultaneously. I also show that all these processes are tightly

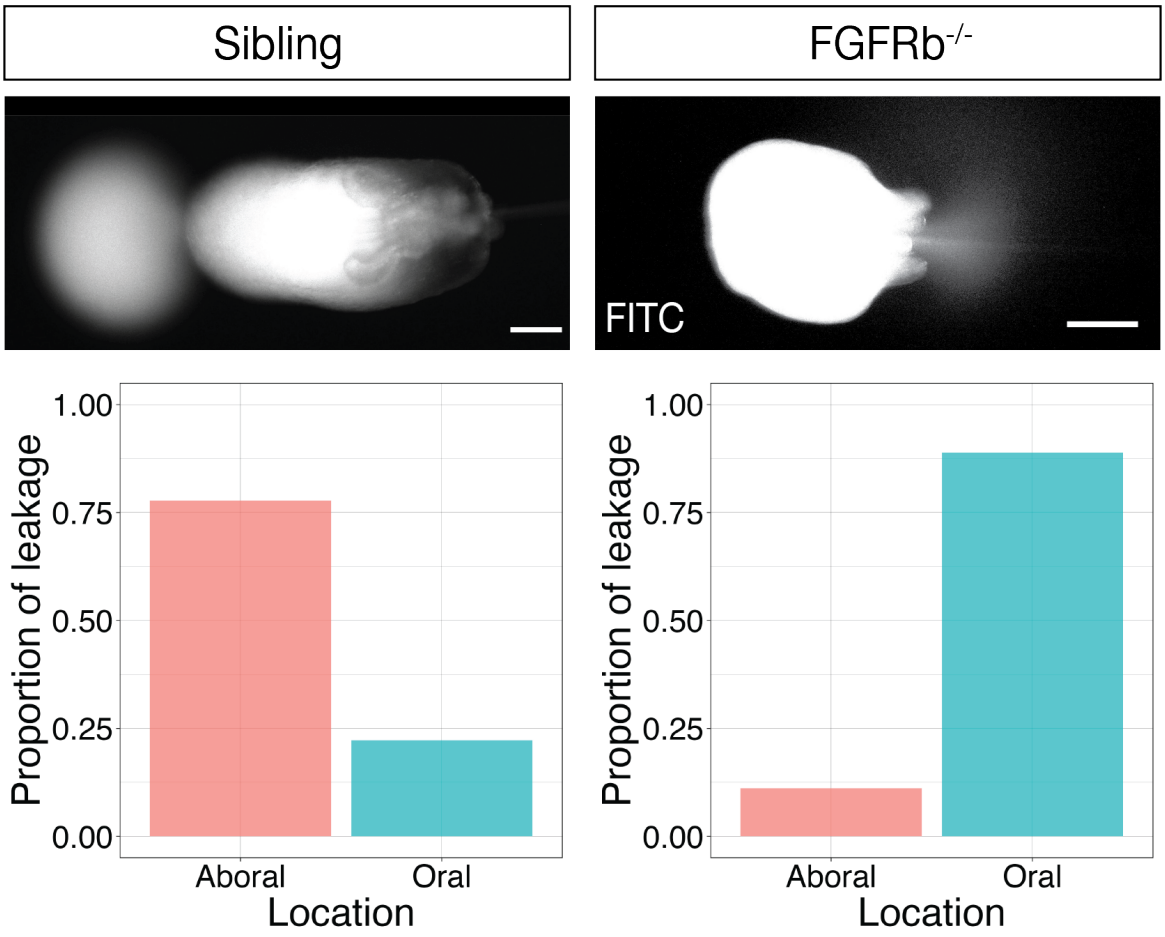

Figure 8.8. FGFRb$^{-/-}$ mutants lack aboral pore leakage with artificial cavity inflation. The mutants fail to open its aboral pore to neutralize excess cavity pressure. Scale bar: 100µm. Quantification of leakage location in siblings and mutants. n = 10 in both cases.

orchestrated by FGF signaling for which the mutant animals lack the aboral pore. Taken together, I propose that the opening of the aboral pore involves both a muscle-controlled valve-like structure and rupture of epidermal tissue allowing cavity fluid expulsion and thereby providing a novel foundation for understanding the diversification of axial properties in metazoans, aiding in the resolution of existing evolutionary controversies.

Chapter 9

Discussions

9.1 On the roles of basement membrane in organismal morphogenesis

I have used the larva-polyp morphogenesis of Nematostella to understand the role of the ECM on organismal morphogenesis, post-embryonically. Using immunostaining and generating endogenously tagged ECM proteins of interest, I was able to characterize and understand the biogenesis of the basement membrane, a part of the ECM that remains adjacent to the overlying germ layers. Furthermore, I have unlocked a possible feedback between the ECM and the muscular system that drives the morphogenetic changes with the generation of active stresses. To account for the strains that permit deformation to generate morphogenesis, I found out two independent mechanisms that is responsible to drive tissue remodeling across the organismal scales. The first regime is dominantly driven by tissue thinning, driving body length from 250µm to 400µm, while the second regime is controlled dominantly by tissue rearrangements. A tight coordination between the muscles and the basement membrane only modulates the second regime.

In order to modulate changes in shape and size, biological systems require the generation of forces, and their maintenance. The principles of cell autonomous forces are already characterized in many other model systems, owing to their respective advantages. Independent of the model system, forces are driven by the dynamics of cytoskeletal motors actin and myosin, giving rise to actomyosin contractility. Organismal morphogenesis can be driven through a same mechanism, where collectives of cells can generate forces independently. Emergent properties may come up from

the interactions between individual cells and the constraints of the system, coming from geometry, mechanics or biochemistry. This is a topic very similar in physical systems, like in the emergence of viscosity in water molecules or temperature in gas. Changes in the emergent material properties like viscosity and stiffness coming from cellular interactions has already been characterized as crucial driving parameters for morphogenesis (Mongera et al. (2018); Petridou et al. (2021)).

Multicellular animals were characterized by the innovation of neuromuscular junctions, that allow the correspondence of stimulus across larger lengthscales over shorter timescales. How does muscle contractions control morphogenesis? The larva-polyp transition poses an interesting problem demonstrating these principles, the mechanisms driving which require a coordination between forces generated autonomously by the contractions of the muscles and constrained by biophysical principles. In order to metamorphose from a larva into a polyp, Nematostella utilizes the physics of hydraulics, where the muscle contractions pump up their inner cavity pressure to generate stresses, which in effect drive tissue remodeling. The anisotropic organization of the muscles drive changes in tissue material properties across the body axis. How the material properties and tissue remodeling is connected across organismal scales is still vastly elusive, primarily due to the lack of accessibility of investigative approaches in post-embryonic development. As discussed in details in section 3, the ECM becomes a non-negotiable element within the context of morphogenesis. The ECM is a dominant contributor to the emergent material properties of the tissue. Hence I tried to understand the link between the ECM and larva-polyp transformation, focusing particularly on the BM. My results revealed an initially increasing and further maintenance of a stable density of BM across the body axis during the entire transition. Stiffening the BM halts morphogenesis and stabilizes the emergent shape, while softening the BM halts morphogenesis and reverts the animal back to its initial spherical geometry.

Furthermore, through morphometric measurements I have revealed a two-step process of tissue remodeling, where cellular rearrangements are responsible for organismal growth beyond 400µm. Cells, sitting on the BM, possibly require a finely tuned BM density to rearrange and intercalate. The stiffness of the BM thus possibly can control the effective fluidity of the tissue, which require a fine adjustment to enable morphogenesis. This will be tested by checking the rearrangement of cells in the pharmacological perturbations targeting the steady state of BM density.

My experiments have also revealed a dynamic pattern of muscle fibers during

the larva-polyp morphogenesis. The muscle fibers grow, intercalate and reach out to the segment boundaries. Individual muscle fibers are unable to cross between segments, so how does the muscles coordinate their contraction throughout the body?

Collagen IV stitches, observed at the boundaries, remain colocalized with the muscle fibers from neighboring segments. Possibly, these stitches help coordinate the individual muscles to contract. Since the softening and stiffening of the basement membrane effectively controls the amount of stitches on the boundaries, this hypothesis could be tested by looking at muscle contractility under these treatments, by analyzing high time resolution movies from the Acquifer microscope.

It is yet unclear what are the driving mechanisms that lie upstream to establish the coordination between the muscles and the matrix to regulate larva-polyp morphogenesis. In other examples like during mouse gastrulation, Nodal signaling is credited to induce spatial gradients of MMP activities that break the organismal symmetry. A similar biochemical or mechanical control can constrain the muscle-matrix coordination that is yet to be answered, If the animal generates active stresses using its muscular hydraulics and modulates its morphogenesis through its ECM, what halts morphogenesis at the polyp stages is yet to be found out.

An important observation in the larva-polyp morphogenesis was the introduction of emergent behavior and morphogenetic patterns. Animals that have different motility patterns direct their morphogenetic trajectory differently. How can this be accounted with my current model still remains an open question.

The effective changes in mechanical properties on morphogenesis could be validated through theoretical discourses. The larva-polyp transition with all its characterizations could unveil novel theoretical frameworks to understand morphogenesis of active matter at organismal scales, and bridge gaps to understanding where experiments are inaccessible. In combination, this could shed light into deeper understanding of how mechanics and morphogenesis is coordinated at such larger spatiotemporal scales.

9.2 What is the identity of the aboral pore?

I have also used the larva-polyp transition to highlight on a more local-scale morphogenesis, situated at the aboral end of the developing animal. My results highlighted in the developmental origins of a cryptic secondary opening in a cnidarian system, which evades common textbook knowledge. The investigation was started with the correla-

tion of a local disruption of collagen IV networks at the aboral end and the sporadic expulsion of material from the aboral end during live imaging. Further experiments revealed a much deeper connection of the ECM and the aboral pore formation, where an upstream molecular signaling events mediated by FGFRb controls morphogenetic events spanning both germ layers. Firstly, muscle fibers within the endoderm at the aboral pole are organized, and phosphorylated, preparing a mechanosensitive valve-like structure, while the ectoderm maintains a flexible ruptured or intact state upon losing its apical organ. The region is prepatterned as a weak spot as the cell-cell contacts and the basement membrane is locally weakened. The activation of the aboral pore only occurs post morphogenesis, as I highlighted with my cavity inflation experiments.

Going beyond morphogenesis, what is the identity of this aboral pore? Could this be an evidence of a through-gut instead of a sac-like gut as hypothesized? Could it be evidences of an early excretory system? Nematostella, like other anthozoans, live a motile larval form, and prior to metamorphosis settles down in its niche. Once settled down, they bury their body column deep within their habitat. Can a secondary opening at the aboral end allow exchange of nutrients in between the external environment and the animal's internal niche? Since the pore is consistently opened during the artificial cavity expansion instead of the mouth, this can be used as an emergency depressurizing valve to offset higher than normal hydrostatic pressure within the cavity. These are still open questions about this questionable opening, as I focused primarily on the morphogenesis of the aboral pore. A way to solve some of these mysteries is to find the molecular identity of the cells surrounding the aboral pore. Since these cells are marked by eGFP::Fgfrb, I can use the eGFP signal as a landmark to sort these cells out and sequence. The results might shed some light on some of these open-ended questions.

Chapter 10

Materials and methods

10.1 Animal husbandry

The seawater used for everything in the lab was artificially prepared by mixing 12 parts per thousand sea salt (Instant Ocean) with water, which is further mentioned as *Nematostella* medium (NM). Adult *Nematostella* were kept under controlled conditions at a temperature of 17°C in darkness immersed in NM in a recirculating system. Every three weeks, spawning was induced by subjecting the organisms to light for a duration of six hours. This light exposure was facilitated using a light box set at a temperature of around 28-30°C and providing a light intensity ranging between 250 and 300 lumens per square foot for about 8 hours, as described by Genikhovich and Technau (2009). Spawning typically occurred within three to four hours following a cold wash wih NM at 17°C. Eggs were collected and fertilized and kept in desired temperatures to control the speed of development.

10.2 Fixation and immunostaining

I anesthetized the animals in 7% Magnesium chloride before fixation. Fixation took place for one hour at room temperature using either 4% paraformaldehyde (EMS, E15710) in PBS for cellular components or Lavdovsky's fixative (3.7% formaldehyde, 50% ethanol, 4% acetic acid) for basement membrane components. Subsequently, I permeabilized the animals in 10% DMSO (Thermo Fisher, 85190) in PBS for 20 minutes and washed them with 1X PBS containing 0.2% Triton (Sigma, T8787) (PTx 0.2%). Following this, I carried out a one-hour incubation in blocking buffer (PTx 0.1%, 0.1% DMSO, 1% BSA (Sigma, A2153), and 5% Goat serum (Sigma,

G9023)). Next, I incubated the samples with the primary antibody in blocking solution overnight at 4 °C. After washing with PTw 0.1%, I incubated the animals with the secondary antibody Alexa-conjugated secondary antibodies at a 1:500 dilution (Thermo Fisher) in PTx 0.1% overnight at 4 °C. For additional staining for F-actin and nuclei, I used phalloidin Alexa Fluor (Thermo Fisher, 1:100) and Hoechst 34580 (Sigma, 63493, 1:1000), respectively, in PTx 0.1% overnight at 4 °C. Finally, I washed the animals in PTw 0.1% and mounted them in Vectashield Plus for confocal imaging.

Antibody	**Organism**	**Clonality**	**Source**	**Catalogue**	**Dilution**
pMLC	Rabbit	Polyclonal	Cell Signaling Technology	#3671S	1:50
eGFP	Rabbit	Polyclonal	MBL	#598S	1:500
eGFP	Mouse	Monoclonal	Abcam	#ab1218	1:500
α-Tubulin	Mouse	Monoclonal	Sigma	T9026	1:250
Laminin-γ	Rabbit	Polyclonal	Gift from Gideon Bergheim	X	1:400
Col IV - JK2	Rat	Monoclonal	Gift from Haruko Tomono	X	1:400

Table 10.1. List of antibodies used for this thesis.

10.3 Endogenous eGFP staining

I anesthetized the animals in 7% Magnesium chloride before fixation. Fixation took place for one hour at room temperature using 4% paraformaldehyde (EMS, E15710) in PBS. Afterwards, I washed the samples 4 times for 5 minutes each with 1X PBS. For additional staining for F-actin and nuclei, I used phalloidin Alexa Fluor (Thermo Fisher, 1:100) and Hoechst 34580 (Sigma, 63493, 1:1000), respectively in 1X PBS for 6 hours at 4 °C. The samples are protected from light post fixation. Finally, the samples are directly mounted in Vectashield Plus for confocal imaging.

10.4 Pharacological treatments

I treated larvae grown to 3 days post fertilization (DPF) and incubated them for 3 more days in the drugs that target the basement membrane remodeling. I used 0.1% DMSO as a control, 50µM GM6001 (Abcam, #ab120845) to stiffen the BM and 50µm 2,2'-Bipyridine (BPY) (Sigma, #1030980005) to soften the BM.

10.5 Live imaging with Acquifer and image analysis

I placed larvae grown 3DPF individually into the wells of a 384 well plate (Corning, 3540) containing 25 l of 12 ppt ASW or drugs using a pipette. Then, I performed imaging using an Acquifer screening microscope equipped with a 4x magnification objective and a brightfield channel set at 20% intensity, maintaining a temperature of 27 °C for three days. All image analyses were conducted using FIJI (Schindelin et al. (2012)) utilizing several FIJI plugins, such as 'AnalyzeSkeleton' (Arganda-Carreras et al. (2010)), MorphoLibJ (Legland et al. (2016)), and the BioFormats plugin (Linkert et al. (2010)). I employed the windowed sinc filter function from the pyBOAT package (Mönke et al. (2020)) to compute smoothed curves from the raw measurements of circularity, body length, average body width, and estimated body column volume. For estimating the body column volume, I subdivided the body column into cylinders with a height of 1 pixel and a radius depending on the local body column width. Subsequently, I summed up the volumes of these cylinders and added the volumes of two half spheres at the two extremities.

10.6 Confocal imaging

All samples were imaged by using a Zeiss LSM880 AiryFast or a Zeiss LSM980 AiryFast microscope with a Plan-Apochromat 20x/0.8 M27 air or a LD-LCI Plan-Apochromat 25x/0.8 Imm autocorr FCS M27 objective for lower resolutions, in the respective microscopes. For higher resolution, images were taken with a C-Apochromat 40x/1.2 W autocorr FCS M27 or a Plan-Apochromat 63x/1.4 Oil DIC M27 objective. Laser lines 405nm, 488nm, 561nm or 633nm were used depending on the sample.

10.7 Dendra2::ColIV photoconversion

Dendra2::ColIV+ larvae were anesthesized with 7% Magnesium chloride, and transfered to a round glass-bottom dish (MatTek, #P35G-1.5-14-C). The photoconversion was performed with a Evident Rapp FV3000 microscope, the conversions done with 375nm laser line. Post morphogenesis, the animals were loaded on a microscopy slide, looked for the photoconverted clone under the microscope and imaged. The laser lines 488nm an 561nm were used to check the unconverted and converted Dendra2 signal.

GFP shRNA	Forward	TAATACGACTCACTATAGGGGCACAAGCTGGAGTACAATTCAAGAGATTGTACTCCAGCTTGTGCCCTT
	Reverse	AAGGGCACAAGCTGGAGTACAATCTCTTGAATTGTACTCCAGCTTGTGCCCCTATAGTGAGTCGTATTA
Tbx20 shRNA	Forward	TAATACGACTCACTATAGGGAACAGCTGCTTAAACATTCAAGAGATGTTTAAGCAGCTGTTCCCTT
	Reverse	AAGGGAACAGCTGCTTAAACATCTCTTGAATGTTTAAGCAGCTGTTCCCTATAGTGAGTCGTATTA
BMP2/4 shRNA	Forward	TAATACGACTCACTATAGGACTGGATATTCAAGTGATTCAAGAGATCACTTGAATATCCAGTCCTT
	Reverse	AAGGACTGGATATTCAAGTGATCTCTTGAATCACTTGAATATCCAGTCCTATAGTGAGTCGTATTA

Table 10.2. Primers used for shRNA KD targeting muscle organization

10.8 shRNA KD

shRNAs were already synthesized by Anniek Stokkermans. I dejellied unfertilized eggs in a 4% cysteine solution (Sigma, #168149) in NM for nine minutes and washed them with NM. Then, I fertilized the eggs and injected them with shRNA using a Femtojet Express (Eppendorf). I mixed shRNA targeting GFP, Tbx20, or BMP2/4 mRNA with Texas Red-labelled Dextran (ThermoFisher, #D3328) to label injected eggs. I kept the embryos at room temperature and transferred them to 27°C the following day.

10.9 Cavity inflation assay

A needle loaded with FITC (Thermo Fisher, #46425) at 1:100 dilution is slowly inserted into the mouth of an animal with a Femtojet Express microinjector. Depending on the needle size, the cavity can be inflated under recording from the stereoscope every second until the leakage appears.

Bibliography

Adachi, T., Tomita, M., and Yoshizato, K. (2005). Synthesis of prolyl 4-hydroxylase subunit and type IV collagen in hemocytic granular cells of silkworm, *Bombyx mori*: Involvement of type IV collagen in self-defense reaction and metamorphosis. *Matrix Biology*, 24(2):136–154.

Arganda-Carreras, I., Fernández-González, R., Muñoz-Barrutia, A., and Ortiz-De-Solorzano, C. (2010). 3d reconstruction of histological sections: Application to mammary gland tissue. *Microscopy research and technique*, 73(11):1019–1029.

Aufschnaiter, R., Zamir, E. A., Little, C. D., Özbek, S., Münder, S., David, C. N., Li, L., Sarras, M. P., and Zhang, X. (2011). In vivo imaging of basement membrane movement: ECM patterning shapes *Hydra* polyps. *Journal of Cell Science*, 124(23):4027–4038.

Bella, J. and Hulmes, D. J. (2017). Fibrillar collagens. *Fibrous proteins: structures and mechanisms*, pages 457–490.

Bonnans, C., Chou, J., and Werb, Z. (2014). Remodelling the extracellular matrix in development and disease. *Nature Reviews Molecular Cell Biology*, 15(12):786–801. Number: 12 Publisher: Nature Publishing Group.

Borchiellini, C., Coulon, J., and Le Parco, Y. (1996). The function of type iv collagen during drosophila muscle development. *Mechanisms of development*, 58(1-2):179–191.

Bordeleau, F., Mason, B. N., Lollis, E. M., Mazzola, M., Zanotelli, M. R., Somasegar, S., Califano, J. P., Montague, C., LaValley, D. J., Huynh, J., Mencia-Trinchant, N., Negrón Abril, Y. L., Hassane, D. C., Bonassar, L. J., Butcher, J. T., Weiss, R. S., and Reinhart-King, C. A. (2017). Matrix stiffening promotes a tumor vasculature phenotype. *Proceedings of the National Academy of Sciences*, 114(3):492–497. Publisher: Proceedings of the National Academy of Sciences.

Boudko, S. P., Ailsworth, O., Bryant, Z., Cole, C., Edward, J., Edwards, D., Farrar, S., Gallup, J., Gallup, M., Gergis, M., Holt, A., Lach, M., Leaf, E., Mahoney, F., McFarlin, M., Moran, M., Murphy, G., Myers, C., Ni, C., Redhair, N., Rosa, R., Servidio, O., Sockbeson, J., Taylor, L., Pedchenko, V. K., Pokidysheva, E. N., Budko, A. M., Baugh, R., Coates, P. T., Fidler, A. L., Hudson, H. M., Ivanov, S. V., Luer, C., Pedchenko, T., Preston, R. L., Rafi, M., Vanacore, R., Bhave, G., Hudson, J. K., and Hudson, B. G. (2023). Collagen IV of basement membranes: III. Chloride pressure is a primordial innovation that drives and maintains the assembly of scaffolds. *Journal of Biological Chemistry*, 299(11). Publisher: Elsevier.

Chan, A., Ma, S., Pearson, B. J., and Chan, D. (2021). Collagen IV differentially regulates planarian stem cell potency and lineage progression. *Proceedings of the National Academy of Sciences*, 118(16):e2021251118. Publisher: Proceedings of the National Academy of Sciences.

Chen, D.-Y., Crest, J., Streichan, S. J., and Bilder, D. (2019). Extracellular matrix stiffness cues junctional remodeling for 3D tissue elongation. *Nature Communications*, 10(1):3339. Number: 1 Publisher: Nature Publishing Group.

Chu, W.-C. and Hayashi, S. (2021). Mechano-chemical enforcement of tendon apical ECM into nano-filaments during Drosophila flight muscle development. *Current biology: CB*, 31(7):1366–1378.e7.

Collinet, C. and Lecuit, T. (2021). Programmed and self-organized flow of information during morphogenesis. *Nature Reviews Molecular Cell Biology*, 22(4):245–265. Number: 4 Publisher: Nature Publishing Group.

Crest, J., Diz-Munoz, A., Chen, D.-Y., Fletcher, D. A., and Bilder, D. (2017). Organ sculpting by patterned extracellular matrix stiffness. *Elife*, 6:e24958.

DeSimone, D. W. and Mecham, R. P. (2013). *Extracellular matrix in development*, volume 10. Springer.

Díaz-de-la Loza, M.-d.-C. and Stramer, B. M. (2024). The extracellular matrix in tissue morphogenesis: No longer a backseat driver. *Cells & Development*, 177:203883.

Fidler, A. L., Darris, C. E., Chetyrkin, S. V., Pedchenko, V. K., Boudko, S. P., Brown, K. L., Gray Jerome, W., Hudson, J. K., Rokas, A., and Hudson, B. G. (2017). Collagen IV and basement membrane at the evolutionary dawn of metazoan tissues. *eLife*, 6:e24176. Publisher: eLife Sciences Publications, Ltd.

Fidler, A. L., Vanacore, R. M., Chetyrkin, S. V., Pedchenko, V. K., Bhave, G., Yin, V. P., Stothers, C. L., Rose, K. L., McDonald, W. H., Clark, T. A., Borza, D.-B., Steele, R. E., Ivy, M. T., The Aspirnauts, Hudson, J. K., and Hudson, B. G. (2014). A unique covalent bond in basement membrane is a primordial innovation for tissue evolution. *Proceedings of the National Academy of Sciences*, 111(1):331–336. Publisher: Proceedings of the National Academy of Sciences.

Fritz, A. E., Ikmi, A., Seidel, C., Paulson, A., and Gibson, M. C. (2013). Mechanisms of tentacle morphogenesis in the sea anemone nematostella vectensis. *Development*, 140(10):2212–2223.

Gao, H., Ren, G., Xu, Y., Jin, C., Jiang, Y., Lin, L., Wang, L., Shen, H., and Gui, L. (2011). Correlation between expression of aquaporins 1 and chondrocyte apoptosis in articular chondrocyte of osteoarthritis. *Zhongguo Xiu Fu Chong Jian Wai Ke Za Zhi= Zhongguo xiufu chongjian waike zazhi= Chinese journal of reparative and reconstructive surgery*, 25(3):279–284.

Genikhovich, G. and Technau, U. (2009). Induction of spawning in the starlet sea anemone nematostella vectensis, in vitro fertilization of gametes, and dejellying of zygotes. *Cold Spring Harbor Protocols*, 2009(9):pdb–prot5281.

Gorres, K. L. and Raines, R. T. (2010). Prolyl 4-hydroxylase. *Critical reviews in biochemistry and molecular biology*, 45(2):106–124.

Guimarães, C. F., Gasperini, L., Marques, A. P., and Reis, R. L. (2020). The stiffness of living tissues and its implications for tissue engineering. *Nature Reviews Materials*, 5(5):351–370. Number: 5 Publisher: Nature Publishing Group.

Haigo, S. L. and Bilder, D. (2011). Global tissue revolutions in a morphogenetic movement controlling elongation. *Science*, 331(6020):1071–1074.

Harmansa, S., Erlich, A., Eloy, C., Zurlo, G., and Lecuit, T. (2023). Growth anisotropy of the extracellular matrix shapes a developing organ. *Nature Communications*, 14(1):1220. Number: 1 Publisher: Nature Publishing Group.

He, S., Del Viso, F., Chen, C.-Y., Ikmi, A., Kroesen, A. E., and Gibson, M. C. (2018). An axial Hox code controls tissue segmentation and body patterning in Nematostella vectensis. *Science (New York, N.Y.)*, 361(6409):1377–1380.

Hejnol, A. and Martindale, M. Q. (2009). The mouth, the anus, and the blastopore—open questions about questionable openings. *Animal Evolution: Genomes, Fossils,*

and Trees, pages 33–40.

Holster, T., Pakkanen, O., Soininen, R., Sormunen, R., Nokelainen, M., Kivirikko, K. I., and Myllyharju, J. (2007). Loss of assembly of the main basement membrane collagen, type IV, but not fibril-forming collagens and embryonic death in collagen prolyl 4-hydroxylase I null mice. *The Journal of Biological Chemistry*, 282(4):2512–2519.

Hynes, R. O. (2004). The emergence of integrins: a personal and historical perspective. *Matrix biology : journal of the International Society for Matrix Biology*, 23(6):333–340.

Ikmi, A., McKinney, S. A., Delventhal, K. M., and Gibson, M. C. (2014). Talen and crispr/cas9-mediated genome editing in the early-branching metazoan nematostella vectensis. *Nature communications*, 5(1):5486.

Ikmi, A., Steenbergen, P. J., Anzo, M., McMullen, M. R., Stokkermans, A., Ellington, L. R., and Gibson, M. C. (2020). Feeding-dependent tentacle development in the sea anemone nematostella vectensis. *Nature communications*, 11(1):1–13.

Isabella, A. J. and Horne-Badovinac, S. (2016). Rab10-mediated secretion synergizes with tissue movement to build a polarized basement membrane architecture for organ morphogenesis. *Developmental cell*, 38(1):47–60.

Jahnel, S. M., Walzl, M., and Technau, U. (2014). Development and epithelial organisation of muscle cells in the sea anemone nematostella vectensis. *Frontiers in zoology*, 11:1–15.

Jayadev, R. and Sherwood, D. R. (2017). Basement membranes. *Current Biology*, 27(6):R207–R211.

Jessen, J. R. (2015). Recent advances in the study of zebrafish extracellular matrix proteins. *Developmental Biology*, 401(1):110–121.

(Jr), S. and P, M. (2012). Components, structure, biogenesis and function of the hydra extracellular matrix in regeneration, pattern formation and cell differentiation. *The International Journal of Developmental Biology*, 56(6-7-8):567–576. Number: 6-7-8 Publisher: UPV/EHU Press.

Karkali, K., Tiwari, P., Singh, A., Tlili, S., Jorba, I., Navajas, D., Muñoz, J. J., Saunders, T. E., and Martin-Blanco, E. (2022). Condensation of the drosophila nerve

cord is oscillatory and depends on coordinated mechanical interactions. *Developmental cell*, 57(7):867–882.

Kato, T., Saika, S., and Ohnishi, Y. (2006). Effects of the matrix metalloproteinase inhibitor GM6001 on the destruction and alteration of epithelial basement membrane during the healing of post-alkali burn in rabbit cornea. *Japanese Journal of Ophthalmology*, 50(2):90–95.

Kim, S., Pochitaloff, M., Stooke-Vaughan, G. A., and Campàs, O. (2021). Embryonic tissues as active foams. *Nature Physics*, 17(7):859–866. Number: 7 Publisher: Nature Publishing Group.

Ku, H.-Y., Harris, L. K., and Bilder, D. (2023). Specialized cells that sense tissue mechanics to regulate drosophila morphogenesis. *Developmental Cell*, 58(3):211–223.

Kyprianou, C., Christodoulou, N., Hamilton, R. S., Nahaboo, W., Boomgaard, D. S., Amadei, G., Migeotte, I., and Zernicka-Goetz, M. (2020). Basement membrane remodelling regulates mouse embryogenesis. *Nature*, 582(7811):253–258.

Labouesse, M. (2012). Role of the extracellular matrix in epithelial morphogenesis. *Organogenesis*, 8(2):65–70.

Lardennois, A., Pásti, G., Ferraro, T., Llense, F., Mahou, P., Pontabry, J., Rodriguez, D., Kim, S., Ono, S., Beaurepaire, E., Gally, C., and Labouesse, M. (2019). An actin-based viscoplastic lock ensures progressive body-axis elongation. *Nature*, 573(7773):266–270.

Layden, M. J., Rentzsch, F., and Röttinger, E. (2016). The rise of the starlet sea anemone nematostella vectensis as a model system to investigate development and regeneration. *Wiley Interdisciplinary Reviews: Developmental Biology*, 5(4):408–428.

Legland, D., Arganda-Carreras, I., and Andrey, P. (2016). Morpholibj: integrated library and plugins for mathematical morphology with imagej. *Bioinformatics*, 32(22):3532–3534.

Lenne, P.-F. and Trivedi, V. (2022). Sculpting tissues by phase transitions. *Nature Communications*, 13(1):664. Number: 1 Publisher: Nature Publishing Group.

Li, Y., Trivedi, V., Truong, T. V., Koos, D. S., Lansford, R., Chuong, C.-M., Warburton, D., Moats, R. A., and Fraser, S. E. (2015). Dynamic imaging of the growth

plate cartilage reveals multiple contributors to skeletal morphogenesis. *Nature Communications*, 6(1):6798. Publisher: Nature Publishing Group.

Linkert, M., Rueden, C. T., Allan, C., Burel, J.-M., Moore, W., Patterson, A., Loranger, B., Moore, J., Neves, C., MacDonald, D., et al. (2010). Metadata matters: access to image data in the real world. *Journal of Cell Biology*, 189(5):777–782.

Liu, X., Wang, L., Ji, J., Yao, W., Wei, W., Fan, J., Joshi, S., Li, D., and Fan, Y. (2014). A mechanical model of the cornea considering the crimping morphology of collagen fibrils. *Investigative ophthalmology & visual science*, 55(4):2739–2746.

Martin-Martin, B., Tovell, V., Dahlmann-Noor, A. H., Khaw, P. T., and Bailly, M. (2011). The effect of MMP inhibitor GM6001 on early fibroblast-mediated collagen matrix contraction is correlated to a decrease in cell protrusive activity. *European Journal of Cell Biology*, 90(1):26–36.

Martindale, M. Q., Pang, K., and Finnerty, J. R. (2004). Investigating the origins of triploblasty:mesodermal'gene expression in a diploblastic animal, the sea anemone nematostella vectensis (phylum, cnidaria; class, anthozoa).

Matsubayashi, Y., Louani, A., Dragu, A., Sanchez-Sanchez, B. J., Serna-Morales, E., Yolland, L., Gyoergy, A., Vizcay, G., Fleck, R. A., Heddleston, J. M., et al. (2017). A moving source of matrix components is essential for de novo basement membrane formation. *Current Biology*, 27(22):3526–3534.

Misko, A., Ferguson, T., and Notterpek, L. (2002). Matrix metalloproteinase mediated degradation of basement membrane proteins in Trembler J neuropathy nerves. *Journal of Neurochemistry*, 83(4):885–894. _eprint: https://onlinelibrary.wiley.com/doi/pdf/10.1046/j.1471-4159.2002.01200.x.

Molnar, K. and Labouesse, M. (2021). The plastic cell: mechanical deformation of cells and tissues. *Open Biology*, 11(2):210006.

Mongera, A., Rowghanian, P., Gustafson, H. J., Shelton, E., Kealhofer, D. A., Carn, E. K., Serwane, F., Lucio, A. A., Giammona, J., and Campàs, O. (2018). A fluid-to-solid jamming transition underlies vertebrate body axis elongation. *Nature*, 561(7723):401–405. Number: 7723 Publisher: Nature Publishing Group.

Mönke, G., Sorgenfrei, F. A., Schmal, C., and Granada, A. E. (2020). Optimal time frequency analysis for biological data-pyboat. *BioRxiv*, pages 2020–04.

Naik, S., Unni, M., Sinha, D., Rajput, S. S., Reddy, P. C., Kartvelishvily, E.,

Solomonov, I., Sagi, I., Chatterji, A., Patil, S., and Galande, S. (2020). Differential tissue stiffness of body column facilitates locomotion of Hydra on solid substrates. *Journal of Experimental Biology*, 223(20):jeb232702.

Olofsson, B. and Page, D. T. (2005). Condensation of the central nervous system in embryonic drosophila is inhibited by blocking hemocyte migration or neural activity. *Developmental biology*, 279(1):233–243.

Paix, A., Basu, S., Steenbergen, P., Singh, R., Prevedel, R., and Ikmi, A. (2023). Endogenous tagging of multiple cellular components in the sea anemone Nematostella vectensis. *Proceedings of the National Academy of Sciences of the United States of America*, 120(1):e2215958120.

Parks, W. C. and Mecham, R. (2011). *Extracellular matrix degradation*. Springer Science & Business Media.

Petridou, N. I., Corominas-Murtra, B., Heisenberg, C.-P., and Hannezo, E. (2021). Rigidity percolation uncovers a structural basis for embryonic tissue phase transitions. *Cell*, 184(7):1914–1928.e19.

Petridou, N. I., Grigolon, S., Salbreux, G., Hannezo, E., and Heisenberg, C.-P. (2019). Fluidization-mediated tissue spreading by mitotic cell rounding and non-canonical Wnt signalling. *Nature Cell Biology*, 21(2):169–178. Number: 2 Publisher: Nature Publishing Group.

Presnell, J. S., Vandepas, L. E., Warren, K. J., Swalla, B. J., Amemiya, C. T., and Browne, W. E. (2016). The presence of a functionally tripartite through-gut in ctenophora has implications for metazoan character trait evolution. *Current Biology*, 26(20):2814–2820.

Pukhlyakova, E. A., Kirillova, A. O., Kraus, Y. A., Zimmermann, B., and Technau, U. (2019). A cadherin switch marks germ layer formation in the diploblastic sea anemone nematostella vectensis. *Development*, 146(20):dev174623.

Qin, X., Park, B. O., Liu, J., Chen, B., Choesmel-Cadamuro, V., Belguise, K., Heo, W. D., and Wang, X. (2017). Cell-matrix adhesion and cell-cell adhesion differentially control basal myosin oscillation and Drosophila egg chamber elongation. *Nature Communications*, 8(1):14708. Number: 1 Publisher: Nature Publishing Group.

Rauzi, M. and Lenne, P.-F. (2011). Cortical forces in cell shape changes and tissue

morphogenesis. *Current topics in developmental biology*, 95:93–144.

Rozario, T. and DeSimone, D. W. (2010). The extracellular matrix in development and morphogenesis: a dynamic view. *Developmental biology*, 341(1):126–140.

Sanchez-Sanchez, B. J., Urbano, J. M., Comber, K., Dragu, A., Wood, W., Stramer, B., and Martín-Bermudo, M. D. (2017). Drosophila embryonic hemocytes produce laminins to strengthen migratory response. *Cell reports*, 21(6):1461–1470.

Sarras, M. P., Yan, L., Grens, A., Zhang, X., Agbas, A., Huff, J. K., St. John, P. L., and Abrahamson, D. R. (1994). Cloning and Biological Function of Laminin in Hydra vulgaris. *Developmental Biology*, 164(1):312–324.

Schindelin, J., Arganda-Carreras, I., Frise, E., Kaynig, V., Longair, M., Pietzsch, T., Preibisch, S., Rueden, C., Saalfeld, S., Schmid, B., et al. (2012). Fiji: an open-source platform for biological-image analysis. *Nature methods*, 9(7):676–682.

Sebé-Pedrós, A., Chomsky, E., Pang, K., Lara-Astiaso, D., Gaiti, F., Mukamel, Z., Amit, I., Hejnol, A., Degnan, B. M., and Tanay, A. (2018). Early metazoan cell type diversity and the evolution of multicellular gene regulation. *Nature ecology & evolution*, 2(7):1176–1188.

Serna-Morales, E., Sánchez-Sánchez, B. J., Marcotti, S., Nichols, A., Bhargava, A., Dragu, A., Hirvonen, L. M., Mink, M., Cox, S., Rayfield, E., et al. (2023). Extracellular matrix assembly stress initiates drosophila central nervous system morphogenesis. *Developmental Cell*, 58(10):825–835.

Shimizu, H., Aufschnaiter, R., Li, L., Sarras, M. P., Borza, D.-B., Abrahamson, D. R., Sado, Y., and Zhang, X. (2008). The extracellular matrix of hydra is a porous sheet and contains type IV collagen. *Zoology (Jena, Germany)*, 111(5):410–418.

Shimizu, H., Takaku, Y., Zhang, X., and Fujisawa, T. (2007). The aboral pore of hydra: evidence that the digestive tract of hydra is a tube not a sac. *Development genes and evolution*, 217:563–568.

Sinigaglia, C., Busengdal, H., Lerner, A., Oliveri, P., and Rentzsch, F. (2015). Molecular characterization of the apical organ of the anthozoan nematostella vectensis. *Developmental biology*, 398(1):120–133.

Stokkermans, A., Chakrabarti, A., Subramanian, K., Wang, L., Yin, S., Moghe, P., Steenbergen, P., Mönke, G., Hiiragi, T., Prevedel, R., Mahadevan, L., and Ikmi,

A. (2022). Muscular hydraulics drive larva-polyp morphogenesis. *Current Biology*, 32(21):4707–4718.e8.

Technau, U. (2020). Gastrulation and germ layer formation in the sea anemone nematostella vectensis and other cnidarians. *Mechanisms of Development*, 163:103628.

Theocharis, A. D., Skandalis, S. S., Gialeli, C., and Karamanos, N. K. (2016). Extracellular matrix structure. *Advanced Drug Delivery Reviews*, 97:4–27.

Tucker, R. P. and Adams, J. C. (2014). Adhesion networks of cnidarians: a postgenomic view. *International Review of Cell and Molecular Biology*, 308:323–377.

Tucker, Richard., Shibata, Bradley., and Blankenship, Thomas N. (2011). Ultrastructure of the mesoglea of the sea anemone Nematostella vectensis. *Invertebrate Biology*.

Töpfer, U. (2023). Basement membrane dynamics and mechanics in tissue morphogenesis. *Biology Open*, 12(8):bio059980.

Töpfer, U., Guerra Santillán, K. Y., Fischer-Friedrich, E., and Dahmann, C. (2022). Distinct contributions of ECM proteins to basement membrane mechanical properties in Drosophila. *Development*, 149(10):dev200456.

Vallet, S. D. and Ricard-Blum, S. (2019). Lysyl oxidases: from enzyme activity to extracellular matrix cross-links. *Essays in biochemistry*, 63(3):349–364.

Van Helvert, S., Storm, C., and Friedl, P. (2018). Mechanoreciprocity in cell migration. *Nature cell biology*, 20(1):8–20.

Zhang, X., Fei, K., Agbas, A., Yan, L., Zhang, J., O'Reilly, B., Deutzmann, R., and Sarras, M. P. (2002). Structure and function of an early divergent form of laminin in hydra: a structurally conserved ECM component that is essential for epithelial morphogenesis. *Development Genes and Evolution*, 212(4):159–172.

Özbek, S., Balasubramanian, P. G., Chiquet-Ehrismann, R., Tucker, R. P., and Adams, J. C. (2010). The Evolution of Extracellular Matrix. *Molecular Biology of the Cell*, 21(24):4300–4305. Publisher: American Society for Cell Biology (mboc).